View metadata, citation and similar papers at core.ac.uk
brought to you by CORE
provided by Publikationsserver der RWTH Aachen University

Stephan Korden

Molecular Density Functional Theory Based on a Hard-Particle Reference Potential

Molecular Density Functional Theory Based on a Hard-Particle Reference Potential

Von der Fakultät für Maschinenwesen der Rheinisch-Westfälischen Technischen Hochschule Aachen zur Erlangung des akademischen Grades eines Doktors der Naturwissenschaften genehmigte Dissertation

vorgelegt von

Stephan Korden

Berichter: Juniorprofessor Dr. rer. nat. Kai Olaf Leonhard
Universitätsprofessor Dr. rer. nat. Roland Roth

Tag der mündlichen Prüfung: 26. Oktober 2015

Diese Dissertation ist auf den Internetseiten der Universitätsbibliothek online verfügbar.

Acknowledgements

In these first lines, I would like to express my gratitude to all people who contributed to this thesis. Especially I would like to thank my supervisor Prof. Kai Leonhard for his support and encouragement over the past years, and whose interest in lattice models was the starting point for the current investigation of classical DFT. Also Prof. Roland Roth from the University of Tübingen for his time and effort to take the part as second reviewer and Prof. Peter Loosen for taking the chair of the doctoral Commitee. Likewise, I would like to thank Prof. André Bardow as head of the Institute of Technical Thermodynamics for his continuous encouragement and Prof. Matthias Schmidt from the University of Bayreuth for his interest in the mathematical approach and bringing me in contact with the FMT community, as well as Prof. Andreas Klamt from the University of Regensburg for helpful insights into his off-lattice model. I would also like to highlight the influence of Matthieu Marechal on this work. His helpful discussions and intense e-mail correspondence were a great motivation. Without his insight into Ree-Hoover diagrams, the solution of the hard-particle problem would not have been complete. Many thanks also goes to Annett Schwarz and Christian Jens for their helpful comments on the manuscripts and to Van Nhu Nguyen for many discussions on the thermodynamics of liquids. Many more have contributed to this work in more indirect ways, especially all colleagues from the Institute of Technical Thermodynamics, who patiently bridged the worlds between engineers and physicists. Finally, I would also thank my family for their long lasting support, patience, and motivation.

Für meine Eltern

Beatrix Korden

und

Joachim Korden

Abstract

The aim of the current doctorate thesis is the development of a density functional theory (DFT) for classical intermolecular interactions. In the first part, we begin with an analysis of the structure of the grand-canonical potential and demonstrate that for pair potentials only two independent representations exists: the direct-correlation functional and its Legendre transformation with respect to the pair potential. Using far-reaching assumptions, this dual grand-canonical potential reduces to the free-energy functions of Flory-Huggins, Staverman-Guggenheim, and Guggenheim, from which again derive the lattice-models UNIQUAC, UNIFAC, and COSMO-RS. We conclude this first part by discussing possible generalizations of this approach to a continuum formulation.

As is well known from quantum mechanics, the central problem of the DFT approach is the derivation of the functionals, which is further complicated for intermolecular interactions by their strongly repulsive potential. A well established approach is the separation of the potential into a flat but long-ranged contribution and the approximation of the repulsive part using the geometry of hard particles. In the second part of this work, we develop the necessary methods for the non-perturbative derivation of their corresponding hard-particle functionals.

We first begin with a discussion of the fundamental measure theory and interpret the semi-heuristic Rosenfeld functional as the leading order of an expansion in the number of intersection centers of the particles. For the generalization of the approach we demonstrate the equivalence between intersection configurations and classes of Ree-Hoover diagrams, whose sum defines a generic functional decoupling into a convolute of intersection kernels. Each such kernel determines the local intersection probability of a set of particles under the group of translations and rotations. For the case of two particles this result has been first derived by Blaschke, Santalo, and Chern. Here, we generalize their approach to an arbitrary set of particles and obtain a closed expression for the free-energy functional and the n-particle densities for any dimension.

As examples, we derive the functional of the free energy for up to four intersection centers, whose leading order agrees with Rosenfeld's result. We then calculate for the 2-particle density an upper limit of the contact probability for hard spheres, which is in excellent agreement with the result of Carnahan and Starling. Comparing the same level of approximation with Kirkwood's superposition ansatz for correlation functions of higher orders, shows that the contact probability of spheres is significantly overestimated by the superposition approximation. Finally, we derive the leading perturbative corrections for long-range interactions.

With the methods developed in the current work, the hard-particle interaction is now the only known example, whose density functionals can be derived systematically to any order of precision. We conclude our work with a discussion of possible applications in biology and chemistry.

Zusammenfassung

Das Ziel der vorliegenden Dissertation ist die Entwicklung einer Dichtefunktionaltheorie (DFT) für klassische intermolekulare Wechselwirkungen. Wir beginnen im ersten Teil der Arbeit mit einer Analyse der Struktur des großkanonischen Potentials und zeigen, dass es für Paarwechselwirkungen nur zwei unabhängige Darstellungen erlaubt: das der direkten Korrelationsfunktion und das seiner Legendre-Transformation bezüglich des Paarpotentials. Es wird gezeigt, dass sich unter weitreichenden Modellannahmen das duale Funktional auf die Ausdrücke der freien Energie von Flory-Huggins, Staverman-Guggenheim und Guggenheim reduziert, aus denen sich wiederum die Gittermodelle UNIQUAC, UNIFAC und COSMO-RS herleiten lassen. Abschließend diskutieren wir mögliche Erweiterungen als Kontinuumsbeschreibung.

Wie aus der Quantenmechanik bekannt, besteht das grundlegende Problem des DFT Ansatzes in der Berechnung der Funktionale, was im Fall der intermolekularen Wechselwirkungen durch den stark repulsiven Anteil zusätzlich erschwert wird. Ein etablierter Ansatz ist daher die Zerlegung des Potentials in einen flachen aber weitreichenden Beitrag und die Näherung des repulsiven Anteils durch die Geometrie eines harten Körpers. Im zweiten Teil der Arbeit entwickeln wir die Methoden für die nichtperturbative Berechnung der Funktionale harter Körper.

Wir beginnen mit einer Einführung in die Fundamental Measure Theory und interpretieren das semi-heuristische Rosenfeld Funktional als die führende Ordnung einer Entwicklung nach der Anzahl der Schnittzentren der Körper. Um diesen Ansatz zu verallgemeinern, zeigen wir die Äquivalenz zwischen Schnittkonfigurationen und Klassen von Ree-Hoover Diagrammen, deren Summe ein generisches Funktional bestimmt, das in ein Konvolut von Schnittkernen zerfällt. Dabei berechnet sich jeder Schnittkern aus der lokalen Schnittwahrscheinlichkeit der Teilchen unter Translationen und Rotationen. Für zwei Körper wurde dieses Ergebnis bereits durch Blaschke, Santalo und Chern berechnet. Hier verallgemeinern wird diesen Ansatz auf eine beliebige Anzahl von Teilchen und geben eine geschlossene Lösung für die freie Energie und die n-Teilchendichten in beliebiger Dimension an.

Als Beispiele berechnen wir das Funktional der freien Energie für bis zu vier Schnittzentren, dessen führende Ordnung mit Rosenfelds Ergebnis übereinstimmt. Ferner leiten wir für die 2-Teilchendichte eine obere Abschätzung der Kontaktwahrscheinlichkeit für harte Kugeln ab, das das Ergebnis von Carnahan und Starling sehr gut wiedergibt. Vergleicht man nun die gleiche Näherung mit Kirkwoods Superpositionsansatz für Korrelationen höherer Ordnung, so zeigt sich ferner, dass die Kontaktwahrscheinlichkeit durch den Superpositionsansatz signifikant überschätzt wird. Schließlich berechnen wir noch die ersten störungstheoretischen Terme für attraktive Korrekturen.

Mit den hier entwickelten Methoden ist das Hartkörperpotential das einzige heute bekannte Beispiel, für das sämtliche Korrelationsfunktionale systematisch berechnet werden können. Wir beenden die Arbeit mit einer Diskussion möglicher Anwendungen in Biologie und Chemie.

Contents

Chapter 1

Preface

As any doctorate thesis, the current text is the result of a dynamic process with unforseen problems and findings. Some results have already been published and others recently submitted. The complete list of texts that have been prepared over the last years include the following articles in chronological order of their writing:

1. S. Korden, N. Van Nhu, J. Vrabec, J. Gross, and K. Leonhard: *On the Treatment of Electrostatic Interactions of Non-Spherical Molecules in Equation of State Models*, Soft Materials, **10**, 81-105, (2012)

2. S. Korden: *Deriving the Rosenfeld Functional from the Virial Expansion*, Phys. Rev. E, **85**, 041150, (2012)

3. S. Korden, *Density Functional Theory for Hard Particles in N Dimensions*, Commun. Math. Phys., **337**, 1369-1395, (2015)

4. M. Marechal, S. Korden, and K. Mecke, *Deriving fundamental measure theory from the virial series: Consistency with the zero-dimensional limit*, Phys. Rev. E, **90**, 042131, (2014)

5. S. Korden, *Distribution Functionals for Hard Particles in N Dimensions*, (2015), arXiv:1502.04393, submitted to Commun. Math. Phys.

6. S. Korden, *Lattice-Fluid Models derived from Density Functional Theory*, (2015), arXiv:1503.02327, submitted to Mol. Phys.

The outgoing problem of the current thesis was the development of fast and universal methods to derive the phase structure of homogeneous fluids from the structure of their molecular compounds. The first approach we followed tried to reduce the overall number of parameters of an equation of state by correlating its values to the data of single molecules calculated by quantum mechanical methods. Article (1) shows this for the example of dipole and quadrupole moments. But the relationship proved to be too irregular to be of practical use. The different types of interactions result in cross-correlations in the fitted parameters, which cannot be decoupled and assigned to individual potentials. A true understanding of the relation between interaction potentials and the phase diagram therefore requires the determination of the density functional of the grand canonical potential itself, which became the topic of the current thesis.

A common approach to construct the grand canonical potential for molecular systems is the perturbative coupling of soft interactions to the correlation functionals of hard particles. But for

a long time a suitable approach for their derivation was not known. It was therefore an important step when Rosenfeld introduced the "fundamental measure theory" for spheres. In Article (2), we analyze this semi-heuristic approach and identify several contradictions in its underlying assumptions. Instead of using Rosenfeld's intuitive approach, we then show that the same functional can be derived from the virial expansion for particles overlapping in a common intersection center, calculating the intersection probability for an infinite set of overlapping particles under translations and rotations, generalizing previous results from Blaschke, Santalo, and Chern.

However, although this result explains the mathematical structure of the Rosenfeld functional, it still fails to extend its applicability to more complex particles than spheres. This problem is solved in Article (3). Starting from an observation of Matthieu Marechal that the intersection pattern of particles is related to Ree-Hoover diagrams, we classify all virial integrals belonging to a given type of intersection networks. Generalizing our previous results from Article (2) to N dimensional particles, we have a now an efficient set of mathematical methods at hand to derive the free-energy functional for a given class of intersection networks.

In a parallel approach, we also followed a set-theoretic ansatz in Article (4) to derive the Rosenfeld functional, confirming our previous results.

But the derivation of the hard-particle direct correlation functionals is not sufficient for the perturbative construction of a molecular DFT. For this it is still necessary to construct the n-particle distribution functionals to couple the soft-interaction potentials to the free energy. This is done in Article (5), using the previous techniques of diagrammatic resummation and integral geometry. With this result, we have all the necessary hard-particle correlation functionals at hand for the construction of a molecular density functional.

The structure of the grand canonical potential is not a unique, but allows different representations related by symmetry transformations. For the pair-potential it is shown in Article (6) that only two possible representations exist. The better known example is the direct correlation functional and its perturbative expansion for weak interactions. But here we argue that for the strong molecular interactions the dual grand potential is to be preferred because of its unique minimum with respect to the pair-correlation functional and its analytical simplicity at first perturbation order. Both properties are demonstrated by comparing the functional to lattice excess free-energy models, completing the cycle to develope the framework and mathematical tools to improve and extend existing models based on DFT.

Chapter 2

Introduction

The investigation of the gas, liquid, and crystalline phases of molecular matter is one of the oldest topics in the history of natural science. And, with a delay of several decades of solid-state dominated physics, it is nowadays at the center of an interdisciplinary revolution triggered by molecular biology and its increasing understanding of inner-cellular processes. The development of new experimental techniques, e.g. X-ray and neutron scattering, NMR, force field, and laser scanning microscopy, to investigate the microscopic properties of fluids and the dynamics of individual molecules is among the major achievements of the last decades and intensified the development of mathematical methods for the prediction of their properties [81, 71].

Most of the chemical and biological processes take place in the liquid state. It is therefore the by far most important phase, whose high particle density and low spacial correlations allow for large collision rates between particles of sufficiently high energies for chemical reactions to take place. A first insight into this microcosmos can be gained from its characteristic values of energies, bonding lengths, and particle distances. As shown in Table 2.1, the ionic and covalent bond energies are considerably larger than the average kinetic energy at 300 K, whereas the translational and rotational oscillations can be assumed to be almost uncorrelated to other interactions. The liquid state is therefore dominated by dispersion forces, electrostatic, and hydrogen-bond interactions, whose potential energies are approximately of the same order as the Boltzmann distributed thermal energy [4].

The other characteristic value for molecular systems is the average particle distance. The covalent bonds and interparticle distances between molecules in the liquid and solid phase are approx-

	energy [eV]		density [mol/m^3]	distance [nm]
ionic bond	8 - 10	gas	0.025	> 4
covalent bond	3 - 9	liquid	30 - 100	0.15 - 0.2
hydrogen bond	0.1 - 0.3	solid	150 - 200	0.15 - 0.2
vibrations	0.1			
vdW bond	0.02 - 0.04	vdW radius		0.12 - 0.18
rotations	0.0001	cov. bond		0.1 - 0.15
300 k_BT	0.026	de Broglie		< 0.1

Table 2.1: Characteristic energies, interparticle distances, bond lengths, and the de Broglie thermal wavelength for organic molecules at 300 K and 1 bar (data taken from [4]).

imately of the same order as the de Broglie wavelength and thus dominated by quantum effects. But due to the rapid exponential decline of the quantum correlations between electrons of different molecules, they are largely suppressed, which justifies the introduction of classical molecular potentials. The only notable exception is the hydrogen atom, whose large thermal wavelength indicates that effects of discrete energies and tunneling can occur for strong interactions, resulting in the hydrogen bonding between polar molecules [4, 57].

Quantum effects arise, e.g., when the attractive potential exceeds critical values in depth and interaction width, leading to the association of molecules [49]. If the lifetime of such a cluster is sufficiently small this is in no contradiction with classical statistical mechanics. But the formation of temporarily long-lived associates is incompatible with the ergodicity assumption of the Boltzmann distribution for classical interactions. Instead of a configurational ensemble, such processes can only be described by an average over time [2]. In the following, we will exclude such systems and assume that the time-scales of associated and dissociated states are sufficiently separated to be considered as thermodynamically individual states.

The description of molecular interactions by effective potentials applies to the most relevant parts of the phase diagram, including the equilibrium states of gases, liquids, and the various crystalline states, but also the metastable non-equilibrium states of granular matter and glasses. In the thermodynamic equilibrium, each phase domain in the diagram is adjacent to at least one other state, with the maximum number of $n+2$ neighboring phases determined by Gibbs' rule for a system of n compounds and separated by a $f = n+2-r$ dimensional boundary for r neighboring states. Any domain is therefore locally represented by a function of $n+3$ variables, depending on temperature T, entropy S, volume V, pressure P, densities ρ_i, and the chemical potentials μ_i for a mixture of $i = 1,\ldots,n$ compounds [50].

Following Ehrenfest's Theorem, each transition in the phase diagram is related to a change in the symmetries of the free-energy functional [71]. This is easily seen for a crystalline state of density $\rho(\vec{r})$ with lattice structure Λ and periodic coordinates $\vec{r} \in \mathbb{R}^3/\Lambda$ or the gas $\rho(\vec{r}) = \text{const.}$ as the state of highest symmetry. The corresponding change of symmetry in the liquid state, on the other hand, is less obviously related to a reduced radial translation invariance. To illustrate this effect, consider two particles with radial-symmetric potential $U(r)$, reduced mass m, and angular momentum L, whose energy $E = m\dot{r}^2/2 + L^2/(2mr^2) + U(r)$ is a function of the translational part $m\dot{r}^2/2$ and the effective potential $U_{\text{eff}}(r) = U(r) + L^2/(2mr^2)$. The relative motion of the two particles is then characterized by the minimum of $U_{\text{eff}}(r)$ as a function of L. The particles are bonded if the minimum is negative and unbonded when positive, with a critical value $U'_{\text{eff}}(L_c) = 0$, where the extremum degenerates to zero. A similar picture applies to the statistical average $\langle U_{\text{eff}} \rangle$ if the system is dominated by pair correlations. Below a critical value of $L_c^2 \sim T_c$, the particles condense into a state of classically bonded particles and move unrestrained for $T \geq T_c$, where $\langle U_{\text{eff}} \rangle$ is zero or strictly repulsive. The effective potential of a fluid near the critical point is therefore similar to the potential surface the ϕ^4-theory with its second order phase transition [99].

The different approaches to derive the phase diagram from molecular potentials can be classified into three groups. The most general method is the molecular dynamic (MD) simulation [2]. The thermodynamic variables are determined as time-averages over particle ensembles derived by solving Newton's equation of motion. This approach applies to equilibrium and non-equilibrium situations alike, and also represents molecules with flexible bond lengths and angles, thus including transitions between conformers and the classical kinetic energies of vibrations and rotations. The second group covers the Markov-Chain Monte Carlo (MC) simulations which uses stochastic ensembles to average over configurational variables [2, 48]. With the kinetic energy decoupled, it

is the preferred simulation technique for equilibrium thermodynamics. The third group is based on density functional theory (DFT) [57, 19]. It determines the thermodynamic equilibrium by minimizing the grand canonical potential with respect to the density $\rho_i(\vec{r})$. But in contrast to the MD/MC techniques, its sampling function is not known in general and far-reaching approximations are often necessary to derive its form. This reduces its accuracy to derive thermodynamic information, but on the other hand also offers a more varied set of approximations that can be used to reduce the considerable numerical efforts accompanied by MD/MC calculations.

Apart from these three groups, there exists two further representations to derive parts of the phase diagram: equations of state (EoS) and lattice models of the excess free-energy [66, 5]. Examples of EoS are the van der Waals model, the statistical associated fluid theories (SAFT) [13, 14, 57], and the Landau free-energy function for liquid crystals [50], each depending on parameters that characterize the change of symmetry related to the phase transition. In contrast to DFT, an EoS parametrizes the minimum of the grand canonical potential for a single realization of the local density. But for most interactions the topology of this hypersurface of the free energy is too complex to be globally representable by a simple function, why any practical realization is restricted to the description of a small domain of the phase diagram. This limitation also extends to the prediction of the properties of mixtures from the parameters of their pure compounds. To describe the related changes in the interparticle correlations, it is thus necessary to define ad hoc mixing rules and mixture coefficients. These parameters are strictly model dependent and contain no further physical information. But their comparatively small number are easily fitted to experimental data sets, why EoS are often used to parametrize the gas-liquid domain of homogeneous fluids [65].

Closely related to DFT are the lattice-fluid models of the excess free-energy. Based on the physically incorrect assumption of a lattice structure as background with tightly packed particles without free volume, the lattice cells form a hard-particle reference fluid with an additional interaction between its cell surfaces [5, 39]. Its phase diagram is thus restricted to a fixed reference value of density and pressure for an artificial state of the liquid phase. This simple ansatz has been implemented by Abrams and Prausnitz in the universal quasichemical model (UNIQUAC), extended by Prausnitz and Maurer by including functional group-activity coefficients (UNIFAC), and the conductor like screening model for real solvents (COSMO-RS) developed by Klamt [56, 1, 22, 65, 39, 38, 40]. These three examples start from the same density functional of the grand-canonical potential but use different strategies for its minimization and different interaction models. Together with the group contribution ansatz, the UNIFAC and COSMO-RS models have both been successfully applied to predict the mixture diagrams of liquids under the given set of assumptions.

These five methods for determining the liquid phase diagram illustrate the dilemma of soft-matter physics. Either one uses the simple but limited methods of EoS and lattice models, or the computationally expensive but universal ansatz of MD/MC. The aim of the current thesis is to find a compromise in the framework of DFT that is numerically manageable but still applies to the full range of the phase diagram. For this purpose we will use the lattice models as a guideline and derive the technical framework to develope further continuum functionals for molecular potentials approximated by a hard-particle core and soft interactions.

In Chapter 3, we begin with a detailed analysis of the representation of the grand-canonical potential. Widely constrained by the Hohenberg, Kohn, Mermin theorem [57], only two realizations exist for pair interactions. One representation is based on the direct correlation functional from which, e.g., the van der Waals and SAFT equations of state descent. The second representa-

tion follows from its Legendre transformation in the pair potentials [7, 59, 60, 61]. Together with the quasichemical approximation, this is the functional from which the lattice excess functionals originate, differing by their various strategies to minimize the grand potential [47]. The Wilson ansatz is used in the UNIQUAC and UNIFAC models, which is shown to yield a physically inconsistent solution of the Euler-Lagrange equation [97], whereas the COSMO-RS model applies the correct Larsen-Rasmussen approach [51]. Deriving both approaches, we show that the lattice variables miss important information about the geometry of the molecules and that long-ranged potentials not only change the free energy but also the self-consistent equation of its lattice models. Including the molecular geometry and the long-range interactions therefore prove problematic if not impossible in this framework and thus require the formulation of an unconstrained density functional, introducing the new problem of deriving the pair-correlation functionals for any intermolecular potential. A common and well tested strategy to reduce the complexity of this task is the approximation of the strongly repulsive part of the molecular interaction by a hard-particle potential and to expand the functional in a perturbative series in the residual soft interactions [57]. This approach reduces the construction of a molecular DFT to the non-perturbative derivation of the hard-particle correlations functionals.

In Chapter 4, we take a first step in this direction and derive an approximate direct correlation functional for hard particles. Using hard spheres as a reference geometry for molecules goes back to van der Waals and Boltzmann, with its mathematical structure first analyzed by Isihara and Kihara, who calculated the second virial integral for convex particles using the Minkowski sum of their domains [37, 36]. This result is the starting point of the scaled particle theory (SPT) developed by Reiss, Frisch, and Lebowitz for spherical particles [72], which has been generalized by Rosenfeld to the fundamental measure theory (FMT) [74, 75, 78] with an alternative representation developed by Rosinberg and Kierlik [35, 62]. Its ansatz is based on three assumptions: 1. the Fourier splitting of the second virial integrand into a convolute of 1-particle weight functions, 2. the scale invariance of the free energy, and 3. the SPT differential equation. However, these rules only determine two of the three terms of the Rosenfeld functional uniquely, while an approximation for the third term has been found only later by Tarzona, focusing on the consistency in the zero-dimensional limit [86, 85]. When compared to simulated data, the predicted phase diagram of the Rosenfeld functional proves to be highly accurate for spheres at packing fractions well below the crystallization point but shows significant deviations at higher packing fractions, for mixtures, and alternative geometries [83, 11, 18, 63]. One reason for this failure has been explained by Wertheim and, independently, by Rosenfeld and Tarazona, who observed the similarity between the second virial integral and the Gauss-Bonnet equation [92, 93, 94, 95, 77]. Using this relation as additional information, Mecke and Hansen-Goos extended the Rosenfeld functional to convex particles [25, 26, 27]. The resulting Rosenfeld-Tarazona functional describes the phase diagram of spheres even for the crystalline state but still shows systematic deviations for mixtures.

A complementary approach to improve the Rosenfeld functional has been taken by Roth et al. [80] and Hansen-Goos and Roth [28], using the Mansoori-Carnahan-Starling-Boublik equation of state to solve for the pressure in the SPT differential equation [53]. The resulting White-Bear II functional shows a significant improvement compared to the Percus-Yevick approximation of the Rosenfeld functional and provides the most reliable functional as of today. For a more detailed introduction to the development of FMT, we refer to the review [79].

However, despite its remarkable success, the construction of the functional leaves many questions unanswered. First of all, higher order virial integrals depend on more than one intersection center. As shown by Wertheim, the third virial integral for elongated convex particles is not

well represented by the 1-center approximation, which neglects important contributions of the 3-particle correlations [92, 93, 94, 95]. Also, the mathematical connection between the second virial integrand, the Gauss-Bonnet equation, and the calculation of Isihara and Kihara is unexplained. Here, we will give a more detailed analysis, demonstrating that most assumptions used in constructing the Rosenfeld functional only apply to spherical particles in odd dimensions. This can be seen for the Fourier decoupling of the second virial integrand, which maps the extrinsic curvature to its intrinsic form, but also for the Minkowski sum as well as its assumed relation to the Gauss-Bonnet equation. As we will show in Chapter 4, the solution of these and more apparent paradoxes is the Blaschke-Santalo-Chern equation of integral geometry [82, 9]. First proven by Chern for two intersecting n-dimensional domains [15, 16, 17], we generalize the theorem to an arbitrary set of particles, overlapping in at least a common point. Its derivation thus depends solely on the extrinsic representation of the imbedded particles and explains the deeper connection to the Gauss-Bonnet identity.

The intersection probability of particles with one intersection center is all that is necessary to derive the Rosenfeld functional from the virial expansion in Mayer diagrams. For higher order corrections, however, the identification and summation of Mayer graphs for a given type of intersection pattern is more complex. As pointed out by Matthieu Marechal, this problem can be reduced by transforming the virial expansion from Mayer to Ree-Hoover diagrams [67, 69], which defines a unique relationship between virial clusters and the intersection pattern of the particles. Classifying the graphs by their intersection patterns, we determine their symmetry factors and sum over all elements of its equivalence class to determine the generic functional for the direct correlations.

In Chapter 5, we extend these methods to derive the r-particle distribution functionals for hard particles from the virial expansion. Starting from the representation in rooted Ree-Hoover diagrams [68, 70], each intersection pattern defines an equivalence class of diagrams that determines a generic distribution functional. Focusing on the example of the pair-correlation functional, this route adds a third approach to its derivation in addition to solving the Bogoliubov-Born-Green-Kirkwood-Yvon integral equation or the Ornstein-Zernike equation in the Percus-Yevick approximation [87, 57]. For the 2-center approximation, we also determine an upper bound for the contact probability of spheres, which is in excellent agreement with the Carnahan-Starling parametrization as well as the Wertheim, Thiele, Baxter solution of the Ornstein-Zernike equation [90, 91, 88, 6]. We also compare the pole-structure of the n-particle correlation functions to its corresponding value predicted by Kirkwood's superposition ansatz, demonstrating that this approximation fails at short distances. Finally, we derive the perturbative expansion of the pair-correlation functionals for soft interactions, which completes our investigation of the molecular grand-canonical potential.

In Chapter 6, we summarize our results and give an outlook to further applications and implementations of molecular DFT.

Chapter 3

Density Functionals and Lattice Models

Before constructing a molecular density functional, one has to decide on its representation. In the following chapter, it will be shown that the Hohenberg-Kohn-Mermin theorem constrains their number for a given potential. For the pair interaction, e.g., only two representations are possible, the free-energy functional Ω^{F} and the dual functional Ω^{D}. In Sec. 3.1, we discuss their structure and respective perturbation expansions. By comparing the excess free energy of the dual functional to the UNIQUAC, UNIFAC lattice, and the COSMO-RS off-lattice models, it is shown in Sec. 3.2 that Ω^{D} is the most promising candidate. It is the only functional that allows the use of COSMO data for its interaction potential, and different levels of approximations can be used to interpolate between the continuum or off-lattice description and the lattice models, customizing the molecular functional to its specific applications.

3.1 The dual Free-Energy Functional

The Hohenberg, Kohn, Mermin theorem shows the unique mutual relationship between interaction and grand-canonical potential [57], forming the foundation of DFT, as it guarantees that different representations of the functional determine the same thermodynamic ground state. It thus constrains the number of alternative representations for a given interaction potential, which are related by similarity transformations. Ignoring mappings that correspond to internal symmetries of the potential or result in contributions which cancel in the Euler-Lagrange equations, the only nontrivial symmetry is the Legendre transformation of the grand potential Ω, exchanging its canonically conjugate variables. For the simplest and most relevant case of pair interactions, it replaces the potential ϕ_{ij} by its dual pair-correlation functional g_{ij}, defined by

$$\frac{\delta\Omega}{\delta\phi_{ij}} = \frac{1}{2}\rho_i\rho_j g_{ij} \,. \tag{3.1}$$

This shows that Ω for 2-particle potentials has only two representations, either as the free-energy functional $\Omega^{\mathrm{F}}(\phi_{ij})$ or its Legendre-dual counterpart $\Omega^{\mathrm{D}}(g_{ij})$.

Most molecular functionals use Ω^{F} as the starting point, as its perturbation expansion in r-particle densities $\rho_{i_1\ldots i_r}$ is algebraically well understood [57]. But it will be shown in the next section that the lattice models derive from the dual functional Ω^{D}, whose analytic form is more complex and the perturbation expansion of g_2 does not result in either the direct or the distribution functionals. For comparison, we will derive both representations, analyze their respective perturbation expansions, and discuss their advantages and limitations.

Beginning with the free-energy representation, the functional $\Omega^{\mathrm{F}}(\beta,\mu_i,\phi_i^{\mathrm{ex}}|\rho_i,\phi_{ij})$ of the particle density ρ_i depends on the inverse temperature $\beta=1/k_{\mathrm{B}}T$, chemical potential μ_i, and external potentials ϕ_i^{ex} for a mixture of $i=1,\dots,M$ compounds. It is an integral

$$\beta\Omega^{\mathrm{F}}=\sum_{i=1}^{M}\int\left[\rho_i(\ln(\rho_i\Lambda_i)-1)-\beta\rho_i(\mu_i-\phi_i^{\mathrm{ex}})\right]d\gamma_i-c_0(\rho_i) \tag{3.2}$$

over the positions and orientations $\gamma_i\in\mathbb{R}^n\times\mathrm{SO}(n)$ of the n-dimensional Euclidean space and depending on the thermal wavelength Λ_i and direct correlation functional $c_0(\rho_i)$.

Its perturbation expansion in the potential $\phi=\phi^{\mathrm{H}}+\phi^{\mathrm{S}}$ of hard-particle ϕ^{H} and soft interaction ϕ^{S} is a formal Taylor series of the logarithm of the grand canonical partition integral, whose first and second order in the Mayer functions f_2^{S} have the form

$$\begin{aligned}\beta\Omega^{\mathrm{F}}=\beta\Omega^{\mathrm{F}}_{\mathrm{H}}-\frac{1}{2}\int\rho^{\mathrm{H}}_{i_1i_2}f^{\mathrm{S}}_{i_1i_2}\,d\gamma_{i_1i_2}-\frac{1}{2}\int\rho^{\mathrm{H}}_{i_1i_2i_3}f^{\mathrm{S}}_{i_1i_2}f^{\mathrm{S}}_{i_2i_3}\,d\gamma_{i_1i_2i_3}\\-\frac{1}{8}\int(\rho^{\mathrm{H}}_{i_1i_2i_3i_4}-\rho^{\mathrm{H}}_{i_1i_2}\rho^{\mathrm{H}}_{i_3i_4})f^{\mathrm{S}}_{i_1i_2}f^{\mathrm{S}}_{i_3i_4}\,d\gamma_{i_1i_2i_3i_4}-\dots\,,\end{aligned} \tag{3.3}$$

where a sum over paired indices is implied [57]. Higher order terms are readily obtained using diagrammatic techniques [46], where each product $[f_2^{\mathrm{S}}]^m$ couples to a homogeneous polynomial of r-particle densities of order $2\le r\le 2m$, integrated over the $(m-1)n(n+1)/2$ coordinates of position and orientation. The rapid increase in the dimensionality of the integrals effectively limits the perturbative approach to the first or second order.

In deriving (3.3), we assumed the particles to interact by pair potentials. But the same approach also applies to irreducible m-particle interactions, with the fully f_2^{S}-bonded subdiagrams $[f_2^{\mathrm{S}}]^m$ replaced by the Mayer function f_m^{S}. For the 3-particle interaction $\phi_{i_1i_2i_3}$, e.g., this adds the leading correction

$$\beta\Omega^{\mathrm{F}}=\beta\Omega^{\mathrm{F}}(\phi_{ij})+\frac{1}{6}\int\rho^{\mathrm{H}}_{i_1i_2i_3}f^{\mathrm{S}}_{i_1i_2i_3}\,d\gamma_{i_1i_2i_3}+\dots \tag{3.4}$$

to the 2-particle functional $\Omega^{\mathrm{F}}(\phi_{ij})$.

The second representation is the dual functional Ω^{D}. First derived by Morita and Hiroike using diagrammatic techniques [59, 60, 61, 7], it replaces ϕ_{ij} by its canonically conjugate variable g_{ij}. To perform the Legendre transformation, we integrate (3.1) over $\delta\phi_{ij}$

$$\Omega=\Omega_{\mathrm{kin}}+\frac{1}{2}\int\rho_i\rho_jg_{ij}\phi_{ij}\,d\gamma_{ij}-\frac{1}{2}\int\rho_i\rho_j\phi_{ij}\delta g_{ij}\,d\gamma_{ij}\,. \tag{3.5}$$

To complete the integration over δg_{ij}, Morita and Hiroike derive the self-consistent closure relation between ϕ_{ij} and g_{ij} [61]:

$$\ln(g_{ij})=-\beta\phi_{ij}+d_{ij}+h_{ij}-c_{ij}\,, \tag{3.6}$$

introducing the bridge functional d_{ij} of 2-path connected clusters, the pair correlation $h_{ij}=g_{ij}-1$, and 2-particle direct correlation functionals c_{ij}. To eliminate the remaining dependence on the free-energy representation, c_{ij} is then replaced by the Ornstein-Zernike equation

$$c_{ij}-h_{ij}=-\int\rho_kh_{ik}c_{kj}\,d\gamma_k=\sum_{n=1}^{\infty}\int(-1)^n\rho_{k_1}\dots\rho_{k_n}h_{ik_1}\dots h_{k_nj}\,d\gamma_{k_1\dots k_n}\,. \tag{3.7}$$

Inserting this result into (3.5), they form the infinite sum over h-bonded ring integrals

$$\int \rho_i \rho_j (c_{ij} - h_{ij})\, \delta h_{ij}\, d\gamma_{ij} = \sum_{n=3}^{\infty} \int \frac{(-1)^n}{n} \rho_{k_1} \dots \rho_{k_n} h_{k_1 k_2} \dots h_{k_n k_1}\, d\gamma_{k_1 \dots k_n} \tag{3.8}$$

in the final representation of the dual grand-canonical potential [61, 7]:

$$\begin{aligned} \beta\Omega^{\mathrm{D}} \;=\; & \sum_i \int \rho_i \ln(\rho_i \Lambda_i) - \rho_i - \beta\mu_i \rho_i\, d\gamma_i + \frac{1}{2} \sum_{ij} \int \rho_i \rho_j \big(g_{ij} \ln(g_{ij}) - g_{ij} + 1 \big)\, d\gamma_{ij} \\ & + \frac{\beta}{2} \sum_{ij} \int \rho_i \rho_j\, g_{ij}\, \phi_{ij}\, d\gamma_{ij} + \frac{1}{2} \sum_{n=3}^{\infty} \int \frac{(-1)^n}{n} \rho_{k_1} \dots \rho_{k_n} h_{k_1 k_2} \dots h_{k_n k_1}\, d\gamma_{k_1 \dots k_n} \\ & - \frac{1}{2} \int \rho_i \rho_j d_{ij}\, \delta g_{ij}\, d\gamma_{ij} \,, \end{aligned} \tag{3.9}$$

where the integration constant $+1$ in the second integral has been chosen to reproduce the ideal gas in the limit $\phi_{ij} \to 0$.

Compared to the free energy representation (3.2), the analytic structure of the dual functional is considerably more complex, although containing exactly the same information for pairwise interacting particles. A common simplification is therefore to set $d_{ij} = 0$ and to use either the Percus-Yevick (PY) or the hypernetted chain approximation (HNC) for the closure relation (3.6)

$$\begin{aligned} \text{PY} \;:\quad & g_{ij} \exp(\beta\phi_{ij}) = \exp(d_{ij} + h_{ij} - c_{ij}) \approx 1 + h_{ij} - c_{ij} \\ \text{HNC}: \quad & \ln(g_{ij}) \;\approx -\beta\phi_{ij} + h_{ij} - c_{ij} \,. \end{aligned} \tag{3.10}$$

In combination with the Ornstein-Zernike equation [57], they provide easier to solve self-consistent integral equations for h_2 and c_2.

Probably the best known example is the PY approximation for hard spheres and its solution for g_2 developed by Wertheim, Thiele, and Baxter [90, 91, 88, 6]. Another example is the Coulomb potential $\phi = q^2/r$ for point-particles of charge $\pm q$. Its slow radial decline allows the long-range approximation $c_2 \approx -\beta\phi$, for which the HNC equation can be solved, using the Fourier transformation $\hat{c}_2 = F(c_2)$ to decouple the Ornstein-Zernike equation

$$\ln(g_2) = -\beta\phi + h_2 - c_2 \approx h_2 = F^{-1}\Big(\frac{\hat{c}_2}{1 - \rho\hat{c}_2} \Big) = -\beta \frac{q^2}{r} \exp(-k_D r) \,. \tag{3.11}$$

This result reproduces the characteristic Debye-Hückel screening for an ionic liquid of wavenumber $k_D = (4\pi\beta\rho q^2)^{1/2}$ and, together with the infinite sum over the ring integrals

$$\int \rho(\hat{c}_2 - \hat{h}_2)\delta\hat{h}_2\, d\hat{\gamma} = \rho\hat{h}_2 - \frac{1}{2}\rho^2\hat{h}_2^2 - \ln(1 + \rho\hat{h}_2) \,, \tag{3.12}$$

yields the Debye-Hückel functional for charged particles [57, 64].

The calculation illustrates how the combination of the Ornstein-Zernike and the closure equation (3.6) improves the low order approximation. Actually, it is an example of a duality transformation that inverts the length scales by exchanging a pair of canonically conjugate variables, mapping the perturbative sector of one functional to the non-perturbative of its dual. This shows that the two representations Ω^{F} and Ω^{D}, although equivalent in their total information, have different application ranges when the perturbation series are restricted to a finite order. In summary,

Ω^{D} depends only on one class of correlation functionals, allows a simple consistency test for its perturbative corrections, and applies for short- and long-range interactions alike. A disadvantage, however, is its limitation to pair interactions. But as higher-order irreducible m-particle potentials are often very short-ranged, they can be coupled perturbatively using the expansion (3.4). Thus, despite its complex structure, the dual functional is the preferred ansatz for the perturbative construction of a molecular model, which will be further supported in the next section, where we make contact with the lattice theories.

3.2 Lattice-Fluid Models derived from the Dual Functional

Lattice models for fluids use a discretized Euclidean space, with molecules represented by linear chains of cells. Instead of the configuration integral, one therefore calculates the partition integral of all allowed particle insertions [23, 66, 65, 5]. To simplify the derivation, two additional assumptions are made: 1. molecules are closely stacked, i.e. the packing fraction for all systems is $\eta = 1$, and 2. interactions only occur between next neighbors.

A mixture of $N = \sum_i N_i$ particles with $i = 1,\ldots,M$ compounds is therefore independent of volume effects, from which follows that the free-energy of mixing

$$F^{\mathrm{M}}(\{x_i\}) = F(\{x_i\}) - \sum_i x_i F_i(x_i = 1) \tag{3.13}$$

is a function only of the temperature and molar fractions $x_i = N_i/N$. This definition compares the overall free energy before and after the mixing process. For practical calculations, however, it is more convenient to consider the influence of the interaction potentials and to subtract the ideal combinatorial entropy contribution, resulting in the definition of the excess free-energy:

$$F^{\mathrm{E}}(\{x_i\}) = F^{\mathrm{M}}(\{x_i\}) - N/\beta \sum_i x_i \ln(x_i) \,. \tag{3.14}$$

To derive the lattice model from the functional Ω^{D}, we have to interpret its two assumptions in terms of the continuum formulation. The first constraint of close packing is readily implemented for a mixture of constant densities $\rho_i = N_i/V$ and their pure-compound systems $\hat{\rho}_i = N_i/V_i$ with partial volumes $V_i = x_i V$ and molecular volumes v_i:

$$1 = \eta = \sum_k \rho_k v_k = \hat{\rho}_i v_i = \hat{\eta}_i \,. \tag{3.15}$$

The second constraint reduces the correlation length of the pair-distribution function to its next neighbors. In a first step, we therefore neglect all g_2 in the functional (3.9) beyond the leading order $\mathscr{O}(g_{ij}^2)$

$$\beta F = \sum_i \int \rho_i \ln(\rho_i \Lambda_i) - \rho_i \, d\gamma_i + \frac{1}{2} \sum_{ij} \int \rho_i \rho_j \big(g_{ij} \ln(g_{ij}) - g_{ij} + 1 + \beta g_{ij} \phi_{ij} \big) \, d\gamma_{ij} \,, \tag{3.16}$$

thus removing the bridge and ring integrals responsible for the Debye-Hückel screening. Next, we restrict the spacial range of g_2 to the first particle shell Λ_{ij}, which comes closest to the idea of next-neighbor correlations between cell elements. Introducing the definitions

$$z_{ij} = \rho_j g_{ij}|_{\Lambda_{ij}} \,, \quad z_i = \sum_j \int_{\Lambda_{ij}} \rho_j g_{ij} \, d\gamma_j \,, \quad z = \frac{1}{2} \sum_{ij} \int_{\Lambda_{ij}} \rho_i \rho_j g_{ij} \, d\gamma_{ij} \,, \tag{3.17}$$

the pair distribution and correlation function can be rewritten

$$\begin{aligned} \rho_i\rho_j g_{ij}|_{\Lambda_{ij}} = \frac{z_{ij}}{z_j}\frac{\rho_j z_j}{z} z = \theta_{ij}\,\theta_j\, z\,, \quad g_{ij}|_{\Lambda_{ij}} = \frac{z_{ij}}{z_j}\frac{z_j}{\rho_i} = \frac{\theta_{ij}}{\theta_i}\frac{z_i z_j}{z} \\ z_i = \frac{\rho_i z_i}{z}\frac{z}{\rho_i} = \frac{\theta_i}{\phi_i}\frac{z}{\rho}\,, \quad \phi_i = \frac{\rho_i}{\hat\rho_i} = \frac{\eta_i}{\eta} \end{aligned} \tag{3.18}$$

in terms of the local coordination number θ_{ij}, surface fraction θ_i, and volume fraction ϕ_i of lattice theories. These variables are not independent, but related by the permutation symmetry $\rho_{ij} = \rho_{ji}$ and normalization

$$\theta_{ij}\theta_j = \theta_{ji}\theta_i\,, \qquad \sum_i \int_{\Lambda_{ij}} \theta_{ij}\, d\gamma_i = 1\,, \qquad \sum_i \int_{\Lambda_{ij}} \theta_i\, d\gamma_i = 1\,. \tag{3.19}$$

Using these identities, the continuum functional (3.16) can now be written in the basis of lattice variables.

Beginning with the potential energy

$$\frac{1}{2}\sum_{ij}\int_{V\times V} \rho_i\rho_j g_{ij}\phi_{ij}\, d\gamma_{ij} = \frac{1}{2}N\sum_{ij}\int_{\Lambda_{ij}} \rho_i\rho_j g_{ij}\phi_{ij}\, d\gamma_{ij} = \frac{1}{2}zN\sum_{ij}\theta_{ij}\,\theta_j\,\varepsilon_{ij}\,, \tag{3.20}$$

the integration over $V\times V$ separates into a sum over $N/2$ particle pairs of volume Λ_{ij}, while the potential ϕ_{ij} is approximated by the constant energy parameter ε_{ij} of neighboring cells. The same transformation also applies to the logarithmic term of (3.16)

$$\begin{aligned} \frac{1}{2}\sum_{ij}\int_{V\times V} \rho_i\rho_j g_{ij}\ln(g_{ij})\, d\gamma_{ij} &= \frac{1}{2}zN\sum_{ij}\theta_{ij}\theta_j \ln\Big(\frac{\theta_{ij}}{\theta_i}\frac{z_i z_j}{z}\Big) \\ &= \frac{1}{2}zN\sum_{ij}\theta_{ij}\,\theta_j \ln\Big(\frac{\theta_{ij}}{\theta_i}\Big) + zN\sum_i \theta_i \ln\Big(\frac{\theta_i}{\phi_i}\Big) + \frac{1}{2}zN\ln\Big(\frac{z}{\rho^2}\Big)\,, \end{aligned} \tag{3.21}$$

whose constant contribution cancels in the excess free energy (3.14). The same applies to the linear term

$$\frac{1}{2}\sum_{ij}\int_{V\times V} \rho_i\rho_j(g_{ij}-1)\, d\gamma_{ij} = \frac{1}{2}N(2z-N)\,. \tag{3.22}$$

Slightly more complicated is the transformation of the kinetic energy, as the integration over the configuration space Λ_{ij} effectively reduces the number of independently moving molecules. The excess kinetic energy of unpaired particles

$$\begin{aligned} \beta F^{\mathrm{E},1}_{\mathrm{kin}} &= \sum_i \int_V (\rho_i\ln(\rho_i\Lambda_i) - \rho_i)\, d\gamma_i - \sum_i \int_{V_i} (\hat\rho_i\ln(\hat\rho_i\Lambda_i) - \hat\rho_i)\, d\gamma_i \\ &= \sum_i N_i \ln\Big(\frac{\rho_i}{\hat\rho_i}\Big) = N\sum_i x_i\ln(\phi_i)\,, \end{aligned} \tag{3.23}$$

has to be corrected by the kinetic energy of clusters. To determine their contribution observe that the translational and rotational degrees of freedom of one particle is bound to the second particle of the cluster. We therefore have to subtract for each pair the kinetic energy of one particle. The

amount of energy bound by the density of $\rho_i z_i/2$ particle pairs is determined by the difference:

$$\begin{aligned}\frac{1}{2}\sum_i \int_V (\rho_i z_i \ln(\rho_i z_i \Lambda_i) - \rho_i z_i)\, d\gamma_i - \frac{1}{2}\sum_i \int_V z_i(\rho_i \ln(\rho_i \Lambda_i) - \rho_i)\, d\gamma_i \\ = \frac{1}{2}\sum_i \int_V \rho_i z_i \ln(z_i)\,.\end{aligned} \tag{3.24}$$

From this derives the excess kinetic energy stored by the clusters

$$\begin{aligned}\beta F^{\mathrm{E},2}_{\mathrm{kin}} &= \frac{1}{2}\sum_i \int_V \rho_i z_i \ln(z_i)\, d\gamma_i - \frac{1}{2}\sum_i \int_{V_i} \hat{\rho}_i \hat{z}_i \ln(\hat{z}_i)\, d\gamma_i \\ &= \frac{1}{2} zN \sum_i \theta_i \ln\left(\frac{\theta_i}{\phi_i}\frac{z}{\rho}\right) - \frac{1}{2} zN \ln\left(\frac{z}{\rho}\right) = \frac{1}{2} zN \sum_i \theta_i \ln\left(\frac{\theta_i}{\phi_i}\right).\end{aligned} \tag{3.25}$$

Subtracting this result from the excess kinetic energy of the free particles (3.23), yields the effective kinetic energy of the lattice fluid

$$\beta F^{\mathrm{E}}_{\mathrm{kin}} = \beta F^{\mathrm{E},1}_{\mathrm{kin}} - \beta F^{\mathrm{E},2}_{\mathrm{kin}} = N\sum_i x_i \ln(\phi_i) - \frac{1}{2} zN \sum_i \theta_i \ln\left(\frac{\theta_i}{\phi_i}\right). \tag{3.26}$$

Combining the previous results (3.20), (3.22), (3.21) with the identities $\hat{\theta}_{ii} = 1$, $\hat{\theta}_i = 1$ for the pure compounds and omitting constant contributions, we finally arrive at the excess free energy of the lattice liquid

$$\beta F^{\mathrm{E}}/N = \sum_i x_i \ln\left(\frac{\phi_i}{x_i}\right) + \frac{z}{2}\sum_i \theta_i \ln\left(\frac{\theta_i}{\phi_i}\right) + \frac{z}{2}\sum_{ij} \theta_{ij}\theta_j \Big[\ln\left(\frac{\theta_{ij}}{\theta_i}\right) + \beta(\varepsilon_{ij} - \varepsilon_{jj})\Big], \tag{3.27}$$

whose first two terms correspond to the Flory-Huggins and Staverman-Guggenheim energies [20, 21, 32, 23]. The corresponding grand canonical excess functional follows by adding the excess chemical potential of paired particles

$$\Omega^{\mathrm{E}}(\theta_{ij}) = F^{\mathrm{E}}(\theta_{ij}) - zN\sum_i \theta_i \mu_i\,. \tag{3.28}$$

Mixtures are now uniquely determined by the four sets of variables θ_{ij}, θ_i, ϕ_i, z, and the constraints (3.19). But only θ_{ij} is fixed by the Euler-Lagrange equations of Ω^{E}. The remaining variables still need to be determined from their definitions (3.17), (3.18), and the assumptions of the lattice model. The molecules, e.g., are flexible, linear chains of cells without self-intersection. Their specific shape is therefore undefined, but the volumes v_i and surfaces a_i are constant and the contact probability independent of positions and orientations $g^{\mathrm{H}}_{ij}|_{\Lambda_{ij}} \approx c$. This corresponds to a hard-particle pair-correlation function

$$g^{\mathrm{H}}_{ij}(t)|_{\Lambda_{ij}} = c e_{ij}(t)\delta(t) \tag{3.29}$$

of particles whose surfaces are separated by a distance $t = 0$.

To derive its coordination numbers (3.17), we use the representation derived in App. A for the integral measure $d\gamma_{ij}$ of two particles with principal curvatures $\kappa^{(i)}_\alpha$ at a distance $t = 0$ and rotation angle $0 \le \phi < 2\pi$. Expanding the determinant (A.10)

$$\begin{aligned}\det[\lambda^{(1)} + u^{-1}\lambda^{(2)}u] = \kappa^{(1)}_1\kappa^{(1)}_2 + \kappa^{(2)}_1\kappa^{(2)}_2 + \sin^2(\phi)(\kappa^{(1)}_1\kappa^{(2)}_1 + \kappa^{(1)}_2\kappa^{(2)}_2) \\ + \cos^2(\phi)(\kappa^{(1)}_1\kappa^{(2)}_2 + \kappa^{(2)}_1\kappa^{(1)}_2)\end{aligned} \tag{3.30}$$

and integrating (3.29) over all relative orientations of the two particles, yields the surface of the Weyl tube:

$$\int_{\Lambda_{ij}} g_{ij}^{\mathrm{H}} d\gamma_i \approx 8\pi^2 c \int e_{ij}^{\mathrm{H}}(t)\delta(t)\,dt\,d\sigma_i = 8\pi^2 c a_i \delta_{ij} \tag{3.31}$$

and the surface of their Minkowski sum:

$$\int_{\Lambda_{ij}} g_{ij}^{\mathrm{H}} d\gamma_{ij} \approx c \int \det[\lambda^{(1)} + u^{-1}\lambda^{(2)}u] d\phi\, d\sigma_i d\sigma_j = 8\pi^2 c(a_i + a_j + \frac{1}{4\pi}\bar{\kappa}^{(i)}\bar{\kappa}^{(j)}) \,. \tag{3.32}$$

This shows that the Minkowski surface is not simply the sum of its individual surfaces but corrected by the product of mean curvatures. Its counterpart in the lattice representation are cell segments adjoined at the edges of the molecule but not its surface segments. These cells, however, are ignored in the next-neighbor approximation, explaining why the lattice models cannot represent the specific geometry of a particle. Thus, omitting the non-additive part and introducing the packing fraction $\eta = \sum_i \rho_i v_i$, determines the remaining three groups of variables

$$\phi_i = \frac{x_i v_i}{\sum_k x_k v_k} \,, \qquad \theta_i = \frac{x_i a_i}{\sum_k x_k a_k} \,, \qquad z = z_0 \sum_k x_k a_k \tag{3.33}$$

as a function of the universal model parameter z_0.

The last, but subtle, step in determining the thermodynamic equilibrium is the minimization of the functional

$$\delta\Omega^{\mathrm{D}} = \frac{\delta\Omega^{\mathrm{D}}}{\delta\rho_k}\delta\rho_k + \frac{1}{2}\frac{\delta\Omega^{\mathrm{D}}}{\delta g_{ij}}\frac{\delta g_{ij}}{\delta\rho_k}\delta\rho_k = 0 \,. \tag{3.34}$$

The Euler-Lagrange equation of the first term defines the chemical potential, while the second reproduces the constraint (3.6) as a self-consistent equation. To compare this equation to its analogue in Ω^{E}, we apply the previous approximations by omitting terms of g_2 beyond the linear order $\ln(g_2) = -\beta\phi + d_2 + h_2 - c_2 \approx -\beta\phi$ and rewrite the correlation function in the basis of the lattice variables (3.18)

$$g_{ij}|_{\Lambda_{ij}} = \frac{\theta_{ij}}{\theta_i}\frac{z_i z_j}{z} \approx \exp(-\beta\phi_{ij})|_{\Lambda_{ij}} = \exp(-\beta\varepsilon_{ij}) \tag{3.35}$$

The corresponding minimization of Ω^{E} with respect to θ_{ij} and the constraints (3.19) yields the Euler-Lagrange equation for the lattice model [23]

$$\frac{\delta\Omega^{\mathrm{E}}}{\delta\theta_{ij}} = 0 \;: \qquad \frac{\theta_{ij}\theta_{ji}}{\theta_{ii}\theta_{jj}} = \exp(-\beta[2\varepsilon_{ij} - \varepsilon_{ii} - \varepsilon_{jj}]) \tag{3.36}$$

for which we introduce use the notations:

$$\tau_{ij}^2 := \exp(-\beta[2\varepsilon_{ij} - \varepsilon_{ii} - \varepsilon_{jj}]) \,, \quad t_{ij} := \exp(-\beta[\varepsilon_{ij} - \varepsilon_{jj}]) \,, \quad \tau_{ij}^2 = t_{ij}t_{ji} \,. \tag{3.37}$$

By inserting (3.35) into $g_{ij}g_{ji}/(g_{ii}g_{jj})$, it is easily seen that the minimum of the continuum functional and that of its lattice counterpart (3.36) agree, therefore proving that the first-shell approximation does not violate the thermodynamic consistency of the functional.

In the literature, two different approximate self-consistent solutions for (3.36) can be found. The first one, developed by Larsen and Rasmussen (LR) [51], uses the symmetry properties (3.19) to derive the square root

$$\Big(\frac{\theta_{ij}}{\theta_j}\Big)^2 = \frac{\theta_{ii}}{\theta_i}\frac{\theta_{jj}}{\theta_j}\tau_{ij}^2 \,, \quad b_i^2 := \frac{\theta_{ii}}{\theta_i} \quad \Rightarrow \quad \frac{1}{b_j} = \sum_i \tau_{ij}\,\theta_i b_i \,, \tag{3.38}$$

which can be numerically solved for b_i and back-inserted to obtain θ_{ij}. The alternative approach goes back to Wilson (W) [97] and uses the ad hoc separation

$$\frac{\theta_{ij}}{\theta_{jj}} = \frac{\theta_i}{\theta_j} t_{ij} \,, \quad \frac{\theta_{ji}}{\theta_{ii}} = \frac{\theta_j}{\theta_i} t_{ji} \qquad \Rightarrow \qquad \theta_{ij} = \frac{\theta_i t_{ij}}{\sum_k \theta_k t_{kj}} \,, \quad \theta_{ji} = \frac{\theta_j t_{ji}}{\sum_k \theta_k t_{ki}} \tag{3.39}$$

to obtain two independent solutions for (3.36) in terms of t_{ij}. This approach, however, is inconsistent, as can be seen from the missing permutation invariance of t_{ij} in its indices and by inserting (3.35) into g_{ij}/g_{jj}:

$$\frac{\theta_{ij}}{\theta_{jj}} = \frac{\theta_i}{\theta_j} \frac{z_j}{z_i} t_{ij} = \frac{\phi_i}{\phi_j} t_{ij} \,. \tag{3.40}$$

The Wilson ansatz is therefore only a formal solution, depending either on the volume or the surface fraction and at most applicable for molecules of similar spherical size $z_i \approx z_j$.

Inserting (3.38), (3.39) into the functional (3.27) and taking account of the two independent solutions of the Wilson model, yields the minimum of the excess free-energy with respect to θ_{ij}

$$\beta F^{\mathrm{E}}_{\mathrm{LR}}/N = \sum_i x_i \ln\left(\frac{\phi_i}{x_i}\right) + \frac{z}{2}\sum_i \theta_i \ln\left(\frac{\theta_i}{\phi_i}\right) + \frac{1}{2} z \sum_i \theta_i \ln\left[\frac{\theta_{ii}}{\theta_i}\right] \,, \tag{3.41}$$

$$\beta F^{\mathrm{E}}_{\mathrm{W}}/N = \sum_i x_i \ln\left(\frac{\phi_i}{x_i}\right) + \frac{z}{2}\sum_i \theta_i \ln\left(\frac{\theta_i}{\phi_i}\right) - z \sum_i \theta_i \ln\left[\sum_j \theta_j t_{ji}\right] \,, \tag{3.42}$$

where the second result corresponds to the UNIQUAC model introduced by Prausnitz, Abrams, and Maurer [56, 1].

The liquid-liquid equilibrium at a given reference point of density and pressure is now determined by the excess free-energy function and the parameters v_i, a_i, τ_{ij} and t_{ij} respectively. Their values can be adjusted to experimental values if a sufficiently large data set is known. This is especially convenient for the analytical solution of the Wilson ansatz (3.39), which partly explains the popularity of the UNIQUAC model. If, however, the data set is too small, one has to resort to further models to specify the geometry and intermolecular potentials. One such approach is the group-contribution approximation, which uses the observation that the chemical and physical properties of organic compounds are often dominated by their functional groups. Together with the lattice assumption of next-neighbor interactions, the potential ϕ_{ij} is replaced by a superposition of interactions $\phi_{\alpha\beta}$ of its $\alpha, \beta = 1, \ldots, N_G$ functional groups

$$\phi_{ij} = \sum_{\alpha\beta} n_i^\alpha n_j^\beta \, \phi_{\alpha\beta} \,, \tag{3.43}$$

related to an analogous transformation of the pair-correlation functionals

$$\frac{\delta\Omega}{\delta\phi_{ij}} = \sum_{\alpha\beta} \frac{\delta\Omega}{\delta\phi_{\alpha\beta}} n_\alpha^i n_\beta^j \;: \quad \rho_{ij} = \sum_{\alpha\beta} \rho_i \rho_j n_\alpha^i n_\beta^j g_{\alpha\beta} \,. \tag{3.44}$$

The functional groups are the lattice equivalent of the site-site interactions used for molecular fluids [57]. But in combination with the next-neighbor approach, they decouple and formally replace the molecules as individual particles in the potential part of the free energy. Writing its contribution in group indices, the transformation leaves the particle density ρ_i and the product of canonically conjugate variables $g_{ij}\phi_{ij} = g_{\alpha\beta}\phi_{\alpha\beta}$ invariant. Only the integral measure $d\gamma_{ij} =$

$n_i^\alpha n_j^\beta d\gamma_{\alpha\beta}$ is changed by the transition $d\sigma_i = |d\sigma_i/dq_\alpha| dq_\alpha$ from surface elements to surface groups or charges q_α. The transformation of the potential energy therefore remains formally invariant

$$\sum_{ij}\int \rho_i\rho_j g_{ij}\phi_{ij} d\gamma_{ij} = \sum_{ij}\sum_{\alpha\beta}\int \rho_i\rho_j g_{\alpha\beta}\phi_{\alpha\beta} n_i^\alpha n_j^\beta d\gamma_{\alpha\beta} = \sum_{\alpha\beta}\int \rho_\alpha\rho_\beta g_{\alpha\beta}\phi_{\alpha\beta} d\gamma_{\alpha\beta} \;, \tag{3.45}$$

if the particle density is redefined as the density of group elements

$$\rho_\alpha = \sum_i n_i^\alpha \rho_i \;. \tag{3.46}$$

Because the partial integration (3.5) commutes with the coordinate change (3.43), the same transformation applies to the complete functional. The excess free energy (3.27) and the models (3.41), (3.42) therefore remain formally invariant, using the substitution $x_i = n_i^\alpha x_\alpha$ for the molar fractions. This yields the lattice variables of the group-contribution models

$$\theta_\alpha = \frac{\sum_i x_i n_i^\alpha a_\alpha}{\sum_k x_k a_k} \;, \quad \theta_{\alpha\beta} \;, \quad \tau_{\alpha\beta} \;, \quad t_{\alpha\beta} \;, \tag{3.47}$$

of the group surface $a_\alpha = n_\alpha^i a_i$ and the group volume $v_\alpha = n_\alpha^i v_i$.

Writing the UNIQUAC equation in the basis of group contributions reproduces the UNIFAC model [22]. Its larger number of fitting parameters improves the accuracy of the UNIQUAC model and allows to interpolate between molecules of similar chemical classes. But its dependence on the Wilson ansatz, the low spacial resolution of the interaction potential, and the heuristic notion of functional groups limits its value as a guideline for further improvements.

An approach that avoids these complications is the COMOS-RS model [38, 39]. Instead of the functional groups it uses partial charges q_{i_α} localized at the segments a_{i_α} of the discretized surface of the molecule. Their values are derived by a quantum mechanical COSMO calculation, approximating the dielectric background of the liquid by the boundary condition of a conducting surface. Solving the Laplace equation and determining the surface charges of the molecule is then a problem simply solved by the method of mirror charges [43]. With the virtual electrical field $\vec{E}$ pointing into the volume of the conductor and thus being antiparallel to the surface vector $\hat{n}_{i_\alpha} \parallel -\vec{E}$ of the segments a_{i_α}, the energy of the electrical field as a function of surface charges σ_i and the potential ϕ_i

$$\begin{aligned} U_{\text{pot}} &= \frac{1}{8\pi}\int_V \vec{E}^2 d^3r = -\frac{1}{8\pi}\int_V \vec{E}\nabla\phi\, d^3r = -\frac{1}{8\pi}\int_V \nabla(\vec{E}\phi) d^3r = \frac{1}{8\pi}\sum_i \phi_i \oint_{\Sigma_i} \hat{n}\vec{E} d^2r \\ &= -\frac{1}{8\pi\varepsilon_0}\sum_i \phi_i\sigma_i \approx \sum_{i_\alpha j_\beta} \phi_{i_\alpha j_\beta} \end{aligned} \tag{3.48}$$

can be approximated by the sum over its discretized surface elements a_{i_α} and point charges q_{i_α}, separated by the distance $t_{i_\alpha j_\beta}$:

$$\phi_{i_\alpha j_\beta} = -\frac{1}{8\pi\varepsilon_0}\, q_{i_\alpha} q_{j_\beta} \frac{\hat{n}_{i_\alpha}\hat{n}_{j_\beta}}{t_{i_\alpha j_\beta}} \;. \tag{3.49}$$

Inserting this result into (3.37) and assuming an average distance $t_0 := t_{i_\alpha j_\beta}$ between all interacting surface segments, yields the interaction matrix of (3.38) for $\kappa := 1/(8\pi\varepsilon_0 t_0)$

$$\tau_{i_\alpha j_\beta} = \exp\left[-\frac{\beta}{2}\kappa(q_{i_\alpha}\hat{n}_{i_\alpha} - q_{j_\beta}\hat{n}_{j_\beta})^2\right] . \tag{3.50}$$

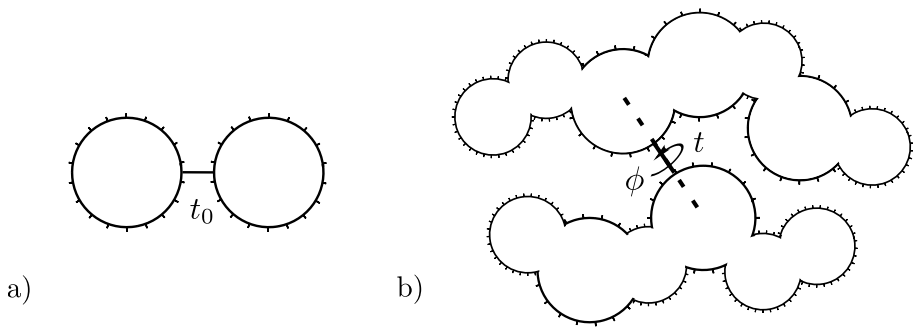

Figure 3.1: Comparing the interaction models of COSMO-RS and the molecular functional: a) The COSMO-RS model maps the surfaces of the molecules to unit spheres, with partial charges interacting over a fixed distance t_0. b) The molecular functional determines the pair-correlation functional, coupling the hard-particle geometry to the soft interaction of partial charges. The grand potential is the integral over all segment-segment combinations, distances t, and axial rotations ϕ.

However, solving the self-consistent equation is still a time-consuming task even for small molecules. Given a mixture of particles with S_i surface segments, the rank of the matrix is $S_1 + \ldots + S_M$, which for binary mixtures is typically of order $\sim 10^3 - 10^4$. To shorten the calculation time, the COSMO-RS model introduces group variables to coarse grain the number of charges $q_\alpha = n^i_\alpha q_{i_\alpha}$ and segments $a_\alpha = n^i_\alpha a_{i_\alpha}$, simplifying the self-consistent equation [39]

$$\frac{1}{b_\beta} = \sum_\alpha \tau_{\alpha\beta}\theta_\alpha b_\alpha \,, \quad \tau_{\alpha\beta} = \exp\left[-\frac{\beta}{2}\kappa(q_\alpha + q_\beta)^2\right] , \tag{3.51}$$

for molecules separated by the average distance t_0 and oppositely positioned surface segments, patched into a common coordinate system by the constraint $\hat{n}_{i_\alpha} = -\hat{n}_{j_\beta}$. Together with the reference geometry of the unit sphere, this corresponds to the interaction model shown in Fig. 3.1a).

A special situation occurs when the local electrostatic binding energy between molecules exceeds a critical limit and the representation by classical mechanics is no longer valid, as in the case of hydrogen bonding (HB). It is known from quantum mechanics [49] that the continuous energy spectrum of a scattered wave function developes discrete eigenvalues, depending on the width and depth of the potential well. This picture can be used as a simplistic model for hydrogen bonding, represented by a particle of mass m inside a spherical well potential of $U(r < t_0) = -U_0 = \kappa_{\mathrm{HB}} q_\alpha q_\beta$ and zero everywhere else. From the continuity condition of the wave function at $r = t_0$ follows that a binding state only forms below $\bar{U}_0 = \hbar^2\pi^2/(8mt_0^2) =: -\kappa_{\mathrm{HB}} q^2_{\mathrm{HB}}$ with a corresponding energy value $\varepsilon = 0$. Lowering the potential depth U_0 by a small amount $|U_0/\bar{U}_0| \ll 0$ while keeping t_0 fixed, results in a corresponding change of the first discrete energy value, which to second order in $U_0/\bar{U}_0$ is $\varepsilon_{\alpha\beta} \approx -\kappa_{\mathrm{HB}}(q_\alpha q_\beta + q^2_{\mathrm{HB}})^2/q^2_{\mathrm{HB}}$ for $q_\alpha q_\beta < q^2_{\mathrm{HB}}$ and $\varepsilon_{\alpha\beta} = 0$ else. The effective potential of a hydrogen bond is of course neither symmetric nor discontinuous, and a more detailed investigation shows that an appropriate description is given by the linear order

$$\varepsilon_{\alpha\beta} = \kappa_{\mathrm{HB}}(T)\min\left(0, q_\alpha q_\beta + q^2_{\mathrm{HB}}\right) , \tag{3.52}$$

which reproduces the experimental data quite satisfyingly [41, 42].

Apart from the electrostatic interaction and hydrogen bonds, the COSMO-RS model also includes dispersion effects, but fails for the Coulomb interaction. This is to be expected, as the

next-neighbor ansatz requires the correlation length to be of the order of the first particle shell, whereas the correlation length of strong electrolytes is significantly longer. As a result, the ring integrals (3.8) can no longer be ignored. A first approximation is therefore to couple the Debye-Hückel (3.12) or Debye-Hückel-Pitzer terms to the grand potential and to derive the new closure identity from the Euler-Lagrange equation for g_2. For the previous example of the electrolyte of point charges $\pm q$, this yields the correction

$$\ln(g_2) = -\beta\phi - F^{-1}\Big(\frac{\rho\hat{h}_2^2}{1+\rho\hat{h}_2}\Big)\,. \tag{3.53}$$

This implicit equation in g_2 cannot be solved algebraically. But the pair correlation is still dominated by ϕ at particle contact $r = t_0$ and only modified by the Debye-Hückel contribution at distances $r_0 = 2\pi/k_D$. If therefore $r_0 \approx t_0$, the screening term is small and can be ignored. If, however, $r_0 \gg t_0$, the pair-correlation function $h_2(r_0)$ can be approximated by (3.11). This adds a background potential to ϕ, while preserving the additive structure required to derive the self-consistent equation of the lattice model (3.38).

Despite this generalization, lattice models remain limited by the fixed reference value of density and pressure and the neglect of the molecular geometry. Any improvement therefore requires the construction of the density functional. A natural link between both descriptions is the COSMO model. The cavity and partial charges provide the relevant information to define the hard-particle geometry and soft interaction, necessary to derive the approximate pair-correlation functional $g_{ij}(\sigma_i,\sigma_j,t_{ij},\phi)$, shown in Fig. 3.1b). It is a function of the surfaces σ_i, σ_j, separated by the distance t_{ij}, and rotated by the axial angle ϕ. It also introduces correlations between several surface segments, thus dismissing the free-segment approximation. This increases the calculation time, but this is a necessary step to generalize the density functional approach to the important problems of biology and chemistry, which are rooted in the detailed spacial structure of the molecules.

Chapter 4

The Direct Correlation Functionals for Hard Particles

The perturbation expansion of the grand potential reduces the problem of determining the functional for the wide range of molecular interactions to the more manageable problem of calculating the hard-particle functionals. In the current chapter, we develope the mathematical methods that are necessary for their derivation. Beginning in Sec. 4.1 with an introduction to the semi-heuristic Rosenfeld functional [74, 76, 86], we show that the underlying idea of its construction is a resummation of intersection networks formed by the particles. In the picture of Ree-Hoover diagrams [68] this corresponds to elements of an equivalence class, whose resummation yields a convolute of integral kernels for each intersection center. The explicit form of this kernel is derived in Sec. 4.2, generalizing the Blaschke-Santalo-Chern equation in App. B. Finally, we derive the free-energy functional in Sec. 4.3 in the approximations for up to four intersection centers.

4.1 The Virial Expansion

The decoupling of the Mayer function of hard particles into a convolute of 1-particle weight function dictates the further structure of the FMT functional which is independent of geometry and dimensions. This is discussed in Sec. 4.1.1 and motivates a change from particle to intersection coordinates. In Sec. 4.1.2 it is shown that this transformation requires a similar change of the virial expansion from Mayer to Ree-Hoover diagrams.

4.1.1 FMT as an expansion in intersection centers

Let us consider a set of $i = 1,\ldots,N$ particles Σ_i imbedded into the finite subset V of the flat, Euclidean space $D_i : \Sigma_i \hookrightarrow V \subset \mathbb{R}^n$. In the thermodynamic limit $N,V \to \infty$, the particle density $\rho = N/V$ is kept constant, while the free energy $F(N,V,T)$ at temperature T becomes the function $F(\rho,T)$. For more than one type of particle, the free energy generalizes correspondingly to $F(\{\rho_k\},T)$ for a mixture of $k = 1,\ldots,M$ compounds.

Following Hohenberg, Kohn, and Mermin, the thermodynamic equilibrium is defined as the minimum of the positive definite grand-canonical free energy $\Omega([\{\mu_k\}],T)$, a functional of the chemical potentials μ_k and the temperature T

$$\Omega([\{\mu_k\}],T) \geq \Omega([\{\mu_k^{(0)}\}],T) \geq -PV \;, \tag{4.1}$$

where $\mu_k^{(0)}$ indicates the chemical potential at thermodynamic equilibrium [57]. Taking into account possible external potentials $\phi_k(\vec{r})$ at $\vec{r} \in \mathbb{R}^n$, the grand-canonical potential is related to the free-energy functional by the Legendre transformation in the local 1-particle densities $\rho_k(\vec{r})$:

$$\Omega([\{\rho_k\}],T) = F([\{\rho_k\}],T) + \sum_{k=1}^{M} \int \rho_k(\vec{r})(\phi_k(\vec{r}) - \mu_k)\, d\gamma\,, \tag{4.2}$$

where we introduced the abbreviation

$$\begin{aligned} \gamma(D) &:= \{\gamma = (\vec{r},\vec{\omega}) \mid \vec{r} \in D, \vec{\omega} \in \mathrm{SO}(n)\} \\ d\gamma_i &= d^n r_i\, d^{\frac{1}{2}n(n-1)}\omega_i \end{aligned} \tag{4.3}$$

for the differential volume element of the Euclidean or isometric group $\mathrm{ISO}(n) = \mathbb{R}^n \ltimes \mathrm{SO}(n)$.

However, the fundamental problem of the DFT approach is that, although the Hohenberg-Kohn theorem assures an almost unique relationship between interaction potential and free energy, it provides no hint for its derivation. It was therefore surprising, when the Rosenfeld functional could be derived from the virial expansion alone [44].

Substituting the Boltzmann function e_{ij} by Mayer's f-function $f_{ij} = e_{ij} - 1$ in the configuration integral and expanding the product in a series of cluster integrals yields the virial representation of the free energy:

$$\begin{aligned} F = F_{\mathrm{id}} + F_{\mathrm{ex}} = k_{\mathrm{B}}T \sum_{k=1}^{M} \int \rho_k(\vec{r})(\ln(\rho_k(\vec{r})\Lambda_k^n) - 1)\, d\gamma \\ + k_{\mathrm{B}}TV \sum_{n=2}^{\infty} \sum_{k_1,\ldots,k_n=1}^{M} \int \frac{1}{n} B_n(\Gamma_n)\, \rho_{k_1}(\vec{r}_1) \ldots \rho_{k_n}(\vec{r}_n)\, d\gamma_1 \ldots d\gamma_n\,, \end{aligned} \tag{4.4}$$

with the "thermal wavelength" Λ_k of the kinetic part F_{id}. The excess energy F_{ex} is an infinite sum over virial integrals, depending on particle densities and sums over products of f-functions $B_n(\Gamma_n)$, with the Mayer clusters (also called diagrams or graphs) Γ_n representing an unordered sum over all labeled, 2-connected star-diagrams $\Gamma_{n,k}$ with $n \geq 2$ nodes and counting index k:

$$\Gamma_n = \sum_k \Gamma_{n,k} \quad \text{for} \quad B_n(\Gamma_{n,k}) := \prod_{i,j \in \Gamma_{n,k}} f_{ij}\,. \tag{4.5}$$

The number of graphs is a rapidly increasing function of n, whose asymptotic dependence for unlabeled diagrams has been estimated by Riddell and Uhlenbeck to be $2^{n(n-1)/2}/n!$ [89, 73]. This diverging number of cluster integrals and the difficulties of their evaluation are the principal reasons why the virial approach is mostly limited to the gaseous state.

In order to go beyond the low-density limit, several alternative approaches have been developed. An early attempt has been taken by Reiss, Frisch, and Lebowitz, resulting in the development of the scaled particle theory for hard spheres [72]. This approach is based on a heuristic but non-perturbative relation between the low- and high-density limit of the free energy and an analytic solution of the second virial integral [33, 37, 36]. Later on, this ansatz has been extended to convex particles based on results from Ishihara and Kihara, who derived B_2 in terms of Minkowski measures [58] and developed further by Rosenfeld into a local formulation in weight functions, suitable for density functionals [76]. However, the equivalence between the volume form of the Minkowski sum of domains and their respective intersection probability is strictly restricted to

convex surfaces and limited to two particles. This approach therefore does not generalize to higher order virial clusters.

Starting from the f-function of hard particles, which is a negative step-function vanishing for non-intersecting domains D_i, D_j:

$$f_{ij} = \begin{cases} -1 & \text{if} \quad D_i \cap D_j \neq 0 \\ 0 & \text{else} , \end{cases} \tag{4.6}$$

Rosenfeld observed that its Fourier transformed integrand factorizes into 1-particle contributions. Transforming back, the Mayer function can be written as the sum over a convolute of distribution and tensor valued 1-particle weight functions:

$$f_{ij}(\vec{r}_i - \vec{r}_j) = -\int C^{A_i A_j} w^i_{A_i}(\vec{r}_i - \vec{r}_a) w^j_{A_j}(\vec{r}_j - \vec{r}_a)\, d\gamma_a , \tag{4.7}$$

with the constant and symmetric coefficient matrix $C^{A_i A_j}$ depending on the dimension of the imbedding space but otherwise independent of the particles' geometry. The transformation introduces the intersection coordinate $\vec{r}_a \in D_i \cap D_j$ as a new variable relative to the particle positions and orientations $\vec{r}_i \in D_i$. Here and in the following, we will omit the orientational dependence for the sake of clarity.

Rosenfeld's weight functions w^i_A are the local counterparts to the Minkowski measures of integral geometry [82, 84]. In 3 dimensions they depend on the normal vector $\vec{\hat{n}}$, Gaussian curvature κ_G, mean curvature $\bar{\kappa}$, curvature difference Δ, surface σ, and the volume v:

$$\begin{aligned} w_G(\vec{r}_i - \vec{r}_a) &= \frac{1}{4\pi}\kappa_G \delta(\vec{\hat{n}}\vec{r}_a) , \quad w_{\kappa L}(\vec{r}_i - \vec{r}_a) = \frac{1}{4\pi}\bar{\kappa}\vec{\hat{n}}^{\otimes L}\delta(\vec{\hat{n}}\vec{r}_a) , \\ w_{\Delta L}(\vec{r}_i - \vec{r}_a) &= \frac{1}{4\pi}\Delta\vec{\hat{n}}^{\otimes L}\delta(\vec{\hat{n}}\vec{r}_a) , \quad w_{\sigma L}(\vec{r}_i - \vec{r}_a) = \vec{\hat{n}}^{\otimes L}\delta(\vec{\hat{n}}\vec{r}_a) , \\ & w_v(\vec{r}_i - \vec{r}_a) = \Theta(\vec{\hat{n}}\vec{r}_a) , \end{aligned} \tag{4.8}$$

where the L-fold tensor product of the normal vector $\vec{\hat{n}}^{\otimes L}$ follows from a Taylor expansion of trigonometric functions, while the theta- and delta-functions restrict the integration to the particle volume, respective surface, as introduced in the appendix of [44].

Because the splitting (4.7) had originally been derived for spherical particles, its general dependence on Δ and the infinite set of tensor-valued weight functions had been obtained only later by Wertheim [92, 93, 94] and, independently by Mecke et al. [25], using the connection between (4.7) and the Gauss-Bonnet identity [77]. Wertheim also introduced the notion of n-point density functions [92, 93]:

$$n_{A_1 \ldots A_n}(\vec{r}_{a_1}, \ldots, \vec{r}_{a_n}) = \sum_{i=1}^{M} \int w^i_{A_1}(\vec{r}_i - \vec{r}_{a_1}) \ldots w^i_{A_n}(\vec{r}_i - \vec{r}_{a_n})\, \rho_i(\vec{r}_i)\, d\gamma_i \tag{4.9}$$

in which any Mayer integral can be rewritten. Given the example of the third virial integral

$$\begin{aligned} B_3 &= \frac{1}{6}\int f_{12} f_{23} f_{31}\, \rho_1 \rho_2 \rho_3\, d\gamma_1 d\gamma_2 d\gamma_3 \\ &= -\frac{1}{6} C^{A_1 A_2} C^{B_2 B_3} C^{C_3 C_1} \int n_{A_1 C_1} n_{A_2 B_2} n_{B_3 C_3}\, d\gamma_a d\gamma_b d\gamma_c , \end{aligned} \tag{4.10}$$

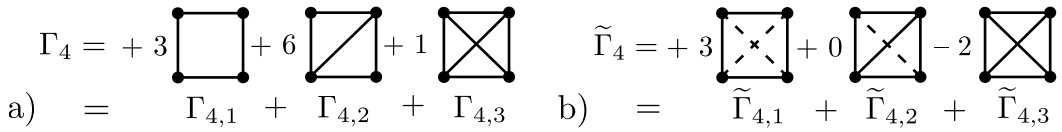

Figure 4.1: The fourth virial diagrams in Mayer Γ_4 and Ree-Hoover $\widetilde{\Gamma}_4$ representation: a) The slow convergence of the virial expansion is partly explained by identical intersection patterns in Mayer diagrams of equal order. b) Ree-Hoover diagrams resolve this problem. With the additional Boltzmann functions, the allowed intersection of particles are constrained. Additionally, the symmetry factors of many diagrams vanish, thus reducing the overall number of integrals entering the virial expansion.

Mayer clusters transform from a representation in particle positions and orientations to a corresponding representation in intersection coordinates $\gamma_i \to \gamma_a$.

Thus, instead of a virial expansion in increasing powers of 1-particle densities (4.4), the expansion in n-point densities suggests an ordering by their number of intersection centers [44]:

$$F_{\rm ex} = k_B T V \sum_{n=1}^{\infty} \int \Phi_n(\vec{r}_{a_1},\ldots,\vec{r}_{a_n})\, d\gamma_{a_1}\ldots d\gamma_{a_n}\,, \tag{4.11}$$

whose leading order in 3 dimensions has the generic form:

$$\Phi_1(\vec{r}_a) = -n_G \ln(1-n_v) + C_{\alpha_1\alpha_2}\frac{n_{\alpha_1}n_{\alpha_2}}{1-n_v} + C_{\alpha_1\alpha_2\alpha_3}\frac{n_{\alpha_1}n_{\alpha_2}n_{\alpha_3}}{(1-n_v)^2}\,, \tag{4.12}$$

where the volume dependence has been separated from the remaining densities $\alpha \in \{\kappa L, \Delta L, \sigma L\}$ and of which the Rosenfeld functional provides a first approximation [86]:

$$\begin{aligned}\Phi_1^{(R)}(\vec{r}_a) = -n_G \ln(1-n_v) &+ \frac{n_{\kappa 0}n_{\sigma 0} - n_{\kappa 1}n_{\sigma 1}}{1-n_v} \\ &+ \frac{1}{24\pi}\frac{n_{\sigma 0}^3 - 3n_{\sigma 0}n_{\sigma 1}^2 + \frac{9}{2}(n_{\sigma 1}n_{\sigma 2}n_{\sigma 1} - n_{\sigma 2}^3)}{(1-n_v)^2}\,.\end{aligned} \tag{4.13}$$

The first two parts of this polynomial in the free-volume $1-n_v$ are uniquely determined by the splitting of the second virial integral (4.7) and the scaled particle theory. The form of the third part, however, is only constrained by the scaling degree of the free-energy density. Several versions have therefore been proposed and tested, comparing its structure to analytical results and computer data [79]. Its exact form and higher order corrections will be determined in Sec. 4.3, making use of the central results summarized in Theorem 1 and Theorem 2.

4.1.2 Resummation of Ree-Hoover Diagrams

The expansion of the free-energy functional in intersection centers (4.11) is not well represented by Mayer diagrams. As can be seen from Fig. 4.1a), any intersection network of the ring diagram $\Gamma_{4,1}$ is also found in $\Gamma_{4,2}$ and $\Gamma_{4,3}$, thus contributing to Φ_1, Φ_3, and Φ_4. This redundancy, which can be found for any diagram of identical number of nodes, explains an observation made by Ree and Hoover in their numerical investigations of Mayer integrals for spheres [67, 69, 68]. Ordering the n-particle virial integrals by their signs into positive and negative contributions $B_n = B_n^+ - B_n^-$, their individual parts are of comparable size $B_n^+ \simeq B_n^-$, but much larger than B_n itself, often by two

orders of magnitude [67]. Thus, in order to reduce the number of redundant intersection patterns, they inserted the identity $1 = e_{ij} - f_{ij}$ for any pair of nodes i, j not bonded by an f-function. The resulting Ree-Hoover (RH) diagrams are completely connected graphs of f- and e-bonds, as shown in Fig. 4.1b). The type of allowed intersections is therefore constrained and comes close to the graphical interpretation of FMT functionals as intersection networks. In the following, we will show that this representation not only significantly simplifies our previous derivation, but also allows the systematic generalization of the approximate free-energy functional to higher orders.

The previous analysis of the Rosenfeld functional started from the observation that its dependence on a single intersection center can only be related to diagrams which allow the particles to intersect in a common point. While this involves all Mayer clusters, it selects the subclass of RH-graphs without e-bonds. It therefore establishes a one-to-one relation between its elements of the virial series and the exclusively f-bonded RH-clusters, with their integration domains restricted to a single intersection center. This relation can now be used as a guideline for the construction of higher order functionals, summarized in four steps: 1. choose an intersection network and find the corresponding class of RH-diagrams, 2. determine their symmetry factors and 3. intersection probabilities, and 4. sum over all elements of the class. In the remaining part of the current section, we will focus on the first two subtopics, saving the last two items to Sec.4.2.

For the two classes of Mayer and RH-diagrams we introduce the following conventions:

Definition 1. *Let $\Gamma_{n,k}$ denote a labeled, 2-path connected Mayer diagram (star-graph) of n nodes (also denoted as vertex or point) and $|\Gamma_{n,k}|$ f-bonds. The Mayer graph $\Gamma_{n,k} \subseteq \Gamma_{n,k'}$ is called a subgraph of $\Gamma_{n,k'}$ if it agrees with $\Gamma_{n,k}$ after removal of a finite number of f-bonds.*

A node can be removed by deleting its vertex with all its bonds $\pi^{-1} : \Gamma_{n,k} \to \{\Gamma_{n-1,k'}, \Gamma^A_{n-1,t}\}$, resulting in a residual diagram which is either a new star-graph $\Gamma_{n-1,k'}$ or a linear chain with articulation points $\Gamma^A_{n-1,t}$.

Definition 2. *Let $\widetilde{\Gamma}_{n,k}$ be a RH-diagram with n nodes and $|\widetilde{\Gamma}_{n,k}|$ f-bonds.*

A node, which is only linked by f-bonds, can be removed from a diagram by deleting its vertex and all its bonds, leaving either a new or the trivial RH-graph $\pi^{-1} : \widetilde{\Gamma}_{n,k} \to \{\widetilde{\Gamma}_{n-1,k'}, 0\}$.

The RH-graph $\widetilde{\Gamma}_{n-m,k'} \subseteq \widetilde{\Gamma}_{n,k}$ is called a subgraph of $\widetilde{\Gamma}_{n,k}$ if it agrees with $\widetilde{\Gamma}_{n-m,k}$ after successive operation with $\pi^{-m} = (\pi^{-1})^m$.

Definition 3. *Mayer- and RH-graphs are subgraphs, $\Gamma_{n,k} \subseteq \widetilde{\Gamma}_{n,k'}$, $\widetilde{\Gamma}_{n,k} \subseteq \Gamma_{n,k'}$, if they agree after removing a finite number of f-bonds and deleting all e-bonds.*

Because the application of π^{-1} on a RH-graph maps to exactly one element, its inverse operation $\pi : \widetilde{\Gamma}_{n-1,k} \to \widetilde{\Gamma}_{n,k'}$ can be defined for $\widetilde{\Gamma}_{n-1,k} \neq 0$, which adds a further node to the graph, linked by f-bonds to all $n-1$ nodes. Thus, each RH-diagram is an element of exactly one class

$$\widetilde{\Lambda}_{n_0,k} = \bigcup_{m=0}^{\infty} \pi^m(\widetilde{\Gamma}_{n_0,k}) \,, \tag{4.14}$$

with the lowest subgraph $\widetilde{\Gamma}_{n_0,k'} \subseteq \widetilde{\Gamma}_{n,k}$ uniquely defined by $\pi^{-1}(\widetilde{\Gamma}_{n_0,k'}) = 0$. One example has already occurred in the discussion of the Rosenfeld functional. Starting from the single node diagram $\widetilde{\Gamma}_{1,1}$, each of the exclusively f-bonded diagrams is then an element of $\widetilde{\Lambda}_{1,1}$. An important property of a class of RH-diagrams is that their intersection networks can be chosen to coincide:

Lemma 1. *The intersection network of the class $\widetilde{\Lambda}_{n_0,k}$ is defined by its lowest subgraph.*

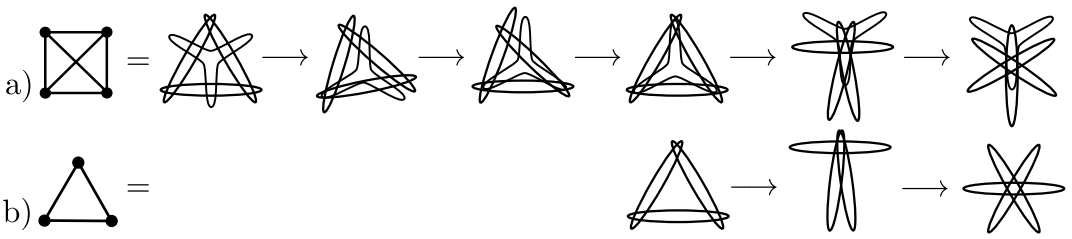

Figure 4.2: Two RH-diagrams and their corresponding representations as intersection networks. a) The particles of the fully f-bonded graph $\widetilde{\Gamma}_{4,3}$ generically intersect in six domains, which are successively contracted down to one. b) The graph $\widetilde{\Gamma}_{3,1}$ of the third virial cluster has three intersection centers, which also can be shifted together into one domain. In both examples, the intersection patterns with one and two centers determine identical intersection probabilities.

This is readily seen using a graphical argument. As can be seen from Fig. 4.1 and Fig. 4.2, for a given diagram $\widetilde{\Gamma}_{n,k}$ there are two types of nodes, those exclusively linked by f-bonds and those belonging to the lowest subdiagram, or "backbone", $\widetilde{\Gamma}_{n_0,k'}$. Choose a specific intersection network for this subgraph. Any further particle can then be attached to this network by overlapping it with all of the previous intersection centers, thus keeping the number of centers unchanged.

Focusing again on the Rosenfeld functional, the first element of the class $\widetilde{\Lambda}_{1,1}$ with a non-trivial intersection center is $\widetilde{\Gamma}_{2,1}$. Thus all RH-graphs with the second virial diagram as its subgraph can be reduced to an intersecting network whose particles overlap in exactly one center. However, one might also choose $\widetilde{\Gamma}_{3,1}$ as the leading element. Then the sum over all RH-integrals of the class $\widetilde{\Lambda}_{3,1}$, contracted to three intersection centers, yields Φ_3. Thus, once a lowest subgraph and its intersection pattern has been selected, its functional is uniquely fixed by its corresponding class. This solves the first of the previously stated four problems.

As the representation of the functional has been shifted from Mayer- to RH-diagrams, it is also necessary to rewrite the functional itself (4.4) in this new basis. This transformation has already been shown by Ree and Hoover to be a linear combination, weighted by the sign of the product of f-functions [68, 34]:

$$\widetilde{\Gamma}_{n,k} = \sum_{k'}^{\widetilde{\Gamma}_{n,k}\subseteq\Gamma_{n,k'}} \Gamma_{n,k'} \;, \quad \Gamma_{n,k} = \sum_{k'}^{\Gamma_{n,k}\subseteq\widetilde{\Gamma}_{n,k'}} (-1)^{|\Gamma_{n,k}|-|\widetilde{\Gamma}_{n,k'}|}\,\widetilde{\Gamma}_{n,k'} \;. \tag{4.15}$$

When inserted into the sum of Mayer clusters of n vertices (4.5), the summation order can be exchanged

$$\Gamma_n = \sum_{k'}\Gamma_{n,k'} = \sum_{k'}\sum_{k}^{\Gamma_{n,k'}\subseteq\widetilde{\Gamma}_{n,k}} (-1)^{|\Gamma_{n,k'}|-|\widetilde{\Gamma}_{n,k}|}\,\widetilde{\Gamma}_{n,k} = \sum_{k} a_{n,k}\,\widetilde{\Gamma}_{n,k} \;, \tag{4.16}$$

leading to the "star-content" of a RH-graph [68]:

$$a_{n,k} = \sum_{k'}^{\Gamma_{n,k'}\subseteq\widetilde{\Gamma}_{n,k}} (-1)^{|\Gamma_{n,k'}|-|\widetilde{\Gamma}_{n,k}|} \;. \tag{4.17}$$

An important property of the star-content, proven by Ree and Hoover, is its recursion relation under removal of an exclusively f-bonded vertex point [68]. When the operator π^{-1} from Def. 1 is applied to Γ_n, the sum separates into star-diagrams $\Gamma_{n-1,k'}$ and 1-path connected graphs with

articulation points $\Gamma^A_{n-1,t}$, each weighted by their sign of f-numbers in order to avoid overcounting of contributions:

$$\begin{aligned}\pi^{-1}(\Gamma_n) = \sum_k \sum_{k'}^{\Gamma_{n-1,k'}\subset\Gamma_{n,k}} (-1)^{|\Gamma_{n,k}|-|\Gamma_{n-1,k'}|}\,\Gamma_{n-1,k'} \\ + \sum_k \sum_{t}^{\Gamma^A_{n-1,t}\subset\Gamma_{n,k}} (-1)^{|\Gamma_{n,k}|-|\Gamma^A_{n-1,t}|}\,\Gamma^A_{n-1,t}\,.\end{aligned} \tag{4.18}$$

Focusing on the first part, the order of summation can be exchanged, resulting in a sum over those $\Gamma_{n,k}$-graphs, which lead to the same $\Gamma_{n-1,k'}$ diagram after the removal of a node. If this node is linked by m bonds, these bonds can be distributed in $(n-1)!/(m!(n-m)!)$ ways among the residual $n-1$ vertex points, each weighted by a sign-factor of $(-1)^m$. The first sum therefore simplifies to:

$$\begin{aligned}&\sum_{k'} \sum_{k}^{\Gamma_{n,k}\supset\Gamma_{n-1,k'}} (-1)^{|\Gamma_{n,k}|-|\Gamma_{n-1,k'}|}\,\Gamma_{n-1,k'} = \sum_{k'}\sum_{m=2}^{n-1}\binom{n-1}{m}(-1)^m\,\Gamma_{n-1,k'} \\ &= (n-2)\,\Gamma_{n-1}\,.\end{aligned} \tag{4.19}$$

The second part is a sum over $\Gamma_{n,k}$ and its 1-path connected subgraphs $\Gamma^A_{n-1,t}$. Again, the order of summation can be exchanged, resulting in a weighted sum over all permutations of $0 \le m \le n-1$ bonds linked to the residual $n-1$ nodes. In order to perform this sum, observe that a 1-path connected diagram is a linear chain of star-graphs, connected by articulation points, here indicated by $'*'$:

$$\Gamma^A_{n-1,t} = \Gamma_{n_1,k_1} * \Gamma_{n_2,k_2} * \ldots * \Gamma_{n_p,k_p}\,, \tag{4.20}$$

with $n-1 = n_1+n_2+\ldots+n_p$ nodes. Any partition of m bonds between the vertex P_n, which is to be removed from $\widetilde{\Gamma}_{n,k}$, and the non-articulation points can now be compensated by a copy of this same diagram with an additional bond between P_n and one of the articulation points. Having the same subgraph but differing by one f-bond, the two diagrams cancel each other in Eq. (4.18). The sum therefore decouples into the partition of bonds on non-articulation vertices and articulation ones. The flanking graphs Γ_{n_1,k_1}, Γ_{n_p,k_p} are each joined by one articulation point, while the center ones carry two. Their individual contributions to the weighted sum are therefore

$$\sum_{m=0}^{n_i-2}\binom{n_i-2}{m}(-1)^m = 0\,, \qquad \sum_{m=1}^{n_i-1}\binom{n_i-1}{m}(-1)^m = -1 \tag{4.21}$$

yielding an overall factor of $(-1)^2 = 1$ and leaving a sum over all permutations of bonds between the articulation points and P_n:

$$\sum_{t} \sum_{k}^{\Gamma_{n,k}\supset\Gamma_{n-1,t}} (-1)^{|\Gamma_{n,k}|-|\Gamma_{n-1,t}|}\,\Gamma_{n-1,t} = \sum_k\sum_{m=0}^{p-1}\binom{p-1}{m}(-1)^m\,\Gamma_{n-1,t} = 0\,. \tag{4.22}$$

Combining the two results (4.19), (4.22), the total sum of (4.18) reduces to the recursion relation of Ree and Hoover [68]:

$$\pi^{-1}(\Gamma_n) = (n-2)\,\Gamma_{n-1}\,. \tag{4.23}$$

An analogous relation can be derived for RH-diagrams, inserting the recursion relation into (4.16) and observing that π^{-1} removes $n-1$ f-bonds from a RH-diagram $\widetilde{\Gamma}_{n,k}$:

$$\begin{aligned}\pi^{-1}(\Gamma_n) &= \sum_k \pi^{-1}(a_{n,k}\widetilde{\Gamma}_{n,k}) = (-1)^{n-1}\sum_k a_{n,k}\widetilde{\Gamma}_{n-1,k} \\ &= (n-2)\,\Gamma_{n-1} = (n-2)\sum_{k'} a_{n-1,k'}\widetilde{\Gamma}_{n-1,k'}\ .\end{aligned} \tag{4.24}$$

Comparing terms, the resulting recursion relation is again independent of k:

$$a_{n,k} = (-1)^{n-1}(n-2)\,a_{n-1,k'} \tag{4.25}$$

and by repeated application yields the star-content [68]:

$$a_{n,k} = (-1)^{\binom{n}{2}-\binom{m}{2}}\frac{(n-2)!}{(m-2)!}\,a_{m,k'}\ . \tag{4.26}$$

Thus, once it has been calculated for the lowest diagram of a class $\widetilde{\Lambda}_{n_0,k}$, the coefficients for all further graphs are known.

So far, we have focused on labeled graphs, ignoring that the physical particles in the partition function are indistinguishable. Transferring to unlabeled RH-diagrams therefore introduces an additional sum over all inequivalent permutations of the labels on the vertex points. For its derivation the e-bonds can be ignored, as they do not change the graph's symmetry, yielding the "symmetry factor" $\sigma_{n,k}$ already known from Mayer clusters. In combination with the star-content, we define the combinatorial prefactor of the virial clusters in RH-graphs:

$$\widetilde{\sigma}_{n,k} = -\frac{1}{n!}\sigma_{n,k}\,a_{n,k}\ , \tag{4.27}$$

where the additional factor $1/n!$ has been inserted for later convenience. The last step in proving the resummability of cluster integrals for a given class $\widetilde{\Lambda}_{n_0,k}$ therefore requires the derivation of a recursion relation for $\sigma_{n,k}$.

The symmetry factor counts the number of inequivalent labelings of a RH- or Mayer graph $\Gamma_{n,k}$ under the permutation group S_n. Its group elements operate on the product of f-functions, which define a representation space by $\lambda : \Gamma_{n,k} \to \mathrm{prod}(f_{ij})$ and are symmetric under exchange of positions and indices:

$$\gamma := \{f_{ij} = f_{ji},\ f_{ij}f_{kl} = f_{kl}f_{ij}\}\ ,\ \ \gamma\lambda(\Gamma_{n,k}) = \lambda(\Gamma_{n,k})\ . \tag{4.28}$$

The group of equivalent labelings is then the automorphism group of its diagram and a subset of the symmetric group S_n

$$\mathrm{Aut}(\Gamma_{n,k}) = \{g \in S_n \mid g\lambda(\Gamma_{n,k}) = \gamma\lambda(\Gamma_{n,k})\} \tag{4.29}$$

subject to the invariance relation $\gamma^{-1}\circ g = \mathrm{id}$. Correspondingly, the set of inequivalent labelings is generated by the coset $S_n/\mathrm{Aut}(\Gamma_{n,k})$, whose number of elements is the symmetry factor of the graph

$$\sigma_{n,k} = \frac{|S_n|}{|\mathrm{Aut}(\Gamma_{n,k})|}\ . \tag{4.30}$$

An extensive list of Mayer diagrams and their automorphism groups has been tabulated by Uhlenbeck and Riddell [89, 73].

In general, determining the automorphism group of a given graph is non-trivial. However, if it is known for the lowest element of a class $\widetilde{\Lambda}_{n_0,k}$, the groups of all further diagrams are known:

Lemma 2. *Let $\widetilde{\Gamma}_{n,k} \in \widetilde{\Lambda}_{n_0,k}$ with lowest element $\widetilde{\Gamma}_{n_0,k}$. Its automorphism group then factorizes into the direct product:*

$$Aut(\widetilde{\Gamma}_{n,k}) = S_{n-n_0} \times Aut(\widetilde{\Gamma}_{n_0,k}) \,. \tag{4.31}$$

The proof is as follows: Because $\widetilde{\Gamma}_{n_0,k}$ is the lowest element of the class, $\pi^{-1}\widetilde{\Gamma}_{n_0,k} = 0$, each vertex is connected to at least one e-bond, whereas the remaining $n-n_0$ nodes are only linked by f-bonds. Shifting an f-bonded label to a vertex with an e-bond would therefore result in an inequivalently labeled diagram. Thus, f-bonded nodes can only be permuted under themselves by S_{n-n_0}, completing the proof.

With the recursion relation for the star content (4.26) and the dimension of the automorphism group

$$|\mathrm{Aut}(\widetilde{\Gamma}_{n,k})| = (n-n_0)!\,|\mathrm{Aut}(\widetilde{\Gamma}_{n_0,k})| \,, \tag{4.32}$$

the RH-diagrams of a given class have the symmetry factor:

Lemma 3. *Let $\widetilde{\Gamma}_{n,k}$ be an element of the class $\widetilde{\Lambda}_{n_0,k}$ of RH-graphs with lowest element $\widetilde{\Gamma}_{n_0,k}$. Its symmetry factor is then:*

$$\begin{aligned} \widetilde{\sigma}_{n,k} &= -(-1)^{\binom{n}{2}-\binom{n_0}{2}} \binom{n-2}{n_0-2} \frac{a_{n_0,k}}{|Aut(\widetilde{\Gamma}_{n_0,k})|} \quad : \quad n_0 \geq 3 \\ \widetilde{\sigma}_{n,k} &= \quad (-1)^{\binom{n}{2}} \frac{1}{n(n-1)} \quad : \quad n_0 = 1 \end{aligned} \tag{4.33}$$

The case $n_0 \geq 3$ follows from the previous calculations. But $n_0 = 1$ and $n_0 = 2$ have to be considered separately, because the recursion relation (4.26) only applies to $n_0 \geq 2$, while (4.31) requires $\widetilde{\Gamma}_{n_0,k}$ to be the lowest element of the class. Observing that $\widetilde{\Gamma}_{1,1} = \pi^{-1}(\widetilde{\Gamma}_{2,1})$ and $a_{2,1} = a_{1,1} = 1$ closes the proof.

It is instructive to derive the symmetry factors for the diagrams of Fig. 4.1. $\widetilde{\Gamma}_{4,3}$ is a fully f-bonded graph and therefore belongs to $\widetilde{\Lambda}_{1,1}$, already covered by (4.33). The next diagram $\widetilde{\Gamma}_{4,2}$ has star-content $a_{4,2}(|) = 0$. Thus, all graphs with a single e-bond drop out of the virial series $\widetilde{\sigma}_n(|) = 0$. Actually, the same applies to roughly half of the RH-diagrams, improving the convergence of the virial expansion. The final example $\widetilde{\Gamma}_{4,1}$ has two separate e-bonds, star-content $a_{4,1}(||) = 1$, and cyclic permutation symmetry $\mathrm{Aut}(\widetilde{\Gamma}_{4,1}) = \mathbb{Z}_4 \times \mathbb{Z}_2$. The prefactors of all related graphs are therefore

$$\widetilde{\sigma}_n(||) = (-1)^{\binom{n}{2}} \frac{1}{16}(n-2)(n-3) \,. \tag{4.34}$$

Eq. (4.33) solves the second of the four problems stated at the beginning of this section and also holds the solution to the fourth one. As has been shown before in 3 dimensions [44], the intersection probability of a network of overlapping particles decouples into a convolute of curvature forms $K_n(\vec{r}_a)$ for each intersection center with n particles. This observation is sufficient to write down a generic functional for a given intersection network and RH-class:

Theorem 1. *Let $\widetilde{\Gamma}_{n_0,k}$ be the lowest element of the class $\widetilde{\Lambda}_{n_0,k}$. The free-energy functional of a network with $p \geq 1$ intersection centers is then determined by*

$$\Phi_1(\widetilde{\Gamma}_{1,1}|\vec{r}_a) = \sum_{n\geq 2} \frac{1}{n(n-1)} \int K_n(\vec{r}_a, \{\gamma_i\}) \rho(\gamma_1) \ldots \rho(\gamma_n)\, d\gamma_1 \ldots d\gamma_n \tag{4.35}$$

for $n_0 = 1$, while higher order functionals for $n_0 > 3$ are derived by

$$\begin{aligned}\Phi_p(\widetilde{\Gamma}_{n_0,k}|\vec{r}_{a_1},\dots,\vec{r}_{a_p}) = -(-1)^{\binom{n_0}{2}} \frac{a_{n_0,k}}{|Aut(\widetilde{\Gamma}_{n_0,k})|} \sum_{n\geq n_0} \binom{n-2}{n_0-2} \\ \times \int K_{n_1}(\vec{r}_{a_1},\{\gamma_{i_1}\})\dots K_{n_p}(\vec{r}_{a_p},\{\gamma_{i_p}\})\rho(\gamma_1)\dots\rho(\gamma_n)\,d\gamma_1\dots d\gamma_n\end{aligned} \tag{4.36}$$

with the integral kernel $K_{n_j}(\vec{r}_a,\{\gamma_i\})$ determining the intersection probability of n_j particles which intersect in $\vec{r}_a$ and with particle positions γ_i for $i = 1,\dots,n_j$.

The first half of the proof determines the numerical prefactor, combining the symmetry factor of (4.33) and the sign of f-bonds $(-1)^{|\widetilde{\Gamma}_{n,k}|}$, which is not accounted for by the intersection forms. It partially cancels with the sign of $\widetilde{\sigma}_{n,k}$ using

$$|\widetilde{\Gamma}_{n,k}| = |\widetilde{\Gamma}_{n_0,k}| + \binom{n}{2} - \binom{n_0}{2}\,, \tag{4.37}$$

leaving a constant only depending on the lowest element of $\widetilde{\Lambda}_{n_0,k}$ and an n-dependent binomial coefficient. The second half of the proof deals with the factorization of the intersection probability into integral kernels, which will be the topic of the next section. There it will also be shown, how to generalize the functionals to e-bonds and mixtures of particles.

4.2 Intersection Probability in N Dimensions

In this section we complete the proof of Theorem 1, determining the intersection probability for networks of overlapping particles. First, the basic idea of integral geometry is summarized, determining the intersection probability of clusters of particles with one intersection center which is then generalized to networks of clusters.

Integral geometry determines the intersection probability between manifolds under translations and rotations with respect to their imbedding space. It has a long history [82, 84], but its modern representation has been founded by Blaschke and Santalo, and further generalized by Chern to n dimensions using differential forms [15, 16, 17]. Chern also explained the connection between the kinematic measure and the Euler form, determining the Blaschke-Santalo-Chern equation for two intersecting manifolds [15, 82]. Up to a sign, this result coincides with Rosenfeld's decoupling of the second virial integral (4.7). Using this approach, we calculated the intersection probability for an arbitrary set of particles overlapping in a common domain, rederiving the Rosenfeld functional for 3 dimensions. This calculation will be simplified in the following and extended to arbitrary dimension n.

For now, let Σ_k be a set of identical, $n-1$ dimensional, smooth, orientable, compact, boundary free, Riemannian manifolds with particle index $k = 1,\dots,N$, imbedded into $D_k : \Sigma_k \hookrightarrow \mathbb{R}^n$. For physical reasons we will further assume that the particles D_k only have cavities that are accessible to all other particles. Each domain is then covered by coordinate patches with an orthonormal, positively oriented coordinate frame $(\hat{e}_1^{(k)},\dots,\hat{e}_n^{(k)})$ at each point $p \in D_k$, with the normal vector $\hat{e}_n^{(k)}$ pointing into the outside direction of the surface $\Sigma_k = \partial D_k$. Being a differential manifold, the geometry of Σ and D is represented by vielbein and connection forms

$$\theta_i = \hat{e}_i dp\,, \quad \omega_{ij} = \hat{e}_i d\hat{e}_j \quad \text{for} \quad i,j = 1,\dots,n\,, \tag{4.38}$$

and the intrinsic forms of torsion and curvature

$$T_i = d\theta_i - \omega_{ij} \wedge \theta_j \,, \quad \Omega_{ij} = d\omega_{ij} - \omega_{ik} \wedge \omega_{kj} \,, \tag{4.39}$$

with the torsion $T_i = 0$ vanishing for a Riemannian manifold. Here and in the following we implicitly assume a sum over pairs of identical indices. Coordinate frames of different patches are connected by $g_{ij} \in \mathrm{SO}(n)$, transforming vectors $e'_i = g_{ij} e_j$ and differential forms

$$\theta'_i = g_{ij}\theta_j \,, \quad \omega'_{ij} = g^{-1}_{ik}\omega_{kl}g_{lj} + g^{-1}_{ik}dg_{kj} \,, \quad \Omega'_{ij} = g^{-1}_{ik}\Omega_{kl}g_{lj} \,. \tag{4.40}$$

Each Riemannian manifold also defines a semisimple group [29], which for the imbedding space $\mathbb{R}^n$ is the isometric or Euclidean group $\mathrm{ISO}(n) = \mathrm{SO}(n) \ltimes \mathbb{R}^n$. Its Lie algebra $\mathrm{iso}(n)$ has a representation in the vielbein and connection forms generating translations and rotations

$$\begin{pmatrix} \omega_{ij} & \theta_i \\ -\theta_j & 0 \end{pmatrix} \in \mathrm{iso}(n) \tag{4.41}$$

and whose volume form, or Haar measure, is the "kinematic measure"

$$K(\mathbb{R}^n) = \bigwedge_{1 \le i < j \le n} \omega_{ij} \bigwedge_{1 \le i \le n} \theta_i \,. \tag{4.42}$$

An alternative interpretation uses the representation as a chain of cosets

$$\mathrm{SO}(k)/\mathrm{SO}(k-1) = S^{k-1} \,, \quad \mathrm{vol}(S^{k-1}) = 2\pi^{k/2}/\Gamma(k/2) \,, \tag{4.43}$$

with the Gamma function Γ, which allows to rewrite products of connection forms into integral measures of spheres

$$dS^{k-1} = \omega_{1,k} \wedge \ldots \wedge \omega_{k-1,k} \,. \tag{4.44}$$

With a particle D imbedded, the vector space of $\mathbb{R}^n$ splits into the tangential $T\Sigma$ and normal space $N\Sigma$ along with a similar decoupling of the rotation group into $\mathrm{SO}(n-1)$ and the coset $\mathrm{SO}(n)/\mathrm{SO}(n-1)$. The kinematic measure (4.42) separates correspondingly into the three parts

$$K(\partial D) = \bigwedge_{\alpha=1}^{n-1} \omega_{\alpha n} \bigwedge_{i=1}^{n} \theta_i \wedge d\mathrm{vol}(\mathrm{SO}(n-1)) \tag{4.45}$$

of the curvature (also Euler or highest Chern-Simons) form, the measure of translations, and the volume form of $\mathrm{SO}(n-1)$.

This result readily generalizes to two and more overlapping domains which intersect in at least a common point. Introducing the notation for identical particles

$$\Sigma^{k_1} \cap D^{k_2} := \underbrace{\Sigma \cap \ldots \cap \Sigma}_{k_1\text{-fold}} \cap \underbrace{D \cap \ldots \cap D}_{k_2\text{-fold}} \,, \tag{4.46}$$

the intersection D^m is again a n dimensional subset of $\mathbb{R}^n$ and therefore applies to the reduced form of the kinematic measure (4.45). When inserted, $K(\partial D^m)$, the boundary of the intersection domain can be expanded in the series

$$\partial D^m = \sum_{1 \le k \le m}^{k \le n} \binom{m}{k} \Sigma^k \cap D^{m-k} \,, \tag{4.47}$$

setting all terms Σ^k for $k \ge n+1$ to zero. This restriction of the sum is a useful consequence of the following rules of K:

Lemma 4. *Let D be a domain in $\mathbb{R}^n$ with hypersurface Σ. The kinematic measure K of intersecting manifolds then has the properties:*

$$K(a_1\Sigma_1 + a_2\Sigma_2) = a_1K(\Sigma_1) + a_2K(\Sigma_2) \tag{4.48}$$

$$K(\Sigma^{k_1} \cap D^{k_2}) = K(\Sigma^{k_1}) \wedge K(D)^{k_2} \tag{4.49}$$

$$K(\Sigma_1 \cap \Sigma_2) = K(\Sigma_2 \cap \Sigma_1) \tag{4.50}$$

$$K(\Sigma^k) = 0 \quad \textit{for } k \geq n+1 \tag{4.51}$$

for $\Sigma_1 \cap \Sigma_2 = 0$ and the constants $a_1, a_2 \in \mathbb{N}$:

The proof: By construction, the differential form (4.42) is a locally defined probability measure, which decouples for $\Sigma_1 \cap \Sigma_2 = 0$, thus showing (4.48). The second identity follows from the observation that the kinematic measure of a point $\mathrm{pt} \in \mathbb{R}^n$ moving in the domain D is trivial $K(\mathrm{pt} \cap D) = K(D)$. Setting $\mathrm{pt} \in \Sigma^{k_1} \cap D^{k_2-1}$ then proves (4.49) by iteration. While the local measure and set theoretic relation $\Sigma_1 \cap \Sigma_2 = \Sigma_2 \cap \Sigma_1$ explains (4.50). The last equation (4.51), which justifies the finite sum (4.47), implies that the intersection probability between a point $\mathrm{pt} \in \Sigma^n$ and a hypersurface Σ is of measure zero. This follows from K being defined on the tangential space of Σ^k, spanned by the normal and tangential vectors $(\hat{e}_n^{(1)}, \ldots, \hat{e}_n^{(k)}, \hat{e}_1, \ldots, \hat{e}_{n-k})$, proving that the coordinate basis is not defined for $k \geq n+1$ and therefore vanishes for dimensional reasons.

Applying these rules to the boundary of intersections (4.47), yields the sum

$$K(\partial D^m) = \sum_{1 \leq k \leq m}^{k \leq n} \binom{m}{k} K(\Sigma^k) \wedge K(D)^{m-k} \,, \tag{4.52}$$

with $K(D)$ and the curvature forms $K(\Sigma^k)$ decoupled. For $m = 1$ this reproduces (4.45). But to derive the remaining differential forms we need an explicit representation of the orthonormal and positively oriented vector field at Σ^k. For simplicity, let us define a fixed ordering of surfaces $\Sigma_1 \cap \ldots \cap \Sigma_k$. The vector

$$(\hat{e}_n^{(1)}, \ldots, \hat{e}_n^{(k)}, \hat{e}_1, \ldots, \hat{e}_{n-k}) \in TD^k \tag{4.53}$$

of the tangential space TD^k then defines a coordinate frame at the intersection, spanned by the k outward pointing normal vectors and the $n-k$ tangential directions which can be chosen by (4.40) to coincide for all surfaces. This frame, however, is neither orthonormal nor positively orientated.

The Gram-Schmidt transformation turns this vector frame into an orthonormal basis

$$v_A = \begin{cases} B_{ab} e_n^{(b)} & \text{for } a, b = 1, \ldots, k \\ e_\alpha & \text{for } \alpha = 1, \ldots, n-k \end{cases} \tag{4.54}$$

whose upper triangular matrix $B_{ab} \in \mathrm{Gl}(k, \mathbb{R})$ combines into the general coordinate mapping:

$$B_{AB} = \begin{pmatrix} B_{ab} & 0 \\ 0 & 1_{\alpha\beta} \end{pmatrix} . \tag{4.55}$$

The coordinate frames of individual surfaces are now related by a rotation of the normal vectors

$$\eta_A = \begin{cases} G_{ab} v_b & \text{for } a, b = 1, \ldots, k \\ v_\alpha & \text{for } \alpha = 1, \ldots, n-k \end{cases} \tag{4.56}$$

generated by $G_{ab} \in \mathrm{SO}(k,\mathbb{R})$ and extended to the matrix representation

$$G_{AB} = \begin{pmatrix} G_{ab} & 0 \\ 0 & 1_{\alpha\beta} \end{pmatrix} . \tag{4.57}$$

Combining both transformations, the connection forms $\eta_{AB} = \eta_A d\eta_B$ at an intersection point can be written in the basis of the tangential $\omega_{\alpha\beta}$ and normal directions $\omega_{\beta n}^{(a)}$ of the coordinate frames of Σ_a keeping the normal vector $de_n^{(a)} = 0$ constant

$$\eta_{AB} = \begin{cases} \eta_{ab} = G_{ac}^{-1}\, dG_{cb} \\ \eta_{a\beta} = G_{ab}\, B_{bc}\, \omega_{\beta n}^{(c)} \\ \eta_{\alpha\beta} = \omega_{\alpha\beta} \end{cases} . \tag{4.58}$$

The curvature form, which generalizes (4.45) to the intersection space Σ^k, is the product of connection forms with one axial direction fixed. Let us choose η_k as the new normal vector, leaving G_{ak} to be an element of the coset space $\mathrm{SO}(k)/\mathrm{SO}(k-1) = S^{k-1}$

$$\begin{aligned} \bigwedge_{\beta=1}^{n-k} \eta_{\beta k} \bigwedge_{a=1}^{k-1} \eta_{ak} &= \Big(\bigwedge_{\beta=1}^{n-k} G_{ka} B_{ab}\, \omega_{\beta n}^{(b)}\Big)\Big(\bigwedge_{a=1}^{k-1} G_{ab}^{-1}\, dG_{bk}\Big) \\ &= \mathrm{Pf}_{1,\ldots,k}^{n-k}(GB\omega) \wedge d\mathrm{vol}_G(S^{k-1}) , \end{aligned} \tag{4.59}$$

introducing the notation $\mathrm{Pf}_{1,\ldots,k}^{n-k}$ for the Pfaffian of an $n-k$-form on the ordered set of surfaces $\Sigma_1 \cap \ldots \cap \Sigma_k$.

In the derivation of (4.59) we ignored the orientation of the coordinate frame of $T\Sigma^k$ which is not fixed by the Gram-Schmidt process. However, changing the orientation, e.g. by permuting the order of the particles in (4.54), changes the sign of (4.59) by $(-1)^{n-1}$. For n odd, this poses no problem. For n even, however, the orientation of the vector frame is relevant and has to be chosen positively orientated to ensure a positive surface form. This uniquely defines the intersection form K_m introduces in Theorem 1:

Theorem 2. *Let $D_{i_1} \cap \ldots \cap D_{i_m}$ be a set of n-dimensional domains overlapping in the common intersection point $\vec{r}_a \in D^m$ and assigned with a positively orientated coordinate frame. Denote by $|S^{k-1}|$ the volume of the S^{k-1} sphere and by $\Theta(D)$ the step function confining the integral measure to the volume of D. Then the integral kernel of the functionals (4.35) and (4.36) has the form:*

$$\begin{aligned} K_{i_1\ldots i_m}(\vec{r}_a, \{\gamma_i\}) = \frac{1}{|S^{n-1}|} \sum_{1\le k\le m}^{k\le n} \binom{m}{k} \int_{G\in S^{k-1}} & Pf(GB\omega)_{i_1\ldots i_k}^{n-k} \wedge dvol_G(S^{k-1}) \\ & \times \Theta(D_{i_{k+1}}) \ldots \Theta(D_{i_m}) , \end{aligned} \tag{4.60}$$

with an integration over the inner area of the Euler sphere S^{k-1}.

This result follows from inserting the curvature form (4.59) into the kinematic measure (4.52) and observing that the vectors $\vec{r}_a$ are already determined by the coordinates $\{\gamma_i\}$ of the 1-particle densities. The integration over γ_i therefore shifts part of the kinematic measure into the definition of the functionals (4.35) and (4.36) and leaves the integral kernel with the step functions $\Theta(D)$ and

the differential form $\mathrm{Pf}(GB\omega)^{n-k}$. Finally, the normalization $|S^{n-1}|$ has been added to compensate the volume form introduced by (4.59).

The curvature form (4.60) defines the integral kernel for one intersection center. To generalize this result to arbitrary networks of overlapping particles, let us introduce the following notation:

Definition 4. *Networks of intersecting particle domains are represented by products of $\gamma_a^{i_1\dots i_m}$ for each intersection center $\vec{r}_a \in D_{i_1} \cap \dots \cap D_{i_m}$ of the intersecting domains $D_{i_1}, \dots, D_{i_m}$.*

When applied to the third virial cluster, shown in Fig. 4.2b), the generic diagram $\Gamma_{3,1}$ is an intersection network of pairwise overlapping domains, which can be successively contracted from three centers into networks of two and one

$$\gamma_a^{i_1 i_2} \gamma_b^{j_2 i_3} \gamma_c^{j_1 i_3} \to \gamma_a^{i_1 i_2 i_3} \gamma_c^{j_1 i_3} \to \gamma_a^{i_1 i_2 i_3} \; . \tag{4.61}$$

While $\Gamma_{4,3}$ has the generic network of six centers, with consecutive contraction into five to one intersection domains, as shown in Fig. 4.2a)

$$\begin{aligned} \gamma_a^{i_1 i_2} \gamma_b^{j_2 i_3} \gamma_c^{j_3 i_1} \gamma_d^{j_1 i_4} \gamma_e^{j_2 i_4} \gamma_f^{j_3 i_4} &\to \gamma_a^{i_1 i_2 i_4} \gamma_b^{j_2 i_3} \gamma_c^{j_3 i_1} \gamma_e^{j_2 i_4} \gamma_f^{j_3 i_4} \to \gamma_a^{i_1 i_2 i_4} \gamma_b^{j_2 i_3 i_4} \gamma_c^{j_3 i_1} \gamma_f^{j_3 i_4} \\ &\to \gamma_a^{i_1 i_2 i_4} \gamma_b^{j_2 i_3 i_4} \gamma_c^{j_1 i_3 i_4} \to \gamma_a^{i_1 i_2 i_3 i_4} \gamma_c^{j_1 i_3 i_4} \to \gamma_a^{i_1 i_2 i_3 i_4} \; . \end{aligned} \tag{4.62}$$

This notation for intersection networks readily translates to the integral kernel:

Lemma 5. *Let γ_a^i and γ_b^j denote intersection clusters at centers $\vec{r}_a$ and $\vec{r}_b$ with particle indices $i = \{i_1, \dots, i_p\}$ and $j = \{j_1, \dots, j_q\}$. And let $e_{k_1 k_2}$ denote a Boltzmann function with arbitrary particle indices k_1, k_2. Introducing the notation $K(\gamma_a^{i_1 \dots i_m}) = K_{i_1 \dots i_m}(\vec{r}_a)$ for the intersection form K, the integral kernel for intersection networks is a linear and multiplicative operator*

$$K(\gamma_a^i + \gamma_b^j) = K_i(\vec{r}_a) + K_j(\vec{r}_b) \tag{4.63}$$

$$K(\gamma_a^i \gamma_b^j) = K_i(\vec{r}_a) K_j(\vec{r}_b) \tag{4.64}$$

$$K(\gamma_a^i e_{k_1 k_2}) = K_i(\vec{r}_a)\, e_{k_1 k_2} \; . \tag{4.65}$$

The first identity (4.63) is a generalization of (4.48), while the product structure (4.64) is a consequence of the properties of f-bonds, whose intersection centers overlap independently. Boltzmann functions, however, do not contribute to the curvature form, but define constraints on the integration domain, justifying (4.65).

Less trivial, however, is the meaning of the indices. In $\gamma_a^{i_1 \dots i_p}$, each index $i_k \in i$ points to an individual domain D_{i_k} of the $i_k = 1, \dots, N$ particles, while the same index in $K_{i_1 \dots i_p}$ points to the compound $i_k = 1, \dots, M$ represented by the 1-particle density ρ_{i_k}. This change of meaning is a consequence of the thermodynamic limit introduced in Sec. 4.1.1 and corresponds to the substitution

$$D_k \to \sum_{i_k=1}^{M} D_{i_k} \rho_{i_k} \; . \tag{4.66}$$

When inserted into the kinematic measure (4.52), the combinatorial prefactors remain unchanged, while the differential forms are weighted by the density functions. Thus each particle index has to be paired by a corresponding density function:

$$\sum_{i_1, i_2, i_3 = 1}^{M} K(\gamma_a^{i_1 i_2} \gamma_b^{j_2 i_3} \gamma_c^{j_3 i_1}) \rho_{i_1} \rho_{i_2} \rho_{i_3} \; . \tag{4.67}$$

The generalization to mixtures completes the proof of Theorem 1. And together with the integral kernel (4.60) and its algebraic structure, we have the necessary tools to systematically derive the density functional for any given class of intersection diagrams. However, to do so efficiently, let us introduce some further notation. First observe that for any k, the curvature form (4.59) can be written as a volume form

$$\begin{aligned} \mathrm{Pf}(GB\omega)^{n-k}_{i_1\dots i_k} &= \det(GBh)_{i_1\dots i_k} \bigwedge_{\alpha=1}^{n-k} \theta_\alpha \\ &= \int_{\mathbb{R}^n} [J \det(GBh)]_{i_1\dots i_k} \delta(\Sigma_{i_1}) \dots \delta(\Sigma_{i_k}) \bigwedge_{i=1}^{n} \theta_i \,, \end{aligned} \tag{4.68}$$

introducing the curvature matrix $\omega_{\alpha,n} = h_{\alpha\beta}\theta_\beta$ and the delta-function $\delta(\Sigma)$, which projects the integration domain from $\mathbb{R}^n$ to the tangential space of the surface Σ. Correspondingly, products of delta-functions project to the intersection space $\Sigma_{i_1} \cap \dots \cap \Sigma_{i_k}$ associated with the Jacobi determinant

$$J_{i_1\dots i_k} = \det(\hat{e}_1, \dots, \hat{e}_{n-k}, \hat{e}_n^{(i_1)}, \dots, \hat{e}_n^{(i_k)}) \,. \tag{4.69}$$

This transformation allows to factor out the overall volume form and to rewrite the integral kernel (4.60) as the derivative of a generating function:

Lemma 6. *Define the weight functions for $k = 1, \dots, n$ intersecting surfaces*

$$w_k^{i_1\dots i_k} = \frac{1}{|S^{n-1}|} \int_{G\in S^{k-1}} [J \det(GBh)]_{i_1\dots i_k} dvol_G(S^{k-1}) \delta(\Sigma_{i_1}) \dots \delta(\Sigma_{i_k}) \tag{4.70}$$

and the weight function for the domain

$$w_0^{i_1} = \Theta(D_{i_1}) \,. \tag{4.71}$$

The integral kernel (4.60) of the intersection form is then the functional derivative of the product of w_0-weights:

$$K(\gamma_a^{i_1\dots i_m}) = \mathscr{D}_a \, w_0^{i_1}(\vec{r}_{ai_1}) \dots w_0^{i_m}(\vec{r}_{ai_m}) \,, \tag{4.72}$$

with the derivative on the weight functions at intersection $\vec{r}_{ai} = \vec{r}_a - \vec{r}_i$ defined by

$$\mathscr{D}_a = \sum_{k=1}^{n} \sum_{i_1\dots i_k} \frac{1}{k!} w_k^{i_1\dots i_k}(\vec{r}_{ai_1}, \dots \vec{r}_{ai_k}) \frac{\delta^k}{\delta w_0^{i_1}(\vec{r}_{ai_1}) \dots \delta w_0^{i_k}(\vec{r}_{ai_k})} \,, \tag{4.73}$$

operating on two and more w_0-weight functions.

To simplify the notation for the functional derivative and its corresponding contraction

$$\frac{\delta}{\delta w_0^i(\vec{r}_{ai})} w_0^j(\vec{r}_{bj}) = \delta(\vec{r}_i - \vec{r}_j)\delta(\vec{r}_a - \vec{r}_b) \;, \quad \int w_0^j(\vec{r}_{ja}) \delta(\vec{r}_i - \vec{r}_j) \, d\gamma_j = w_0^i(\vec{r}_{ia}) \,, \tag{4.74}$$

we introduced the Kronecker delta-functional in the definition of (4.73), which transforms the operations

$$\frac{\delta}{\delta w_0^i(\vec{r}_{bi})} w_0^j(\vec{r}_{aj}) =: \delta_i^{\,j} \delta_a^b \;, \qquad \sum_j \delta_j^i w_0^j(\vec{r}_{aj}) = w_0^i(\vec{r}_{ai}) \,, \tag{4.75}$$

into a tensor-like representation. The proof of (4.72) then reduces to the derivation of a conventional polynomial, whose coefficients coincide with those of (4.60).

Less trivial, however, is the observation that the curvature form (4.68) and therefore the weight functions are symmetric in the particle indices. This is a consequence of the coupled coordinate system of $T\Sigma^k$, which can be diagonalized using the $\mathrm{SO}(n-k)\times\mathrm{SO}(k)$ invariance of its vector basis. Its explicit calculation gives no further insight and therefore is postponed to App. B, completing the proof of Theorem 2.

The derivative (4.73), which is a consequence of (4.47), simplifies the construction of a functional in two aspects: first, it hides the sum over the $k = 1,\dots,n$ differential forms in the intersection kernel (4.60). Second, it leaves the volume weight w_0^i as the only variable in the sums of (4.35), (4.36). Thus each functional is the derivative of a generating function in the virial series of w_0^i. In combination with Theorem 1, this reveals that:

Lemma 7. *The virial series of the free-energy functional for a finite number of intersection centers is convergent.*

The proof is as follows: It is sufficient to show that the generating function is a convergent series. If γ_0 is the intersection diagram of the lowest element $\widetilde{\Gamma}_{n_0,k}$ with p intersection centers. Then, the integral kernel of any higher order element $\pi^m\widetilde{\Gamma}_{n_0,k}$ decouples:

$$\int K(\pi^m\gamma_0)\rho^{n_0+m} = (x_{a_1\dots a_p})^m \int K(\gamma_0)\rho^{n_0}\ , \tag{4.76}$$

with the density function defined by

$$x_{a_1\dots a_p} = \int w_0^i(\vec{r}_{a_1 i})\dots w_0^i(\vec{r}_{a_p i})\rho_i d\gamma_i\ . \tag{4.77}$$

When inserted into the functionals (4.35), (4.36), the sum simplifies to a polynomial in x with singularities in $x = 1$ and $x = 0$. However, the virial series is finite in the low-density limit and therefore $x = 0$ a regular point. This leaves $x = 1$ as the only singularity. At thermodynamic equilibrium and with all intersection centers collapsed into a single point, the packing fraction approaches $\eta = 1$, proving that the functional is convergent for $\eta < 1$.

This final result proves the resummability of the approximate density functional and solves the last of the four problems presented at the beginning of Sec. 4.1.2.

4.3 The Rosenfeld Functional and Beyond

This last section presents four examples, which provide some insight into the construction of functionals. We begin with the integral kernel for 3 dimensions and derive the functional with one intersection center. It is then shown that Rosenfeld's result is an approximation for almost perpendicular normal vectors. The remaining examples then focus on the functionals with two, three, and four intersection centers.

Starting point for the construction of any functional is the derivation of the integral kernel. This has to be done once for any dimension and is independent of the particle geometry or boundary conditions. For $n = 3$ dimensions, only three differential forms exist:

The case $k=1$ is elementary. With $G=B=1$ and assuming a positively oriented orthonormal coordinate frame, the Pfaffian reduces to the Euler form $\mathrm{Pf}^2_{i_1}(GB\omega)=\omega_{13}^{(i_1)}\wedge\omega_{23}^{(i_1)}$ and a trivial integral over the S^0-sphere

$$\int \mathrm{Pf}^2_{i_1}(GB\omega)\wedge d\mathrm{vol}(S^0)=\omega_{13}^{(i_1)}\wedge\omega_{23}^{(i_1)}\,. \tag{4.78}$$

For $k=2$, the Gram-Schmidt scheme and $\mathrm{SO}(2)$ rotation have the matrix representation:

$$\begin{gathered} B=\begin{pmatrix} 1 & 0 & 0\\ -\dfrac{\cos(\phi_{i_1i_2})}{\sin(\phi_{i_1i_2})} & \dfrac{1}{\sin(\phi_{i_1i_2})} & 0\\ 0 & 0 & 1\end{pmatrix}\,,\quad G=\begin{pmatrix}\cos(\alpha) & \sin(\alpha) & 0\\ -\sin(\alpha) & \cos(\alpha) & 0\\ 0 & 0 & 1\end{pmatrix}\\ \phi_{i_1i_2}=\arccos(\hat{e}_3^{(i_1)}\hat{e}_3^{(i_2)})\quad,\qquad 0\le\alpha\le\phi_{i_1i_2}\le 2\pi\,, \end{gathered} \tag{4.79}$$

depending on the intersection angle $\phi_{i_1i_2}$. The associate Pfaffian yields the 1-form:

$$\mathrm{Pf}^1_{i_1i_2}(GB\omega)=\big[\cos(\alpha)-\frac{\cos(\phi_{i_1i_2})}{\sin(\phi_{i_1i_2})}\sin(\alpha)\big]\,\omega_{13}^{(i_1)}+\frac{1}{\sin(\phi_{i_1i_2})}\sin(\alpha)\,\omega_{13}^{(i_2)} \tag{4.80}$$

whose integral over $\alpha\in S^1$ simplifies to

$$\int_{\alpha\in S^1}\mathrm{Pf}^1_{i_1i_2}(GB\omega)\wedge d\mathrm{vol}_\alpha(S^1)=\frac{1-\cos(\phi_{i_1i_2})}{\sin(\phi_{i_1i_2})}\big[\omega_{13}^{(i_1)}+\omega_{13}^{(i_2)}\big]\,. \tag{4.81}$$

Finally, for $k=3$ the integral over the curvature form (4.59) reduces to the area of the spherical triangle $\Delta\subseteq S^2$

$$\int_{G\in S^2}\mathrm{Pf}^0_{i_1i_2i_3}(GB\omega)\wedge d\mathrm{vol}_G(S^2)=\mathrm{area}(\Delta\subseteq S^2)=2\pi-\phi^{i_1}_{i_2i_3}-\phi^{i_2}_{i_1i_3}-\phi^{i_3}_{i_1i_2} \tag{4.82}$$

whose value is determined by the Euler or dihedral angles $\phi^{i_3}_{i_1i_2}$ [31]:

$$\phi^{i_1}_{i_2i_3}=\arccos(\hat{E}_{i_2}\hat{E}_{i_3})\,,\qquad \hat{E}_{i_1}=\frac{\hat{e}_3^{(i_2)}\times\hat{e}_3^{(i_3)}}{|\hat{e}_3^{(i_2)}\times\hat{e}_3^{(i_3)}|}\,. \tag{4.83}$$

Comparing these results to the definition (4.70) and taking into account the permutation symmetry in the particle indices, we obtain the three weight functions:

$$\begin{gathered} w_1^{i_1}=\frac{1}{4\pi}\det(h^{(i_1)})\delta(\Sigma_{i_1}),\; w_2^{i_1i_2}=\frac{1}{2\pi}\frac{1-\cos(\phi_{i_1i_2})}{\sin(\phi_{i_1i_2})}[Jh_{12}]^{(i_1)}\delta(\Sigma_{i_1})\delta(\Sigma_{i_2})\\ w_3^{i_1i_2i_3}=\frac{1}{4\pi}(2\pi-3\phi^{i_1}_{i_2i_3})J_{i_1i_2i_3}\delta(\Sigma_{i_1})\delta(\Sigma_{i_2})\delta(\Sigma_{i_3})\,. \end{gathered} \tag{4.84}$$

These agree with the weight function $w_2^{i_1i_2}$ first derived by Wertheim [92, 93] and rediscovered in [25], while $w_3^{i_1i_2i_3}$ first occurred in [54].

Next, we will illustrate the application of the derivative and generating function on the functional restricted to one intersection center $\Phi|_1$. It is therefore of type (4.35), and the virial series sums up to the generating function in the x-variable (4.77) of the volume weight:

$$\begin{aligned}\Phi|_1(\widetilde{\Gamma}_{1,1},\vec{r}_a) &= \int \sum_{m=2} \frac{1}{m(m-1)} K(\gamma_a^{i_1\dots i_m}) \rho_{i_1}\dots\rho_{i_m} d\gamma_{i_1}\dots d\gamma_{i_m} \\ &= \mathscr{D}_a \int \sum_{m=2} \frac{1}{m(m-1)} w_0^{i_1}(\vec{r}_a)\dots w_0^{i_m}(\vec{r}_a)\rho_{i_1}\dots\rho_{i_m} d\gamma_{i_1}\dots d\gamma_{i_m} \\ &= \mathscr{D}_a \sum_{m=2} \frac{1}{m(m-1)} x_a^m = \mathscr{D}_a[(1-x_a)\ln(1-x_a)+x_a] \,.\end{aligned} \tag{4.85}$$

Introducing the weight density

$$n_k(\vec{r}_a) = \int w_k^{i_1\dots i_k}(\vec{r}_{ai_1},\dots,\vec{r}_{ai_k})\,\rho_{i_1}(\vec{r}_{i_1})\dots\rho_{i_k}(\vec{r}_{i_k})\,d\gamma_{i_1}\dots d\gamma_{i_k} \,, \tag{4.86}$$

the derivative of the generating function yields the three terms

$$\Phi|_1(\widetilde{\Gamma}_{1,1},\vec{r}_a) = -n_1\ln(1-n_0) + \frac{1}{2}\frac{n_2}{1-n_0} + \frac{1}{6}\frac{n_3}{(1-n_0)^2} \tag{4.87}$$

whose structure is well known from the Rosenfeld functional (4.13). It is well established that the weight functions (4.8) derive from a Taylor expansion in the *sin* and *cos* terms of the intersection angles. This has been shown before for n_2 in [25, 26] and by using differential forms [44]. For n_3, however, we made an inconvenient choice of coordinates for $\Delta \in S^2$ and give here a clearer argument. A more detailed discussion that also includes the zero-dimensional limit is presented in App. C.

Let us introduce the notation $\hat{e}_i := \hat{e}_n^{(i)}$ for the $i = 1,2,3$ normal vectors of Σ_1, Σ_2, Σ_3 and $e_{ij} := \hat{e}_i\hat{e}_j$ for their scalar product. Further assume that the three vectors approximately set up an orthonormal basis

$$\hat{e}_1 \approx \hat{e}_2 \times \hat{e}_3 \,. \tag{4.88}$$

The area of the spherical triangle is then $\Delta \approx \pi/2$ with the Jacobi determinant $J_{123} = \det(\hat{e}_1,\hat{e}_2,\hat{e}_3)) \approx 1$ and Euler angles ϕ_{ij}^k close to zero. Thus expanding the argument of *arccos* up to the 5'th order

$$z := \hat{E}_1\hat{E}_2 = (e_{23}e_{13}-e_{12})(1+\frac{1}{2}e_{23}^2)(1+\frac{1}{2}e_{13}^3) + \mathscr{O}(e_{ij}^5) \,, \tag{4.89}$$

yields the small-angle correction of Δ:

$$\begin{aligned}2\pi - 3\arccos(z) &= \frac{\pi}{2} + 3(z+\frac{1}{6}z^3) + \mathscr{O}(z^5) \\ &= \frac{\pi}{2} - 3\big[e_{12} - e_{23}e_{13} + \frac{1}{2}e_{12}(e_{23}^2+e_{13}^2) + \frac{1}{6}e_{12}^3\big] + \mathscr{O}(e_{ij}^4)\end{aligned} \tag{4.90}$$

where only e_{12}^3 follows from order z^3. Rewritten in the weight densities (4.8), n_3 is to first order in the Euler angle:

$$n_3 = \frac{\pi}{2}n_{\sigma 0}^3 - 3n_{\sigma 0}n_{\sigma 1}^2 + 3[n_{\sigma 1}n_{\sigma 2}n_{\sigma 1} - n_{\sigma 1}n_{\sigma 2}n_{\sigma 3}] - \frac{1}{2}n_{\sigma 3}^2 n_{\sigma 0} + \mathscr{O}(e_{ij}^4\rho^3). \tag{4.91}$$

The second term agrees with the Rosenfeld functional, while the prefactor of the third term is 4.5 compared to our 3, which is acceptable given that the terms of (4.13) have been fitted to numerical data. The fourth term disagrees, but is of lower order. More remarkably, the prefactor of the first term disagrees also. Choosing a different point of reference for the Taylor expansion can set the coefficient of the leading term from $\pi/2$ to 0, but never to 1. Here, Tarazona's term for the 3-particle intersection is a better approximation [86], which also includes additional terms from the third order in z. For a more detailed discussion, we refer to App. C.

Our next example derives the functional for three intersection centers, whose lowest RH-diagram is $\widetilde{\Gamma}_{3,1}$, which belongs to the class $\widetilde{\Lambda}_{1,1}$. Its intersection diagram is the exact third virial cluster $\gamma_a^{j_1 i_2}\gamma_b^{j_2 i_3}\gamma_c^{j_3 i_1}$ as shown in Fig. 4.2b). The next particle added to the triangle diagram has to overlap with all three intersection centers, as illustrated by the fourth figure of Fig. 4.2a) and represented by $\gamma_a^{j_1 i_2 i_4}\gamma_b^{j_2 i_3 i_4}\gamma_c^{j_3 i_1 i_4}$. Adding more particles includes copies of the last one, corresponding to the intersection pattern

$$\gamma_a^{j_1 i_2 i_4 \dots i_m}\gamma_b^{j_2 i_3 i_4 \dots i_m}\gamma_c^{j_3 i_1 i_4 \dots i_m} \,. \tag{4.92}$$

To further simplify the notation, let us define $w_a^i := w_0^i(\vec{r}_{ai})$ for the volume weight at intersection center $\vec{r}_a$ and particle position $\vec{r}_i$. The functional (4.35) for the 3-center diagrams then factorizes into weight densities of 2 and 3 centers:

$$\begin{aligned}
&\sum_{m=3}^{\infty} \frac{1}{m(m-1)} \int K(\gamma_a^{j_1 i_2 i_4 \dots i_m}\gamma_b^{j_2 i_3 i_4 \dots i_m}\gamma_c^{j_1 i_3 i_4 \dots i_m})\, \rho_{i_1} \dots \rho_{i_m}\, d\gamma_{i_1} \dots d\gamma_{i_m} \\
&= \mathscr{D}_a \mathscr{D}_b \mathscr{D}_c \sum_{m=3}^{\infty} \frac{1}{m(m-1)} \int (w_a^{i_1} w_c^{i_1} \rho_{i_1})(w_a^{i_2} w_b^{i_2} \rho_{i_2})(w_b^{i_3} w_c^{i_3} \rho_{i_3}) \\
&\qquad\qquad \times (w_a^{i_4} w_b^{i_4} w_c^{i_4} \rho_{i_4}) \dots (w_a^{i_m} w_b^{i_m} w_c^{i_m} \rho_{i_m})\, d\gamma_{i_1} \dots d\gamma_{i_m} \,.
\end{aligned} \tag{4.93}$$

Introducing the x-densities of (4.77) and adding the second virial, we finally arrive at the functional restricted to three and less intersection centers:

$$\begin{aligned}
\Phi|_3(\widetilde{\Gamma}_{1,1}, \vec{r}_a, \vec{r}_b, \vec{r}_c) &= \frac{1}{2}\mathscr{D}_a x_a^2 \\
&\quad + \mathscr{D}_a \mathscr{D}_b \mathscr{D}_c \left[\frac{x_{ab} x_{bc} x_{ac}}{x_{abc}^3} \left((1 - x_{abc}) \ln(1 - x_{abc}) + x_{abc} - \frac{1}{2} x_{abc}^2 \right) \right] .
\end{aligned} \tag{4.94}$$

With three intersection centers, it is exact in the second and third virial order, but also significantly more complex due to additional correlation and autocorrelation functions such as $w_1^{i_4}(\vec{r}_a) w_1^{i_4}(\vec{r}_b) w_1^{i_4}(\vec{r}_c)$, which have been shown by Wertheim to be nontrivial to evaluate [93, 94, 95].

Nevertheless, Lemma 6 is an efficient tool to derive new functionals. To compare different levels of approximation, let us summarize all cases of up to four intersection centers. With one center covered by (4.85), the next level is the 2-center approximation, beginning with the partially contracted third virial cluster, shown in Fig. 4.2b). All further intersection diagrams are then of the form:

$$\gamma_a^{j_1 i_2 i_3\, i_4 \dots i_m}\gamma_b^{j_2 i_3\, i_4 \dots i_m} \,. \tag{4.95}$$

The case of three centers has already been covered by (4.92). This leaves the functional with four intersection centers of the two RH-classes $\widetilde{\Gamma}_{4,1}$ and $\widetilde{\Gamma}_{4,3}$, while the star-content of $\widetilde{\Gamma}_{4,2}$ vanishes.

The corresponding intersection graphs are:

$$\begin{aligned}\gamma_a^{i_1 i_2\, i_5\ldots i_m}\gamma_b^{j_2 i_3\, i_5\ldots i_m}\gamma_c^{j_3 i_4\, i_5\ldots i_m}\gamma_d^{j_1 i_4\, i_5\ldots i_m} e_{i_1 i_3} e_{i_2 i_4} \\ +\ \gamma_a^{i_1 i_2}\gamma_b^{j_2 i_3\, i_4\ldots i_m}\gamma_c^{j_1 i_3\, i_4\ldots i_m}\gamma_d^{j_2 i_4\ldots i_m}\ ,\end{aligned} \tag{4.96}$$

with the Boltzmann functions e_{ij} included. Determining their generating functions and adding the lower order virial terms, yields the complete list of functionals up to four intersection centers

$$\begin{aligned}\Phi|_1 &= \mathscr{D}_a[(1-x_a)\ln(1-x_a)+x_a] \\ \Phi|_2 &= \frac{1}{2}\mathscr{D}_a x_a^2 + \frac{1}{2}\mathscr{D}_a\mathscr{D}_b\frac{x_a+x_b}{x_{ab}}\left[(1-x_{ab})\ln(1-x_{ab})+x_{ab}-\frac{1}{2}x_{ab}^2\right] \\ \Phi|_3 &= \frac{1}{2}\mathscr{D}_a x_a^2 + \mathscr{D}_a\mathscr{D}_b\mathscr{D}_c\,\frac{x_{ab}x_{bc}x_{ac}}{x_{abc}^3}\left[(1-x_{abc})\ln(1-x_{abc})+x_{abc}-\frac{1}{2}x_{abc}^2\right] \\ \Phi|_4 &= \frac{1}{2}\mathscr{D}_a x_a^2 + \frac{1}{6}\mathscr{D}_a\mathscr{D}_b\mathscr{D}_c x_{ab}x_{bc}x_{ac} \\ &\quad + \mathscr{D}_a\mathscr{D}_b\mathscr{D}_c\mathscr{D}_d\frac{x_{ac}x_{bc}x_{abd}}{x_{bcd}^4}\left[(1-x_{bcd})\ln(1-x_{bcd})+x_{bcd}-\frac{1}{2}x_{bcd}^2-\frac{1}{6}x_{bcd}^3\right] \\ &\quad - \frac{1}{8}\mathscr{D}_a\mathscr{D}_b\mathscr{D}_c\mathscr{D}_d\frac{y_{ab|cd}y_{ad|bc}}{(1-x_{abcd})^3}\ ,\end{aligned} \tag{4.97}$$

where we replaced $x_a \to (x_a+x_b)/2$ in $\Phi|_2$ to satisfy the diagram's symmetry and defined the Boltzmann weighted density

$$y_{ab|cd} = \int (w_a^i w_b^i \rho_i)(w_c^j w_d^j \rho_j)\, e_{ij}\, d\gamma_i d\gamma_j\ . \tag{4.98}$$

However, not all intersection networks result in different functionals. The probability measure for two centers, e.g., is identical to the 1-center functional as the orientation and position of the first determines the coordinates of the second. $\Phi|_1$ and $\Phi|_2$ are therefore of the same order of precision. To go beyond the Rosenfeld functional one has to apply $\Phi|_3$, which reduces to $\Phi|_1$ in the limit of coincident intersection centers $\vec{r}_b, \vec{r}_c \to \vec{r}_a$. Further corrections can be added by allowing for the the e-bonded part of $\Phi|_4$, whose negative contribution compensates the tendency of the fully f-bonded terms to overrate tightly packed particle configurations. As an improved model we therefore propose

$$\begin{aligned}\Phi = &\frac{1}{2}\mathscr{D}_a x_a^2 + \mathscr{D}_a\mathscr{D}_b\mathscr{D}_c\,\frac{x_{ab}x_{bc}x_{ac}}{x_{abc}^3}\left[(1-x_{abc})\ln(1-x_{abc})+x_{abc}-\frac{1}{2}x_{abc}^2\right] \\ &- \frac{1}{8}\mathscr{D}_a\mathscr{D}_b\mathscr{D}_c\mathscr{D}_d\frac{y_{ab|cd}y_{ad|bc}}{(1-x_{abcd})^3}\end{aligned} \tag{4.99}$$

as a reasonable approximation, whose integrals can be evaluated by Wertheim's application of the Radon transformation [93].

The formalism of Lemma 6 is not restricted to the free energy but applies to any thermodynamic object representable by Mayer or RH-graphs. As a final example, let us consider the leading order of the pair-correlation function g_2. As has been shown for spheres in [68, 70], the dominating RH-graphs are again the fully f-bonded diagrams with two rooted points connected by an e-bond. The network with the lowest number of intersection centers is therefore

$$\gamma_a^{i_1\, i_3\ldots i_m}\gamma_b^{j_2\, i_3\ldots i_m}\, e_{i_1 i_2}\ , \tag{4.100}$$

whose combinatorial prefactors have been shown in [70] to combine to 1. The sum over all diagrams then yields g_2 approximated by two intersection centers

$$g_{i_1 i_2}|_2(\vec{r}_{i_1}, \vec{r}_{i_2}|\vec{r}_a, \vec{r}_b) = e_{i_1 i_2}\left(1 + \mathscr{D}_a \mathscr{D}_b \frac{w_a^{i_1} w_b^{i_2}}{1 - x_{ab}}\right), \tag{4.101}$$

without summation over the particle indices i_1, i_2. Higher order correlation functionals and their application in perturbation theory will be considered in the next chapter.

Chapter 5

The Distribution Functionals for Hard Particles

The transformation between Mayer, Ree-Hoover, and intersection diagrams allows the derivation of any hard-particle functional that can be expanded in a virial series. In the current chapter, we use this relationship to derive the remaining class of distribution functionals. In analogy to the previous line of reasoning, Sec. 5.1 translates their virial expansion from rooted Mayer diagrams to rooted Ree-Hoover graphs, from which follows the generic distribution functional. Examples will be presented in Sec. 5.2, where the 2- and 3-particle distributions for up to four intersection centers are presented. We also compare the leading order of the contact probability of spheres to the Wertheim, Thiele, and Baxter solution and conclude by deriving the perturbation expansion of the pair-correlation functional.

5.1 The Generic Distribution Functional for Hard Particles

The main difference between the free-energy and the distribution functionals is their respective virial expansion in Mayer clusters. Once this is known, it is a mere technicality to identify their intersection classes and to write the functional in intersection kernels. In the following, we will therefore first derive the Mayer representation of the r-particle distribution functionals $\rho_{i_1\dots i_r}$, or more conveniently of their normalized form $g_{i_1\dots i_r}$, translate them into Ree-Hoover diagrams, from which follows the generic correlation functional.

A convenient starting point for the derivation of the Mayer representation is the perturbation expansion of the grand canonical potential [57]. Introducing the hard ϕ^{H} and soft ϕ^{S} contributions of the interaction potential $\phi_{ij} = \phi^{\mathrm{H}}_{ij} + \phi^{\mathrm{S}}_{ij}$ results in a corresponding splitting of the Boltzmann functions

$$e_{ij} = e^{\mathrm{H}}_{ij} + e^{\mathrm{H}}_{ij} f^{\mathrm{S}}_{ij} = e^{\mathrm{H}}_{ij} + \lambda F_{ij} \quad \text{for} \quad \lambda = 1\,, \tag{5.1}$$

where we introduced the auxiliary variable λ to count the number of F-terms. Next observe that the partition function of N particles is a fully e-bonded cluster integral of N labeled nodes $\Gamma_N(e)$ and that the expansion of the product $\prod(e^{\mathrm{H}}_{ij} + \lambda F_{ij})$ yields a sum of products, with a subset of e-bonds replaced by F-bonds. Using the invariance of the partition function under relabeling of particle numbers, it is always possible to define a unique, labeled subgraph $\Gamma_{r,k}(e^{\mathrm{H}}, F)$ of r nodes and counting index k, such that each node is linked to at least one F-bond. The Taylor expansion

of the partition function in λ can now be written as a functional derivative of cluster diagrams

$$D_\lambda = \sum_{r=2}^{\infty} \sum_{k=1}^{|\Gamma_r|} \frac{\lambda^{[\Gamma_{r,k}|}}{|\Gamma_{r,k}|!} \frac{\sigma_{r,k}}{r!} \Gamma_{r,k}(e^{\mathrm{H}}, F) \frac{\delta}{\delta \Gamma_r(e)}\Big|_{\lambda=0} , \tag{5.2}$$

where $|\Gamma_{r,k}|$ denotes the number of F-bonds, $|\Gamma_r|$ the total number of $\Gamma_{r,k}$ diagrams, and $\sigma_{r,k}$ the number of inequivalent particle labelings.

The Taylor expansion of the partition function $\Xi(\lambda)$ up to second order includes the three leading diagrams:

$$\begin{aligned} \Xi(\lambda) &= \sum_{N=0}^{\infty} \frac{z^N}{N!} Z_N(\lambda) = \sum_{N=0}^{\infty} \frac{z^N}{N!} \int \prod_{i,j=1}^{N} (e_{ij}^{\mathrm{H}} + \lambda F_{ij})\, d\gamma_{i_1 \dots i_N} = \sum_{N=0}^{\infty} \frac{z^N}{N!} Z_N(0) \big[1 + D_\lambda \frac{Z_N(\lambda)}{Z_N(0)}\big] \\ &= \Xi(0) \big[1 + \lambda \int \frac{1}{2} \rho_{i_1 i_2}^{\mathrm{H}} f_{i_1 i_2}^{\mathrm{S}}\, d\gamma_{i_1 i_2} + \frac{\lambda^2}{2} \int (\rho_{i_1 i_2 i_3}^{\mathrm{H}} f_{i_1 i_2}^{\mathrm{S}} f_{i_2 i_3}^{\mathrm{S}} + \frac{1}{4} \rho_{i_1 i_2 i_3 i_4}^{\mathrm{H}} f_{i_1 i_2}^{\mathrm{S}} f_{i_3 i_4}^{\mathrm{S}})\, d\gamma_{i_1 i_2 i_3 i_4} \\ &\quad + \mathcal{O}(\lambda^3)\big] \end{aligned} \tag{5.3}$$

introducing the grand-canonical r-particle distribution functionals $\rho_{i_1 \dots i_r}^{\mathrm{H}}$ as a function of $z_i := \exp(\beta(\mu_i - \phi_i)$. Expanding its logarithm and setting $\lambda = 1$ reproduces the well known perturbation expansion of the grand-canonical potential [57]

$$\begin{aligned} \beta\Omega = \beta\Omega_{\mathrm{H}} &- \frac{1}{2} \int \rho_{i_1 i_2}^{\mathrm{H}} f_{i_1 i_2}^{\mathrm{S}}\, d\gamma_{i_1 i_2} - \frac{1}{2} \int \rho_{i_1 i_2 i_3}^{\mathrm{H}} f_{i_1 i_2}^{\mathrm{S}} f_{i_2 i_3}^{\mathrm{S}}\, d\gamma_{i_1 i_2 i_3} \\ &- \frac{1}{8} \int (\rho_{i_1 i_2 i_3 i_4}^{\mathrm{H}} - \rho_{i_1 i_2}^{\mathrm{H}} \rho_{i_3 i_4}^{\mathrm{H}}) f_{i_1 i_2}^{\mathrm{S}} f_{i_3 i_4}^{\mathrm{S}}\, d\gamma_{i_1 i_2 i_3 i_4} - \dots \end{aligned} \tag{5.4}$$

where an implicit sum over paired indices is understood. Higher order corrections are determined likewise by successive insertion of further F-bonds into the cluster diagrams.

This calculation shows that the operator D_λ not only provides a compact notation for the perturbation expansion but also for the correlations, where each diagram $\Gamma_{r,k}(e^{\mathrm{H}}, F)$ corresponds to exactly one functional $\rho_{i_1 \dots i_r}^{H}$. Reinserting $F = e^{\mathrm{H}} f^{\mathrm{S}}$, $e^{\mathrm{H}} = f^{\mathrm{H}} + 1$ and expanding the graph in the virial series

$$\Gamma_{r,k}(f^{\mathrm{H}} + 1, F) = [f^{\mathrm{S}}]^{|\Gamma_{r,k}|} \sum_{n \geq r}^{\infty} \Gamma_{n,k}^{(r)}(f^{\mathrm{H}}, e^{\mathrm{H}}) \tag{5.5}$$

yields a corresponding representation in terms of r-rooted Mayer diagrams $\Gamma_{n,k}^{(r)}$

$$g_r(\vec{r}_1, \dots, \vec{r}_r) = \sum_{n \geq r} \sum_{k} \frac{\sigma_{n,k}^{(r)}}{(n-r)!} \int \Gamma_{n,k}^{(r)}(f, e)\, \rho_{i_{r+1}} \dots \rho_{i_n}\, d\gamma_{i_{r+1}} \dots d\gamma_{i_n} , \tag{5.6}$$

where we omitted the hard-particle index and introduced the symmetry factor $\sigma_{n,k}^{(r)}$, transforming from labeled to unlabeled graphs [73, 89].

An alternative representation can be derived by observing that completely e- and f-bonded graphs are uniquely related $\Gamma_r(e) \sim \Gamma_r(f)$ by the substitution $e = f + 1$ and ignoring all diagrams of lower order

$$\Gamma_r(e) = \Gamma_r(f) + \sum_{k}^{|\Gamma_{r,k}| < |\Gamma_r|} \Gamma_{r,k}(f) . \tag{5.7}$$

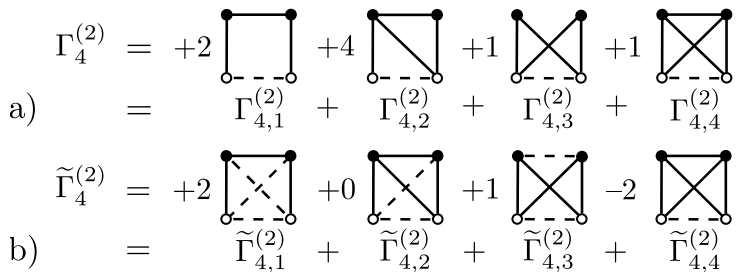

Figure 5.1: The fourth virial order of the 2-particle correlation function in a) Mayer and b) Ree-Hoover diagrams. The continuous lines denote f-bonds, while the dashed lines correspond to e-bonds. The rooted points are always mutually e-bonded.

This relation allows to replace $\Gamma_r(e)$ in (5.2) by $\Gamma_r(f)$ and to change the representation of D_λ from the fully connected e-bonded graphs to Mayer diagrams. The resulting operator then applies to the virial expansion of Ω, where the functional derivative substitutes any subgraph $\Gamma_r(f) \subset \Gamma_{n,k}(f)$ in a Mayer diagram by $\Gamma_r(e)$

$$g_r = -\beta r! \Gamma_r(e) \frac{\delta}{\delta \Gamma_r(f)} \Omega \,, \tag{5.8}$$

which reproduces the definition of the normalized r-particle functional. At the level of individual diagrams, this operation can also be written as

$$\Gamma_{n,k}^{(r)}(f,e) = \Gamma_r(e) \frac{\delta}{\delta \Gamma_r(f)} \Gamma_{n,k}(f) \,. \tag{5.9}$$

Examples for the 2-rooted diagrams of fourth virial order are shown in Fig. 5.1a).

In the following, we will use the close relationship between the virial expansion (5.6) and the functional derivative (5.8) to transfer the methods developed in the last chapter to derive the r-particle correlation functionals. This approach is again divided into two steps: the first one translates the Mayer into intersection diagrams, while the second determines their intersection probabilities. Let us first summarize the central ideas and notations from [45].

The main step in the construction of the correlation functional is again the transformation of the virial series (5.6) from rooted Mayer diagrams to a corresponding set of intersection networks. And in analogy to the star-graphs, this transformation requires the intermediate step of inserting $1 = e_{ij} - f_{ij}$ for each pair i, j of nodes not bonded by f-functions, resulting in a change of the virial series from Mayer to r-rooted RH-diagrams $\widetilde{\Gamma}_{n,k}^{(r)}$ [68, 70]. Examples for 2-rooted graphs of the fourth virial order are shown in Fig. 5.1b).

Following the conventions of Chapter 4, we define the notation for rooted diagrams:

Definition 5. *Let $\Gamma_{n,k}^{(r)}$ denote a labeled r-rooted Mayer diagram with r white and $n-r$ black nodes, free of articulation nodes, and the rooted points mutually e-bonded.*

A black node can be removed by deleting its vertex and all associated f-bonds $\pi^{-1} : \Gamma_{n.k}^{(r)} \to \{\Gamma_{n-1,k'}^{(r)}, \Gamma_{n-1,t}^{(r)}\}$, leaving a residual diagram, which is either a new r-rooted Mayer graph $\Gamma_{n-1,k'}^{(r)}$ or a sum of disjunct diagrams with articulation points $\Gamma_{n-1,t}^{(r)}$.

Definition 6. *Let $\widetilde{\Gamma}_{n,k}^{(r)}$ denote a labeled r-rooted RH-diagram with r white and $n-r$ black nodes. All points are mutually linked by either e- or f-bonds, with the f-bonded subdiagrams free of articulation points.*

A black node without e-bonds can be removed by deleting its vertex and all associated f-bonds $\pi^{-1}:\widetilde{\Gamma}^{(r)}_{n,k}\to\{\widetilde{\Gamma}^{(r)}_{n-1,k'},\,0\}$*, leaving either a new or the trivial RH-graph.*

To rewrite the virial integrals (5.6) in rooted RH-diagrams, observe that the rooting-process (5.9) only exchanges fully f-bonded subdiagrams $\Gamma_r(f)\subseteq\Gamma_{n,k}$ by its corresponding e-bonded graph $\Gamma_r(e)$, whereas the Ree-Hoover transformation only operates on pairs of unbonded nodes. The two operations are therefore mutually exclusive and commute. From this follows that the same functional derivative (5.9), which transforms star-diagrams into rooted Mayer graphs, also applies to RH-diagrams

$$\Gamma_r(e)\frac{\delta}{\delta\Gamma_r(f)}\widetilde{\Gamma}_{n,k}=\widetilde{\Gamma}^{(r)}_{n,k}\,. \tag{5.10}$$

The previously derived results for unrooted RH-graphs therefore remain valid for its rooted forms.

This connection can be immediately applied to rewrite the transformation between Mayer and RH-diagrams

$$\widetilde{\Gamma}^{(r)}_{n,k}=\sum_{k'}^{\widetilde{\Gamma}^{(r)}_{n,k}\subseteq\Gamma^{(r)}_{n,k'}}\Gamma^{(r)}_{n,k'}\,,\quad \Gamma^{(r)}_{n,k}=\sum_{k'}^{\Gamma^{(r)}_{n,k}\subseteq\widetilde{\Gamma}^{(r)}_{n,k'}}(-1)^{|\Gamma^{(r)}_{n,k}|-|\widetilde{\Gamma}^{(r)}_{n,k'}|}\,\widetilde{\Gamma}^{(r)}_{n,k'} \tag{5.11}$$

and to express the sum over rooted RH-diagrams

$$\Gamma^{(r)}_{n}\;=\sum_{k'}\Gamma^{(r)}_{n,k'}\;=\sum_{k}a^{(r)}_{n,k}\,\widetilde{\Gamma}^{(r)}_{n,k} \tag{5.12}$$

in terms of the "root-content"

$$a^{(r)}_{n,k}=\sum_{k'}^{\Gamma^{(r)}_{n,k'}\subseteq\widetilde{\Gamma}^{(r)}_{n,k}}(-1)^{|\Gamma^{(r)}_{n,k'}|-|\widetilde{\Gamma}^{(r)}_{n,k}|}\,, \tag{5.13}$$

which satisfies an analogous recursion relation as the star-content (4.25) under removal of a black node. This is readily seen by commuting π^{-1} with the functional derivative (5.9) and using (4.25)

$$\pi^{-1}(\Gamma^{(r)}_{n})=\Gamma_r(e)\frac{\delta}{\delta\Gamma_r(f)}\pi^{-1}(\Gamma_n)=\Gamma_r(e)\frac{\delta}{\delta\Gamma_r(f)}(n-2)\,\Gamma_{n-1}=(n-2)\,\Gamma^{(r)}_{n-1}\,, \tag{5.14}$$

with the corresponding relation for RH-diagrams, where the removal of a black node and its $n-1$ f-bonds

$$\begin{aligned}\pi^{-1}(\Gamma^{(r)}_{n})&=\sum_{k}\pi^{-1}(a^{(r)}_{n,k}\,\widetilde{\Gamma}^{(r)}_{n,k})=(-1)^{n-1}\sum_{k'}a^{(r)}_{n,k'}\,\widetilde{\Gamma}^{(r)}_{n-1,k'}\\&=(n-2)\,\Gamma^{(r)}_{n-1}=(n-2)\sum_{k'}a^{(r)}_{n-1,k'}\,\widetilde{\Gamma}^{(r)}_{n-1,k'}\end{aligned} \tag{5.15}$$

yields the recursion relation

$$a^{(r)}_{n,k}=(-1)^{n-1}(n-2)\;a^{(r)}_{n-1,k}\,. \tag{5.16}$$

The successive application of π^{-1} traces each diagram to a unique lowest element $\pi^{-1}(\Gamma^{(r)}_{n_0,k})=0$, which is the first element of the RH-class

$$\widetilde{\Lambda}^{(r)}_{n_0,k}=\bigcup_{m=0}^{\infty}\pi^{m}(\widetilde{\Gamma}^{(r)}_{n_0,k})\,, \tag{5.17}$$

defined by the inverse map $\pi : \widetilde{\Gamma}^{(r)}_{n-1,k} \to \widetilde{\Gamma}^{(r)}_{n,k'}$ which attaches a node to the previous $n-1$ vertices by f-bonds. The set of rooted RH-diagrams therefore separates into RH-classes, whose root-contents can be recursively calculated by (5.16), proving

Lemma 8. *The root-content of* $\widetilde{\Gamma}^{(r)}_{n,k} \in \widetilde{\Lambda}^{(r)}_{n_0,k}$ *with lowest element* $\widetilde{\Gamma}^{(r)}_{n_0,k}$ *is determined by*

$$a^{(r)}_{n,k} = (-1)^{\binom{n}{2}-\binom{n_0}{2}} \frac{(n-2)!}{(n_0-2)!}\, a^{(r)}_{n_0,k'} \,. \tag{5.18}$$

The last step in rewriting the correlation function (5.6) in RH-graphs is the transition from labeled to unlabeled diagrams. As for the star-diagrams (4.27), (4.30), the symmetry factor $\sigma^{(r)}_{n,k}$ counts the number of inequivalent permutations of particle indices, determined by the coset of the permutation and automorphism group of rooted diagrams.

Lemma 9. *Let* $\widetilde{\Gamma}^{(r)}_{n,k} \in \widetilde{\Lambda}^{(r)}_{n_0,k}$ *denote an element of the RH-class with lowest element* $\widetilde{\Gamma}^{(r)}_{n_0,k}$. *Its inequivalent labelings of the r white and* $n-r$ *black nodes are permuted by the coset group*

$$S_r \times S_{n-r} / Aut(\widetilde{\Gamma}^{(r)}_{n,k}) \tag{5.19}$$

whose automorphism group factorizes into the direct product

$$Aut(\widetilde{\Gamma}^{(r)}_{n,k}) = S_{n-n_0} \times Aut(\widetilde{\Gamma}^{(r)}_{n_0,k}) \,. \tag{5.20}$$

This is shown as follows: The white and black nodes are labeled independently, resulting in the decoupling of the permutation group $S_r \times S_{n-r}$, proving (5.19). Whereas the automorphism group factorizes, because each of the n_0 nodes is linked to at least one e-bond, while the residual $n-n_0$ nodes are completely f-bonded. Any exchange of labels between these two groups therefore results in an inequivalent permutation, leaving the $n-n_0$ vertices as an invariant set under relabeling, proving (5.20).

To rewrite the virial expansion (5.6) in RH-diagrams, let us define the symmetry factor of RH-integrals

$$\widetilde{\sigma}^{(r)}_{n,k} = \frac{1}{(n-r)!} \sigma^{(r)}_{n,k}\, a^{(r)}_{n,k} \,, \tag{5.21}$$

combining the root-content (5.18) and the number of inequivalent labelings

$$\sigma^{(r)}_{n,k} = \frac{|S_r \times S_{n-r}|}{|\mathrm{Aut}(\widetilde{\Gamma}^{(r)}_{n,k})|} = \frac{r!(n-r)!}{(n-n_0)!} \frac{1}{|\mathrm{Aut}(\widetilde{\Gamma}^{(r)}_{n_0,k})|} \,, \tag{5.22}$$

which yields the numerical prefactor of the rooted RH-class:

Corollary 1. *The symmetry factor of the r-rooted RH-diagram* $\widetilde{\Gamma}^{(r)}_{n,k} \in \widetilde{\Lambda}^{(r)}_{n_0,k}$ *with lowest element* $\widetilde{\Gamma}^{(r)}_{n_0,k}$ *for* $r \geq 2$ *is determined by*

$$\widetilde{\sigma}^{(r)}_{n,k} = (-1)^{\binom{n}{2}-\binom{n_0}{2}} \binom{n-2}{n_0-2} \frac{r!\, a^{(r)}_{n_0,k}}{|Aut(\widetilde{\Gamma}^{(r)}_{n_0,k})|} \,. \tag{5.23}$$

This result follows by inserting (5.18), (5.22) into (5.21).

Up to now, no approximation has been made on the virial expansion (5.6). The next step is therefore to simplify the integrals by restricting the number of intersection centers in which the particles are allowed to overlap. A useful observation is the following property of intersection diagrams of a RH-class:

Lemma 10. *The intersection network of the class $\widetilde{\Lambda}^{(r)}_{n_0,k}$ is defined by its lowest subgraph.*

The proof begins with the intersection diagram of the lowest element. Any further particle, added by π, can then be chosen to overlap with the previous intersection centers. This shows that a new particle can be added without changing their number. Repeated operation with π then completes the proof.

The intersection diagram with the lowest number of intersection centers therefore defines the "backbone" diagram for the entire RH-class. This is the basic idea for the resummation of RH-diagrams of a given RH-class and the approximation transferring the virial series (5.6) to the generic r-particle correlation functional:

Theorem 3. *Let $\widetilde{\Gamma}^{(r)}_{n_0,k}$ denote the lowest element of the RH-class $\widetilde{\Lambda}^{(r)}_{n_0,k}$. The generic r-particle correlation functional of the intersection network $\gamma^{I_1}_{a_1}\dots\gamma^{I_p}_{a_p}[e\dots e]$ with particle indices $I\in(i_1,\dots,i_n)$ is determined by*

$$\begin{aligned} g_{i_1\dots i_r}|_p(\vec{r}_{i_1},\dots,\vec{r}_{i_r}|\vec{r}_{a_1},\dots,\vec{r}_{a_p}) &= \widetilde{\Gamma}^{(r)}_{r,1}(e)\delta_{n_0,r}\delta_{AI}+(-1)^{|\widetilde{\Gamma}^{(r)}_{n_0,k}|}\frac{r!\,a^{(r)}_{n_0,k}}{|Aut(\widetilde{\Gamma}^{(r)}_{n_0,k})|} \\ \times\sum_{n\geq n_0}\sum_{I}\binom{n-2}{n_0-2}&\int K(\gamma^{I_1}_{a_1}\dots\gamma^{I_p}_{a_p}[e\dots e])\,\rho_{i_{r+1}}\dots\rho_{i_n}\,d\gamma_{i_{r+1}}\dots d\gamma_{i_n}\,, \end{aligned} \tag{5.24}$$

with the notation $\delta_{AI}=\delta(\vec{r}_{a_1 i_1})\dots\delta(\vec{r}_{a_r i_r})\delta(\vec{r}_{a_{r+1}})\dots\delta(\vec{r}_{a_p})$ for the product of delta-functions.

This result follows from inserting (5.23) into the cluster expansion (5.6) and the cancelation of signs due to the identity

$$|\widetilde{\Gamma}^{(r)}_{n,k}|=|\widetilde{\Gamma}^{(r)}_{n_0,k}|+\binom{n}{2}-\binom{n_0}{2}\,, \tag{5.25}$$

which leaves an overall constant, depending only on the lowest element of the RH-class and an n-dependent binomial coefficient. An exception provides the leading diagram $n_0=r$ of each r-correlation functional. Without an f-bond, its intersection probability vanishes and therefore has to be included separately. Finally, the delta-functions δ_{AI} have been added in (5.24) to achieve a symmetric formulation of the integrals

$$[g_{i_1 i_2}f_{i_1,i_2}](\vec{r}_{i_1},\vec{r}_{i_2})=\int g_{i_1,i_2}|_3(\vec{r}_{i_1},\vec{r}_{i_2}|\vec{r}_a,\vec{r}_b,\vec{r}_c)f_{i_1 i_2}(\vec{r}_{i_1},\vec{r}_{i_2})\,d\gamma_a d\gamma_b d\gamma_c \tag{5.26}$$

$$[g_{i_1 i_2}f_{i_1,i_2}](\vec{r}_a,\vec{r}_b,\vec{r}_c)=\int g_{i_1,i_2}|_3(\vec{r}_{i_1},\vec{r}_{i_2}|\vec{r}_a,\vec{r}_b,\vec{r}_c)f_{i_1 i_2}(\vec{r}_{i_1},\vec{r}_{i_2})\,d\gamma_{i_1} d\gamma_{i_2} \tag{5.27}$$

in the particle and intersection coordinates, which proves useful in later applications.

5.2 Examples of R-Particle Correlation Functionals

This last section presents four examples. We begin with the explicit derivation of the 2-particle correlation functional with two intersection centers and compare its contact probability with the Ornstein-Zernike solution of Wertheim, Baxter, and Thiele. The 2- and 3-particle correlations are then calculated for up to four intersection centers and compared to the Kirkwood superposition approximation.

The first f-bonded RH-diagram of the 2-particle correlation functional $g_{i_1 i_2}$ is $\widetilde{\Gamma}^{(2)}_{3,1}$, whose two white and one black nodes define a backbone diagram with two intersection centers. All further networks of the same RH-class can then be contracted to the pattern

$$\widetilde{\Lambda}^{(2)}_{2,1} : \quad e_{i_1 i_2} + e_{i_1 i_2}\, \gamma_a^{j_1 i_3 \dots i_n} \gamma_b^{j_2 i_3 \dots i_n} \,. \tag{5.28}$$

Applying the rules of Lemma 5 and Lemma 6 for the representation of the intersection kernel and introducing the notation $w_a^i = w_0^i(\vec{r}_{ai})$ for the volume weight, the virial series sums up to the generating function

$$\begin{aligned}
&g_{i_1 i_2}|_2(\vec{r}_{i_1}, \vec{r}_{i_2}|\vec{r}_a, \vec{r}_b) \\
&= e_{i_1 i_2}\delta_{AI} + \sum_{n\geq 2} \sum_{i_3 \dots i_n} \int K(\gamma_a^{j_1 i_3 \dots i_n} \gamma_b^{j_2 i_3 \dots i_n}\, e_{i_1 i_2})\, \rho_{i_3} \dots \rho_{i_n} d\gamma_{i_3} \dots d\gamma_{i_n} \\
&= e_{i_1 i_2}(\delta_{AI} + \sum_{n\geq 2} \sum_{i_3 \dots i_n} \mathscr{D}_a \mathscr{D}_b \int w_a^{i_1} w_a^{i_3} \dots w_a^{i_n} w_b^{i_2} w_b^{i_3} \dots w_b^{i_n}\, \rho_{i_3} \dots \rho_{i_n}\, d\gamma_{i_3} \dots d\gamma_{i_n}) \\
&= e_{i_1 i_2}(\delta_{AI} + \mathscr{D}_a \mathscr{D}_b\, w_a^{i_1} w_b^{i_2} \sum_{n\geq 2} x_{ab}^{n-2}) \,,
\end{aligned} \tag{5.29}$$

where we used the x-variable (4.77) and the property of Lemma 6 that the intersection probability for a single particle is zero $\mathscr{D}_a w_a^{i_1} = 0$. The final correlation functional has then the analytic form

$$g_{i_1 i_2}|_2(\vec{r}_{i_1}, \vec{r}_{i_2}|\vec{r}_a, \vec{r}_b) = e_{i_1 i_2}\Big(\delta(\vec{r}_{a i_1})\delta(\vec{r}_{b i_2}) + \mathscr{D}_a \mathscr{D}_b\, \frac{w_a^{i_1} w_b^{i_2}}{1 - x_{ab}} \Big) \,. \tag{5.30}$$

This result is exact up to the third virial order, but significantly improved by the additional pole at $x_{ab} = 1$. To illustrate this effect of the resummation process, let us derive the approximate contact probability for a system of 3-dimensional balls $B : S^2 \hookrightarrow \mathbb{R}^3$ of radius R and diameter $D = 2R$ at constant density ρ. The expansion of the derivatives of (5.30) to leading order in x_{ab} results in two terms

$$\begin{aligned}
g_{12}|_2(\vec{r}_1, \vec{r}_2) &= e_{12} \int \Big(\delta_{AI} + \mathscr{D}_a \mathscr{D}_b \frac{w_a^1 w_b^2}{1 - x_{ab}} \Big)\, d\gamma_a d\gamma_b \\
&= e_{12} \int \Big(\delta_{AI} + \mathscr{D}_a \frac{w_a^1 \int w_a^3 \mathscr{D}_b (w_b^2 w_b^3) \rho_3\, d\gamma_3 + \dots}{(1 - x_{ab})^2} \Big)\, d\gamma_a d\gamma_b \\
&= e_{12} \int \Big(\delta_{AI} + \frac{1}{(1 - x_{ab})^2} \int (\mathscr{D}_a w_a^1 w_a^3)(\mathscr{D}_b w_b^2 w_b^3) \rho_3\, d\gamma_3 + \mathscr{O}(\rho^2) \Big)\, d\gamma_a d\gamma_b \,,
\end{aligned} \tag{5.31}$$

corresponding to the resummed second and third virial contributions. For the particle positions $\vec{r}_i \in B_i$ of $i = 1, 2, 3$ and intersection coordinates $\vec{r}_a \in B_1 \cap B_3$, $\vec{r}_b \in B_2 \cap B_3$, the correlation function $x_{ab}(\vec{r}_{ab})$ for $\vec{r}_{ab} = \vec{r}_a - \vec{r}_b$ reduces to the volume of a lens-shaped domain

$$x_{ab}(\vec{r}_{ab}) = \int_{\vec{r}_3 \in B_3} w_0^3(\vec{r}_3 - \vec{r}_a) w_0^3(\vec{r}_3 - \vec{r}_b) \rho\, d\gamma_3 = \frac{4\pi}{3} R^3 \rho \Big[1 - \frac{3}{4}\frac{r_{ab}}{R} + \frac{1}{16}\Big(\frac{r_{ab}}{R}\Big)^3 \Big] \tag{5.32}$$

multiplied by ρ. To evaluate the residual integrals observe that x_{ab} is a strictly monotonic decreasing function in $0 \le r_{ab}/R \le 2$ with packing fraction η as its maximum. To simplify the remaining part of the integral, we approximate the denominator by its upper bound $(1-x_{ab})^{-2} \le (1-\eta)^{-2}$, which allows to exchange the integration over $\vec{r}_3$ with that of $\vec{r}_a, \vec{r}_b$

$$\int (\mathscr{D}_a w_a^1 w_a^3)(\mathscr{D}_b w_b^3 w_b^2)\, d\gamma_a d\gamma_b = f_{13} f_{32}, \tag{5.33}$$

reproducing the Mayer functions f_{13}, f_{32} of the third virial order of g_2. The final integration over $\vec{r}_3$ then again yields the volume of a lens-like domain

$$\int_{\vec{r}_3 \in B_3} f_{13} f_{32}\, \rho\, d\gamma_{i_3} = \frac{4\pi}{3} D^3 \rho \Big[1 - \frac{3}{4}\frac{r_{12}}{D} + \frac{1}{16}\Big(\frac{r_{12}}{D}\Big)^3\Big] = \frac{5}{2}\eta \tag{5.34}$$

for $r_{12} = |\vec{r}_1 - \vec{r}_2| = D$, cut out by the intersection of B_1 with the volume of the Minkowski sum $S_2^2 \oplus S_3^2$.

The upper bound of the contact probability for $1 \ll \eta$ is therefore

$$g_{12}(D) = 1 + \frac{5}{2}\frac{\eta}{(1-\eta)^2} + \mathscr{O}\Big(\frac{\eta^2}{(1-\eta)^3}\Big), \tag{5.35}$$

which is in excellent agreement with the result of Carnahan and Starling [12]:

$$g_{12}^{(\mathrm{CS})}(D) = \frac{1-\eta/2}{(1-\eta)^3} \tag{5.36}$$

as well as the Wertheim, Thiele, Baxter solution of the Ornstein-Zernike equation derived by the virial (V) and compressibility (C) route [57, 88, 90, 91]:

$$g_{12}^{(\mathrm{V})}(D) = \frac{1+\eta/2}{(1-\eta)^2}\,, \qquad g_{12}^{(\mathrm{C})}(D) = \frac{1-\eta/2+\eta^2/4}{(1-\eta)^3}. \tag{5.37}$$

The latter observation is especially interesting because its closing condition $c_2(r>D) = 0$ corresponds to the 1-center approximation of the functional expansion, whereas (5.35) reflects the 2-center representation of g_2. To obtain the same accuracy for the distribution functional therefore requires a larger number of intersections centers than for its dual direct correlation.

Deriving higher order functionals is now a matter of simple algebra. Here we list the leading orders of the 2-particle correlations with up to four intersection centers. The corresponding intersection diagrams for the RH-classes in the notation of Fig. 5.1b) are obtained by successive contraction of pair-wise intersection centers

$$\begin{aligned}
\widetilde{\Lambda}_{2,1}^{(2)} &: e_{i_1 i_2} + e_{i_1 i_2}\, \gamma_a^{j_1 i_3 \ldots i_n} \gamma_b^{j_2 i_3 \ldots i_n} \\
\widetilde{\Lambda}_{2,1}^{(2)} + \widetilde{\Lambda}_{4,1}^{(2)} &: e_{i_1 i_2} + e_{i_1 i_2}\, \gamma_a^{j_1 i_3} \gamma_b^{j_3 i_2} + e_{i_1 i_2}\, \gamma_a^{j_1 i_3 i_5 \ldots i_n} \gamma_b^{j_2 i_3 i_4 i_5 \ldots i_n} \gamma_c^{j_1 i_4 i_5 \ldots i_n} \\
&\quad + e_{i_1 i_2} e_{i_2 i_3} e_{i_1 i_4}\, \gamma_a^{j_1 i_3 i_5 \ldots i_n} \gamma_b^{j_3 i_4 i_5 \ldots i_n} \gamma_c^{j_2 i_4 i_5 \ldots i_n} \\
\widetilde{\Lambda}_{2,1}^{(2)} + \widetilde{\Lambda}_{4,3}^{(2)} &: e_{i_1 i_2} + e_{i_1 i_2}\, \gamma_a^{j_1 i_3} \gamma_b^{j_3 i_2} + e_{i_1 i_2}\, \gamma_{a_1}^{j_1 i_3 i_5 \ldots i_n} \gamma_{a_2}^{j_1 i_4 i_5 \ldots i_n} \gamma_{b_1}^{j_2 i_3 i_5 \ldots i_n} \gamma_{b_2}^{j_2 i_4 i_5 \ldots i_n} \\
&\quad + e_{i_1 i_2} e_{i_3 i_4}\, \gamma_{a_1}^{j_1 i_3 i_5 \ldots i_n} \gamma_{a_2}^{j_1 i_4 i_5 \ldots i_n} \gamma_{b_1}^{j_2 i_3 i_5 \ldots i_n} \gamma_{b_2}^{j_2 i_4 i_5 \ldots i_n}\,,
\end{aligned} \tag{5.38}$$

with the corresponding 2-particle correlation functionals

$$
\begin{aligned}
g_{i_1i_2}|_2 &= e_{i_1i_2}\Big(\delta_{AI} + \mathscr{D}_a\mathscr{D}_b\,\frac{w_a^{i_1}w_b^{i_2}}{1-x_{ab}}\Big)\\
g_{i_1i_2}|_3 &= e_{i_1i_2}\Big(\delta_{AI} + \mathscr{D}_a\mathscr{D}_b w_a^{i_1}w_b^{i_2}x_{ab} + \mathscr{D}_a\mathscr{D}_b\mathscr{D}_c w_a^{i_1}w_b^{i_2}w_c^{i_1}\,\frac{x_{ab}x_{bc}}{1-x_{abc}}\\
&\qquad - \mathscr{D}_a\mathscr{D}_b\mathscr{D}_c\frac{w_a^{i_1}w_c^{i_2}y_{abc}^{i_1i_2}}{(1-x_{abc})^3}\Big)\\
g_{i_1i_2}|_4 &= e_{i_1i_2}\Big(\delta_{AI} + \mathscr{D}_{a_1}\mathscr{D}_{b_1}w_{a_1}^{i_1}w_{b_1}^{i_2}x_{a_1b_1}\\
&\qquad + \mathscr{D}_{a_1}\mathscr{D}_{a_2}\mathscr{D}_{b_1}\mathscr{D}_{b_2}(w_{a_1}^{i_1}w_{a_2}^{i_1})(w_{b_1}^{i_2}w_{b_2}^{i_2})\frac{x_{a_1b_1}x_{a_2b_2}}{1-x_{a_1a_2b_1b_2}}\\
&\qquad + \frac{1}{2}\mathscr{D}_{a_1}\mathscr{D}_{a_2}\mathscr{D}_{b_1}\mathscr{D}_{b_2}\frac{w_{a_1}^{i_1}w_{a_2}^{i_2}w_{b_1}^{i_1}w_{b_2}^{i_2}y_{a_1a_2b_1b_2}}{(1-x_{a_1a_2b_1b_2})^3}\Big)\,,
\end{aligned}
\tag{5.39}
$$

where we introduced the Boltzmann weighted densities

$$
\begin{aligned}
y_{abc}^{i_1i_2} &= \sum_{i_3,i_4}\int e_{i_1i_4}e_{i_2i_3}w_a^{i_3}w_b^{i_3}\,\rho_{i_3}\,w_b^{i_4}w_c^{i_4}\,\rho_{i_4}\,d\gamma_{i_3}d\gamma_{i_4}\\
y_{a_1a_2b_1b_2} &= \sum_{i_3,i_4}\int e_{i_3i_4}w_{a_1}^{i_3}w_{b_1}^{i_3}\,\rho_{i_3}w_{a_2}^{i_4}w_{b_2}^{i_4}\,\rho_{i_4}\,d\gamma_{i_3}d\gamma_{i_4}\,.
\end{aligned}
\tag{5.40}
$$

As a last example, we present the leading term of the 3-particle correlation functional with 3 intersection centers. Its intersection diagram has the form

$$
\widetilde{\Lambda}_{3,1}^{(3)}\ :\qquad e_{i_1i_2}e_{i_2i_3}e_{i_1i_3} + e_{i_1i_2}e_{i_2i_3}e_{i_1i_3}\gamma_a^{i_1i_4\ldots i_n}\gamma_b^{i_2i_4\ldots i_n}\gamma_c^{i_3i_4\ldots i_n}\,,
\tag{5.41}
$$

with the corresponding correlation functional

$$
g_{i_1i_2i_3}|_3 = e_{i_1i_2}e_{i_2i_3}e_{i_1i_3}\Big(\delta_{AI} + \mathscr{D}_a\mathscr{D}_b\mathscr{D}_c\frac{w_a^{i_1}w_b^{i_2}w_c^{i_3}}{(1-x_{abc})^2}\Big)\,.
\tag{5.42}
$$

The contact probability is therefore to leading order $g_3 \sim (1-\eta)^{-3}$, which shows that the Kirkwood approximation $g_{i_1i_2i_3} \approx g_{i_1i_2}g_{i_2i_3}g_{i_3i_1} = [g_2]^3 \sim (1-\eta)^{-6}$ is not applicable when all three particles are close together, in accordance with results obtained from computer simulations [87]. It is not difficult to generalize this result to an arbitrary r-particle correlation function, whose leading term is $g_r \sim (1-\eta)^{-r}$, whereas the Kirkwood approximation suggests $[g_2]^{r(r-1)/2} \sim (1-\eta)^{-r(r-1)}$. This excludes the superposition approximation as a construction principle for any distribution functional.

With the derivation of this second class of correlation functionals, we can finally solve the last problem stated in chapter 3, the perturbative expansion of g_2 for the molecular dual grand canonical potential. Contrary to (3.3), the perturbation theory for Ω^{D} is an expansion of g_2 in the soft-correction term $F_{ij} = e_{ij}^{\mathrm{H}}f_{ij}^{\mathrm{S}}$ of the Mayer function $f_{ij} = f_{ij}^{\mathrm{H}} + F_{ij}$. Its lowest order diagrams are shown in Fig. 5.2, illustrating the successive replacement of f^{H}-bonds by F-functions. The corresponding substitution in the functional is generated by the formal derivative

$$
\begin{aligned}
g_{ij} &= e_{ij}^{\mathrm{S}}g_{ij}^{\mathrm{H}} + e_{ij}^{\mathrm{S}}\int\frac{\delta g_{ij}^{\mathrm{H}}}{\delta f_{ik}^{\mathrm{H}}}F_{ik}\,d\gamma_k + \frac{1}{2}e_{ij}^{\mathrm{S}}\int\frac{\delta g_{ij}^{\mathrm{H}}}{\delta f_{k_1k_2}^{\mathrm{H}}}F_{k_1k_2}\,d\gamma_{k_1k_2} + \ldots\\
&\approx g_{ij}|_{2,0} + g_{ij}|_{2,1} + g_{ij}|_{4,1} + \ldots\,,
\end{aligned}
\tag{5.43}
$$

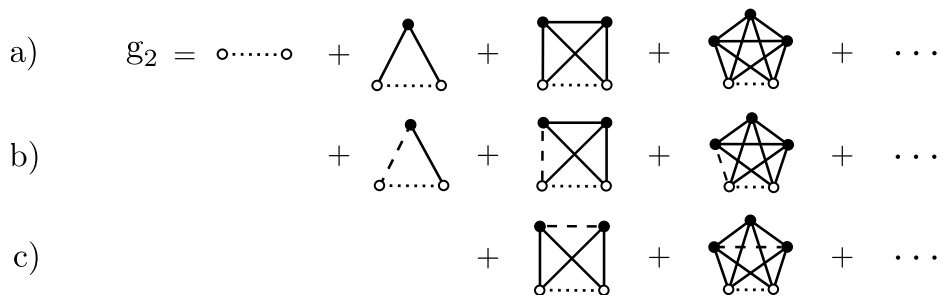

Figure 5.2: The perturbative expansion of the pair-correlation functional g_2 written in Mayer diagrams: solid lines indicate f^{H}-bonds, dashed lines correspond to F-bonds, and dotted ones represent the product $e_2^{\mathrm{S}}e_2^{\mathrm{H}}$ of hard- and soft- Boltzmann functions. The main contribution derives from the fully bonded diagrams a) with no internal F-bond $g_2|_{2,0}$, b) one F-bond linked to a rooted node $g_2|_{2,1}$, and c) one internal F-bond $g_2|_{4,1}$.

whose contributions can be further approximated by a series of correlations $g_2|_{n,k}$ of n hard-particle intersection centers and k internal F-bonds. Using the notation of intersection diagrams, the functionals of lowest intersection order and with at most one internal F-bond have the form:

$$\begin{aligned}
\widetilde{\Lambda}^{(2)}_{2,1} &: \quad e_{i_1i_2} + e_{i_1i_2}\gamma_a^{i_1i_3\ldots i_n}\gamma_b^{i_2i_3\ldots i_n} \\
\widetilde{\Lambda}^{(2)}_{3,1} &: \quad e_{i_1i_2}F_{i_2i_3}\gamma_a^{i_1i_4\ldots i_n}\gamma_b^{i_2i_3i_4\ldots i_n} \\
\widetilde{\Lambda}^{(2)}_{4,1} &: \quad e_{i_1i_2}F_{i_3i_4}\gamma_a^{i_1i_3i_5\ldots i_n}\gamma_b^{i_1i_4i_5\ldots i_n}\gamma_c^{i_2i_3i_5\ldots i_n}\gamma_d^{i_2i_4i_5\ldots i_n} ,
\end{aligned} \tag{5.44}$$

whose resummation yields the functionals

$$\begin{aligned}
g_{i_1i_2}|_{2,0} &= e^{\mathrm{S}}_{i_1i_2}e^{\mathrm{H}}_{i_1i_2}(\delta_{AI} + \mathscr{D}_a\mathscr{D}_b\frac{w_a^{i_1}w_b^{i_2}}{1-x_{ab}}) \\
g_{i_1i_2}|_{2,1} &= -e^{\mathrm{S}}_{i_1i_2}e^{\mathrm{H}}_{i_1i_2}\mathscr{D}_a\mathscr{D}_b\int\frac{w_a^{i_1}w_b^{i_2}F_{i_1i_3}w_b^{i_3}\rho_{i_3}}{(1-x_{ab})^2}\,d\gamma_{i_3} \\
g_{i_1i_2}|_{4,1} &= -e^{\mathrm{S}}_{i_1i_2}e_{i_1i_2}\mathscr{D}_a\mathscr{D}_b\mathscr{D}_c\mathscr{D}_d\frac{(w_a^{i_1}w_b^{i_1})(w_c^{i_2}w_d^{i_2})y_{acbd}}{(1-x_{abcd})^3} ,
\end{aligned} \tag{5.45}$$

with the correlation integral of the inner bond

$$y_{abcd} = \int F_{i_3i_4}(w_a^{i_3}w_c^{i_3}\rho_{i_3})(w_b^{i_4}w_d^{i_4}\rho_{i_4})\,d\gamma_{i_3i_4} . \tag{5.46}$$

These examples show that the representation in intersection centers can also be extended to the perturbative expansion of g_2 in Ω^{D}, completing our previous results for the direct and distribution functionals. But for many applications it will be sufficient to restrict the series to the first order in the hard-particle correlations and to use $g_2 \approx e_2^{\mathrm{S}}g_2^{\mathrm{H}}|_{2,0}$ as approximation. This convention has the additional advantage to satisfy the two constraints $g_2(\vec{r}) \geq 0$ and $g_2(r\to\infty) = 1$ for any $\vec{r}\in\mathbb{R}^n$. These two conditions are easily tested and provide an important advantage over Ω^{F}, where no such lower bounds exists. Because $-1 \leq f_2^{\mathrm{S}} < \infty$ and the discontinuity of g_2^{H} at particle contact, the integral of its first approximation order $f_2^{\mathrm{S}}g_2^{\mathrm{H}}$ is indefinite and very sensitive to changes of the hard-particle geometry and soft-interaction potential. Another disadvantage is the dependence of (3.3) on c_0^{H} and g_2^{H}, which contain identical information but require two separate calculations.

Chapter 6

Discussion and Conclusion

The results of the current thesis can be viewed from three different perspectives: the mathematics of integral geometry, the physics of DFT, and the lattice excess free-energy models used by engineers. In combination, they contribute to the development of the molecular density functional theory. But they are also topics of their own, which can be further extended in their individual directions. In the following, we will thus focus on each of these three topics seperately and finally conclude with an overview of possible applications.

The mathematical aspects: The central observation necessary for the derivation of the Rosenfeld functional from the virial expansion is its connection to integral geometry. It explains the relation between the second virial integral and the Gauss-Bonnet equation and also clarifies the arguments used by Isihara and Kihara, who derived the intersection probability from the Minkowski sum of its surfaces instead of the kinematic measure. Using the Blaschke-Santalo-Chern equation also avoids the Fourier decomposition of the second virial integrand that fails in even dimensions where the Euler-characteristic is trivially zero.

The introduction of integral geometry not only clarifies the mathematical basis of the Rosenfeld functional, it also allows its generalization. A particularly satisfying result is the simple algebraic structure obtained by the introduction of the functional derivative, $\mathscr{D}$, to combine the n-particle weight functions into a single expression to sum over all w_0. In principal, it would be possible to follow the lines of Rosenfeld and Wertheim and to expand these weight functions in an infinite series of 1-particle weight functions. But for non-spherical particles the evaluation of the resulting integrals cannot be done analytically and the splitting would provide no advantage compared to the unrestricted use of the n-particle weights.

The occurrence of the functional derivative in this framework is no coincidence. As has been argued in [44], the boundary operator for the surface of the intersection domains translates to a corresponding operator on the differential forms of the kinematic measure and thus on the weight functions of the particle volume $\partial \to \mathscr{D}$. For a single complex manifold, a similar structure has been discussed by Chern and Simons, leading to the corresponding Chern-Simons classes [3], which contain important geometric information about the underlying complex manifolds. From a mathematical point of view, it would therefore be interesting to extend the free-energy functional to particles with such a complex structure imbedded in either $\mathbb{C}^n$ or $\mathbb{CP}^n$. Another direction is the inclusion of surfaces $\Sigma_k \hookrightarrow \mathbb{R}^n$ of codimension $n-k>1$ to allow for threads of polymers or random coils as 1-dimensional curves, making contact to topics of knot theory and complex topology [10].

The hard-particle functional also provides unique insight into the characterization of non-local

geometry, described by the convolute of local differential forms. Determining, e.g., the packing fraction for a periodic particle distribution is comparatively simple, as the lattice structure maps the infinite space to its primary cell and thus to an almost local problem. But less symmetrical or even random partitions are more difficult to distinguish. Using the pair-correlation functional is therefore an obvious first ansatz, while a more manageable representation is the free-energy functional itself. But it would also be of interest to understand the dependence of the crystalline lattice structure as a function of the particle geometry.

The physical aspects: The intersection kernel together with the symmetry factors of the Ree-Hoover diagrams determine the hard-particle direct correlation and distribution functionals for any given equivalence class of Ree-Hoover diagrams. As of today, the hard-particle potential is therefore the only example whose density functionals can be explicitly calculated in a convergent series with increasing precision using a larger number of intersection centers. This expansion also explains the shortcomings of the Rosenfeld functional, whose 1-center approximations is insufficient to determine the correlations between particles of non-spherical geometry, for mixtures, and at higher packing fractions.

However, as the calculational complexity increases significantly with the number of intersection centers, any progress in FMT will require the development of further approximation methods. For particles with a distinct symmetry axis, e.g., the functionals can be expanded in tensor products of their descriptive vectors, resulting in phase-field crystal models, reproducing the Landau-Ginzburg and Swift-Hohenberg free energies for nematic fluids [98].

An equally important aspect, one that had not been considered systematically in the literature before, is the choice of an optimal representation for the grand-canonical potential. Most approaches start from the direct correlation functional and use perturbation theory to couple further soft potentials. But this low-order expansion is not the best ansatz for strong interactions. Also the combination of the direct and distribution functionals in the free energy is redundant, while ill-chosen splitting of hard and soft potentials can violate the positivity of the grand potential. The Legendre-dual grand-canonical potential, on the other hand, is a function of the pair correlation alone with exactly one minimum for short-ranged interactions. It is therefore well behaved for almost all molecular potentials, and even approximate pair correlations provide stable solutions for the self-consistent equation, as the unphysical Wilson ansatz shows.

The engineering aspects: To obtain a better understanding of the dual grand-canonical potential, we rederived the lattice free-energy in the quasichemical approximation from its continuum counterpart. The calculation shows that the Flory-Huggins, Staverman-Guggenheim, and the Guggenheim excess energies are independent of the underlying lattice structure, with the parameter z_0 determined by the 2-particle density integrated over the first particle shell. The derivation also justifies the validity of the excess functionals under the given constraints on the packing fraction and the next-neighbor interactions. These results are almost exclusively consequences of the unique structure of the two possible representations of the grand potential for pair interactions, but independent of the actual state of phase the model has been designed for, justifying the application of the excess lattice energy from the crystal to the liquid state.

As the derivation of the lattice models indicates, the single minimum of the dual functional is exceptionally stable under variations of the pair correlations, explaining why the UNIQUAC and UNIFAC models provide reasonable results despite their usage of the inconsistent Wilson ansatz. And it also explains, why the quasichemical approximation is incompatible with the inclusion of the detailed molecular geometry, whose additive structure of the lattice variables is a consequence of the neglect of its curvature terms.

Another aspect of the continuum and lattice theory is the relationship between the Euler-Lagrange equation for the pair-correlation functional and the self-consistent equation of the lattice models. Solving this equation corresponds to minimizing the grand potential for a homogeneous density. Together with the Larsen-Rasmussen approach, it also provides an alternative derivation of the self-consistent equation of COSMO-RS that is complementary to the approach by Klamt and clarifies some of its assumptions. E.g., the chemical potential derived by COSMO-RS is the canonical dual to the pair-correlation function and not of the particle density, which is constant and therefore not a dynamical variable of the lattice ansatz. Another misleading idea, often found in the literature, is the idea of the surface charges as "free segments" [52, 30]. As the Euler-Lagrange equation shows, the self-consistent identity is a local function and therefore applies to each pair of surface segments individually. The spacial correlation between separate segments is therefore part of the integral of the free energy, which in the next-neighbor approximation is replaced by a sum over pairs of segments. It is also customary to create new models by ad hoc combinations of separate energy terms. An example, where this approach has failed so far, is the inclusion of the Coulomb potential. But we have shown, the self-consistent equation and the free-energy functional are related by the Euler-Lagrange equation and cannot be modified independently. This has been demonstrated for the Debye-Hückel ansatz of the Coulomb interaction for which we derived the generalization of the continuum model and its possible extension to COSMO-RS.

Prospective developments: The derivation of the COSMO-RS model from the continuum functional is based on far reaching approximations. Probably the most restrictive one is the neglect of the particle geometry apart from volume and surface. A first step to generalize this ansatz is therefore the transition from the lattice to the continuum description, containing the full geometric information while holding on to the simplified representation of the pair-correlation function $g_{ij} \sim ce_{ij}$. The resulting model would still be independent of a free volume, but depending on the hard-particle geometry defined by the COSMO cavity. For a homogeneous liquid, the minimization of the grand potential now includes the integration over all particle orientations at a fixed distance, summing over all segment pairs of the molecules for any axial rotation angle, as shown in Fig. 3.1b).

This model should be sufficient to calculate the contact probability between molecules of complex geometries in the liquid state. For enzymatic reactions, e.g., the affinity between the enzyme and the dissolved substrates is an important information. The same applies to high-performance liquid chromatography, where the optimal selection of the substrate is central for the separation of enantiomer mixtures into their chiral compounds. Another field of applications is the calculation of the solubility of protein conformers to distinguish between the large number of possible tertiary folding structures.

The next level of generalization is the replacement of the constant c by a reference pair-correlation function $g_2(\rho_0; r_0)$ of spheres with volumes of molecular size. The resulting model is a coarse approximation of the density dependence of homogeneous gases and liquids, whose maximum of the first shell is replaced by the radial particle distance r_0 calculated for the given densities. For inhomogeneous fluids and crystals, however, such an approximation is no longer appropriate and the pair-correlation functionals for the hard-particle geometry has to the determined at least to leading order in the 2-center approximation $g_{2|2}(\rho(\vec{r}); t_0)$ at a fixed average distance t_0. But its computational costs for a triangulated surface are comparable or even higher than for MD/MC simulations, and the advantage of the DFT ansatz is lost. However, scanning through the 1700 molecules of the COSMO-SAC database, one finds that almost all particle surfaces are sufficiently regular to be representable by elementary polynomials. Thus instead of a triangulated

surface, the intersection domains can be determined by numerically solving algebraic equations. Whereas the small group of concave molecules can be represented by Voronoi tesselation, reducing the Euler form into a sum over convex subdomains of complementary intersections.

It is interesting to speculate, which of the current results will reach a wider audience over the coming years. The mathematical interest in integral geometry is currently dominated by the notion of valuations [8], whereas the proof of the generalized Blaschke-Santalo-Chern equation is based on the local representation of differential forms. The hard-particle functionals are therefore outside the current mathematical mainstream. Similarly pessimistic is the prospect for the extension of the Rosenfeld functional. Although the current derivation of the hard-particle correlation functional closes a chapter that was started more than a hundred years ago by van der Waals and Boltzmann, the equations of state are outdated by the current progress of MD/MC simulations. This leaves us with the derivation of the lattice models from the dual grand potential. Actually, the simplest result might prove the most useful. The generalization of the lattice models to include the particle geometry is easily implemented, while offering a wide range of applications. But as stated in the Preface of the current thesis, it is not possible to predict research's future course.

Appendix A

The Integral Measure of the Minkowski Sum

The r-particle correlation functionals are always accompanied by an integration over the kinematic measure $d\gamma_{i_1\ldots i_r}$ of translations and rotations of r particles. For the most common case of $r = 2$, we will now derive an explicit realization using methods from integral geometry [96, 24, 31, 58].

Let Σ_k denote a $n-1$ dimensional, smooth, boundary free, convex, Riemannian manifold, imbedded into $D_k : \Sigma_k \hookrightarrow \mathbb{R}^n$. Each point $p_k \in \Sigma_k$ is then related to an orthonormal, positively oriented coordinate frame $(\hat{e}_1^{(k)}, \ldots, \hat{e}_n^{(k)})$ with the outward pointing normal vector $\hat{e}_n^{(k)}$ and the differential basis and connection forms

$$dp = \theta_i \hat{e}_i \,, \quad d\hat{e}_i = \omega_{ij}\hat{e}_j \,, \quad d\hat{e}_n = \omega_{n\alpha}\hat{e}_\alpha = h_{\alpha\beta}\theta_\beta \hat{e}_\alpha \,, \quad \lambda_{\alpha\beta} := h^{-1}_{\alpha\beta} \,. \tag{A.1}$$

Each point of the smooth surface is uniquely related to a tangential plane up to an axial rotation around $\hat{e}_n^{(k)}$. From this follows that the tangential planes of two convex surfaces Σ_1, Σ_2, touching in a common point $p_1 = p_2$, also agree up to an axial rotation and an inversion of their normal vectors $\hat{e}_n^{(1)} = -\hat{e}_n^{(2)}$. This property remains unchanged even when the particles are shifted apart in the normal direction. Surface points of closest distance $t \in \mathbb{R}^+$ and their frames are therefore related by

$$p_2 = p_1 + t\hat{e}_n^{(1)} \,, \quad \hat{e}_n^{(1)} = -\hat{e}_n^{(2)} \,, \quad \hat{e}_\alpha^{(1)} = u_{\alpha\beta}\hat{e}_\beta^{(2)} \quad \text{for} \quad u_{\alpha\beta} \in \mathrm{SO}(n-1) \tag{A.2}$$

using the index conventions $i, j = 1, \ldots, n$ and $\alpha, \beta = 1, \ldots, n-1$.

Having defined the relative coordinate frames for the two particles, we can now write the integral

$$\int g_{12}(\vec{r}_1, \vec{r}_2)\, d\gamma_1 d\gamma_2 = \int g_{12}(\vec{r}_1 - \vec{r}_2)\, d\widetilde{\gamma}_{12} d\gamma = V \mathrm{vol}(\mathrm{SO}(n)) \int g^{\mathrm{H}}_{12}(\vec{r}_1 - \vec{r}_2)\, d\widetilde{\gamma}_{12} \tag{A.3}$$

in a comoving $d\widetilde{\gamma}_{12}$ and a reference system $d\gamma$. The integral of the latter can be carried out, contributing the volume $V = \mathrm{vol}(\mathbb{R}^n)$ and the volume of the group $\mathrm{SO}(n)$. The analogous transformation in the representation of base forms corresponds to the shift

$$d\gamma_1 d\gamma_2 = \bigwedge_{k=1,2} \bigwedge_i \theta_i^{(k)} \bigwedge_{i<j} \omega_{ij}^{(k)} = \bigwedge_i (\theta_i^{(1)} - \theta_i^{(2)}) \bigwedge_{i<j} \omega_{ij}^{(1)} \bigwedge_i \theta_i^{(2)} \bigwedge_{i<j} \omega_{ij}^{(2)} = d\widetilde{\gamma}_{12} d\gamma \tag{A.4}$$

as can be seen by expanding the skew-symmetric product and setting $d\gamma = d\gamma_2$ for the reference system.

The trivial contribution $d\gamma$ will be ignored in the following, leaving us with the transformation of $d\widetilde{\gamma}_{12}$. To simplify the calculation, observe that the translation of Σ_2 can also be written as $p_2 + t_2\hat{e}_2^{(2)} = p_1 + t_1\hat{e}_n^{(1)}$ for any $t_1, t_1 \in \mathbb{R}^+$ and $t_1 + t_2 = t$. This allows to first determine Weyl's half-tube $\Sigma(t) : p(t) = p + t\hat{e}_n$ for Σ_1, Σ_2 separately and then to derive their Minkowski sum $\Sigma_1(t_1) \oplus \Sigma_2(t_2)$ at $p_1(t_1) = p_2(t_2)$ [96, 58].

The differential forms $\theta_i(t), \omega_{ij}(t)$ of the half-tube surface $\Sigma(t)$ are determined by differentiating each point $p(t) = p + t\hat{e}_n$

$$dp(t) = dp + \hat{e}_n dt + t\,\omega_{n\alpha}\,\hat{e}_\alpha \tag{A.5}$$

and separating their components into the directions of $\hat{e}_n$ and $\hat{e}_\alpha$

$$\theta_n(t) = \theta_n + dt\ , \quad \theta_\alpha(t) = \theta_\alpha + t\,\omega_{n\alpha} = (\delta_{\alpha\beta} + t h_{\alpha\beta})\theta_\beta\ . \tag{A.6}$$

The new basis also determines the connection forms, as the orthonormal vectors $\hat{e}_\alpha$ and their differentials are invariant under translations

$$\omega_{n\alpha}(t) = \omega_{n\alpha} \quad \Rightarrow \quad h_{\alpha\beta}\,\theta_\beta(t) = h_{\alpha\beta}\,\theta_\beta\ . \tag{A.7}$$

Inserting (A.6), finally yields the curvature matrix and its inverse for the half-tube $\Sigma(t)$

$$h_{\alpha\beta}(t) = h_{\alpha\gamma}(\delta_{\gamma\beta} + t h_{\gamma\beta})^{-1}\ , \quad \lambda_{\alpha\beta}(t) = t\,\delta_{\alpha\beta} + \lambda_{\alpha\beta} \tag{A.8}$$

The second step requires to determine the differential volume element for the domain $\Sigma_1(t_1) \oplus \Sigma_2(t_2)$, covered by $\Sigma_1(t_1)$ while circling $\Sigma_2(t_2)$. To write $d\widetilde{\gamma}_{12}$ in a common coordinate frame we use the transformation (A.2), which relates the connection forms $\omega_{n\alpha}^{(1)} = -u_{\alpha\beta}\,\omega_{n\beta}^{(2)}$ of the two particles at their intersection point $p_1(t_1) = p_2(t_2)$ and also defines the transformation of their basis forms using the inverse Weingarten map λ. With $\Sigma_2(t_2)$ as the reference system, the forms of $\Sigma_1(t_1)$ are rotated into the new coordinate frame

$$\theta_\alpha^{(2)} = \lambda_{\alpha\beta}^{(2)}\omega_{n\beta}^{(2)}\ , \quad \theta_\alpha^{(1)} = u_{\alpha\beta}\,\theta_\beta^{\prime(1)} = -u_{\alpha\beta}\lambda_{\beta\gamma}^{(1)}u_{\gamma\mu}\,\omega_{n\mu}^{(2)}\ . \tag{A.9}$$

Inserting this result into (A.4), together with the transformation of the normal component $\theta_n^{(1)} - \theta_n^{(2)} = -dt$ and the Jacobi determinant $J = -1$, yields the reduced kinematic measure

$$\begin{aligned} d\widetilde{\gamma}_{12} &= \bigwedge_i (\theta_i^{(1)} - \theta_i^{(2)}) \bigwedge_{i<j} \omega_{ij}^{(1)} \\ &= \bigwedge_\alpha (u\lambda^{(1)}(t_1)u^{-1} + \lambda^{(2)}(t_2))_{\alpha\beta}\,\omega_{n\beta}^{(2)} \wedge dt \bigwedge_\alpha \omega_{n\alpha}^{(1)} \bigwedge_{\alpha<\beta} \omega_{\alpha\beta}^{(1)} \\ &= \det(\lambda^{(1)} + t\delta + u^{-1}\lambda^{(2)}u)\,\kappa_G^{(1)}\kappa_G^{(2)}\,d\sigma_1 \wedge d\sigma_2 \wedge d\mathrm{SO}(n-1) \wedge dt\ , \end{aligned} \tag{A.10}$$

where we introduced the unit matrix δ, the Gaussian curvature $\wedge_\alpha \omega_{n\alpha} = \kappa_G\, d\sigma$, the differential surface element $d\sigma$, used the orthonormal property $\det(u) = 1$ and (A.8) to write the final result in a symmetric form.

Appendix B

Proof of the generalized Blaschke-Santalo-Chern Equation

The current section completes the proof Lemma 6, demonstrating that the weight functions (4.70) are symmetric in the particles indices and permuted by $\mathrm{SO}(k)$ rotations.

For the surfaces $\Sigma_1,\ldots,\Sigma_k$, let us define the k coordinate frames

$$\Sigma_m \;:\; (\underbrace{\hat{e}_1^{(m)},\ldots,\hat{e}_{n-m}^{(m)}}_{\text{tangential}},\underbrace{\hat{e}_{n-m+1}^{(m)},\ldots,\hat{e}_n^{(m)}}_{\text{normal}}) \quad \text{for} \quad m=1,\ldots,k \tag{B.1}$$

and the Pfaffian form (4.68)

$$\mathrm{Pf}(GB\omega)_{1\ldots k}^{n-k} = \det(GBh)_{1\ldots k} \bigwedge_{\alpha=1}^{n-k} \theta_\alpha^{(1)} \,. \tag{B.2}$$

This choice of the vector basis defines a specific ordering of the particles' indices $1,\ldots,k$, which can be viewed as a nested intersection of surfaces

$$(((\Sigma_1\cap\Sigma_2)\cap\Sigma_3)\cap\Sigma_4)\ldots\,, \tag{B.3}$$

with Σ_1 as the reference system. The intersection product therefore fails the permutation invariance of the intersection probability. However, not the curvature form but the kinematic measure (4.50) has to be $\mathrm{SO}(n-k)\times\mathrm{SO}(k)$ invariant. We therefore have to prove the permutation symmetry of the integral

$$\begin{aligned}&\int K(\Sigma_1\cap\ldots\cap\Sigma_k)\wedge K(D_2)\wedge\ldots\wedge K(D_k)\\ &\qquad=\int \det(GBh)_{1\ldots k}\bigwedge_{\alpha=1}^{n-k}\theta_\alpha^{(1)}\frac{d\mathrm{vol}(\mathrm{SO}(n-k))}{|\mathrm{SO}(n-k)|}\wedge K(D_2)\wedge\ldots\wedge K(D_k)\,.\end{aligned} \tag{B.4}$$

Generalizing Chern's arguments for two intersecting surfaces [16, 82], the translational measure of Σ^k has been extended by $\mathrm{SO}(n-k)$ to the kinematic measure of $\mathbb{R}^{n-k}$. This leaves us to rotate the normal vectors $\hat{e}_n^{(2)},\ldots,\hat{e}_n^{(k)}$ into the tangential direction of Σ_1. For the nested coordinate frame (B.3), we can chose the $\mathrm{SO}(m)$ transformations of the "normal" directions to rotate $\hat{e}_n^{(m)}$ into the basis of Σ_1 while keeping the vectors of $\Sigma_2,\ldots,\Sigma_{m-1}$ fixed:

$$\Sigma_m\to\Sigma_1 \;:\quad \mathrm{SO}(m)/\mathrm{SO}(m-1)=S^{m-1}\,. \tag{B.5}$$

Introducing the spherical vector $(x_1^{(m)},\ldots,x_m^{(m)}) \in S^{m-1}$, the normal vector of Σ_m transforms into the basis of Σ_1

$$\hat{e}_n^{(m)} = \sum_{p=1}^{m} x_p^{(m)}\, \hat{e}_{n-p+1}^{(1)} \quad \text{for} \quad \sum_{p=1}^{m} (x_p^{(m)})^2 = 1 \tag{B.6}$$

and their corresponding dual differential forms

$$\begin{aligned} \theta_n^{(m)} = \sum_{p=2}^{m} x_p^{(m)}\, \theta_{n-p+1}^{(1)} = x_m^{(m)} \theta_{n-m+1}^{(1)} + \mathscr{O}(\theta_\alpha^{(1)}) \\ \text{for} \quad n-m+2 \le \alpha \le n-1 \,. \end{aligned} \tag{B.7}$$

Here the symbol $\mathscr{O}(\theta_\alpha^{(1)})$ indicates elements which drop out when inserted into the skew symmetric product (B.4) as they already occur at a lower m. This transforms the normal directions into the tangential forms of Σ_1

$$\theta_n^{(2)} \wedge \ldots \wedge \theta_n^{(k)} = x_2^{(2)} \ldots x_k^{(k)}\, \theta_{n-1}^{(1)} \wedge \ldots \wedge \theta_{n-k+1}^{(1)} \,, \tag{B.8}$$

which are complementary to the already existing elements in (B.4).

The analogous transformation has to be done for the connection forms. Adopting the notation of (B.1), we separate the forms into two groups

$$\Sigma_m : \quad \underbrace{\omega_{1,n}^{(m)} \wedge \ldots \wedge \omega_{n-m,n}^{(m)}}_{\text{tangential}} \wedge \underbrace{\omega_{n-m+1,n}^{(m)} \wedge \ldots \wedge \omega_{n-1,n}^{(m)}}_{\text{normal}} \,. \tag{B.9}$$

Again, the tangential directions transform by the coset elements of S^{m-1}

$$\begin{aligned} \omega_{\alpha,n}^{(m)} = x_m^{(m)}\, \omega_{\alpha,n-m+1}^{(1)} + \mathscr{O}(\omega_{\alpha,\beta}^{(1)}) \\ \text{for} \quad 1 \le \alpha \le n-m \,,\ n-m+2 \le \beta \le n-1 \,, \end{aligned} \tag{B.10}$$

whose products provide the complementary part to the $\mathrm{SO}(n-k)$ form of (B.4)

$$\bigwedge_{m=2}^{k} \bigwedge_{\alpha=1}^{n-m} \omega_{\alpha,n}^{(m)} = \Big[\prod_{m=2}^{k} (x_m^{(m)})^{n-m}\Big] \bigwedge_{m=2}^{k} \bigwedge_{\alpha=1}^{n-m} \omega_{\alpha,n-m+1}^{(1)} \,. \tag{B.11}$$

On the other hand, the normal components of the connection forms (B.9) transform under the adjoint of $g_{\alpha\beta} \in \mathrm{SO}(m)$

$$\begin{aligned} \omega_{\alpha,n}^{(m)} = g_{\alpha\beta}^{-1} \hat{e}_\beta^{(1)}\, d(g_{n\gamma} \hat{e}_\gamma^{(1)}) = g_{\alpha\beta}^{-1} dg_{n\beta} + \mathscr{O}(\omega_{\beta\gamma}^{(1)}) \\ \text{for} \quad n-m+1 \le \beta < \gamma \le n-1 \end{aligned} \tag{B.12}$$

with the coset element $g_{n\alpha} \in \mathrm{SO}(m)/\mathrm{SO}(m-1)$ leaving the normal vectors invariant. Forming their product, they combine into the group measure of $\mathrm{SO}(k)$ modulo further connections

$$\begin{aligned} \bigwedge_{m=2}^{k} \bigwedge_{\alpha=n-m+1}^{n-1} \omega_{\alpha,n}^{(m)} &= \bigwedge_{m=2}^{k} [d\mathrm{vol}(S^{m-1}) + \mathscr{O}(\omega_{\beta\gamma}^{(1)})] \\ &= d\mathrm{vol}(\mathrm{SO}(k)) + \mathscr{O}(\omega_{\beta\gamma}^{(1)}) \,. \end{aligned} \tag{B.13}$$

Finally, inserting the transformed normal components into the kinematic measure (B.4), yields a differential form which is obviously $\mathrm{SO}(k)$ invariant

$$\begin{aligned}&\int K(\Sigma_1 \cap \ldots \cap \Sigma_k) \wedge K(D_2) \wedge \ldots \wedge K(D_k) \\ &\quad = \int \frac{\det(GBh)}{|\mathrm{SO}(n-k)|} \prod_{m=2}^{k} \left(x_m^{(m)}\right)^{n-m+1} d\mathrm{vol}(\mathrm{SO}(k)) \wedge K(\Sigma_1) \wedge \ldots \wedge K(\Sigma_k) \,.\end{aligned} \tag{B.14}$$

The product of $x_m^{(m)}$ terms is the Jacobian J of the transformation into spherical coordinates with the parameterization in terms of $\mathrm{SO}(m)$ rotation angles for $m = 1, \ldots, k$

$$x_m^{(m)} = \prod_{\alpha=1}^{m-1} \sin(\phi_{\alpha,m}) \,, \tag{B.15}$$

proving the invariance of the weight functions (4.70) under $\mathrm{SO}(k)$-generated permutations of particles indices and thus completing the proof of Lemma 6.

Appendix C

Deriving Rosenfeld's 1-particle Weight Functions

In the following, we will give a short account of how to transform the 2- and 3-particle Euler form (4.81) to the coordinate dependent representation of 1-particle weight functions introduced by Rosenfeld, Wertheim, and Tarazona [76, 92, 85]

The Euclidean metric η_{ij} in the orthonormal principal frame $(\vec{v}_1, \vec{v}_2, \vec{n})$ is the diagonal tensor

$$\eta_{ij} = e_i \otimes e_j = \mathbb{I}_{ij} = (\vec{v}_1 \otimes \vec{v}_1 + \vec{v}_2 \otimes \vec{v}_2 + \vec{n} \otimes \vec{n})_{ij} \,. \tag{C.1}$$

with the corresponding connection tensor written in the normal vector $e_3 = \vec{n}$:

$$\begin{aligned} de_3 = \omega_{3\alpha} e_\alpha = \kappa_\alpha \theta_\alpha \otimes e_\alpha = \kappa_\alpha e_\alpha \otimes e_\alpha d\vec{p} = \big(\kappa_\alpha e_\alpha \otimes e_\alpha\big)\vec{t}\, ds \\ = \big(\kappa_1 \vec{v}_1 \otimes \vec{v}_1 + \kappa_2 \vec{v}_2 \otimes \vec{v}_2\big)\vec{t}\, ds = \mathbb{K}\,\vec{t} ds \end{aligned} \tag{C.2}$$

using Rodrigues formula $de_n = \kappa_\alpha v_\alpha e_\alpha$, the representation of the vielbein $\theta_\alpha = e_\alpha d\vec{p}$, and by observing that the tangential vector at each point $\vec{p} \in \Sigma_1 \cap \Sigma_2$ lies in the direction of $\vec{t} \sim \vec{n}^{(1)} \times \vec{n}^{(2)}$. The derivative $d\vec{p} = \vec{t}\, ds$ therefore is the differential line element ds pointing into the direction of $\vec{t}$.

In order to separate the normal vectors from the principal frame, Wertheim rewrites the connection form [92]:

$$\begin{aligned} \mathbb{K} &= \frac{1}{2}\big(\kappa_1 \vec{v}_1 \otimes \vec{v}_1 + \kappa_2 \vec{v}_2 \otimes \vec{v}_2\big) + \frac{1}{2}\kappa_1\big(\mathbb{I} - \vec{n} \otimes \vec{n} - \vec{v}_2 \otimes \vec{v}_2\big) + \frac{1}{2}\kappa_2\big(\mathbb{I} - \vec{n} \otimes \vec{n} - \vec{v}_1 \otimes \vec{v}_1\big) \\ &= \frac{1}{2}\big(\kappa_1 + \kappa_2\big)(\mathbb{I} - \vec{n} \otimes \vec{n}) + \frac{1}{2}\big(\kappa_1 - \kappa_2\big)(\vec{v}_1 \otimes \vec{v}_1 - \vec{v}_2 \otimes \vec{v}_2) \\ &=: \bar{\kappa}\,\big(\mathbb{I} - \vec{n} \otimes \vec{n}\big) + \Delta \end{aligned} \tag{C.3}$$

introducing the mean and tangential curvatures $\bar{\kappa}$, Δ. The connection form then yields the form

$$\omega_{13} = e_1 de_3 = \vec{t}\,\mathbb{K}\vec{t}\, ds \,. \tag{C.4}$$

In a second step, the normal vector $\vec{n}^{(2)}$ is separated from the curvature depending parts of particle 1:

$$(\vec{n}^{(1)} \times \vec{n}^{(2)})\, \mathbb{K}_{(1)}\, (\vec{n}^{(1)} \times \vec{n}^{(2)}) = -\vec{n}^{(2)} \times \vec{n}^{(1)}\, \big(\kappa_1 \vec{v}_1 \otimes \vec{v}_1 + \kappa_2 \vec{v}_2 \otimes \vec{v}_2\big)\vec{n}^{(1)} \times \vec{n}^{(2)}$$

$$= -\vec{n}^{(2)}\big(\kappa_1\vec{n}^{(1)}\times\vec{v}_1\otimes\vec{v}_1\times\vec{n}^{(1)} + \kappa_2\vec{n}^{(2)}\times\vec{v}_2\otimes\vec{v}_2\times\vec{n}^{(1)}\big)\vec{n}^{(2)}$$
$$= \vec{n}^{(2)}\big(\kappa_1\vec{v}_2\otimes\vec{v}_2 + \kappa_2\vec{v}_1\otimes\vec{v}_1\big)\vec{n}^{(2)} = \vec{n}^{(2)}\,\mathbb{K}^{\dagger}_{(1)}\,\vec{n}^{(2)}\,,$$

using the orthonormal relation $\vec{v}_1\times\vec{v}_2 = \vec{n}$ and introducing the adjoint connection tensor:

$$\mathbb{K}^{\dagger} = \bar{\kappa}\left(\mathbb{I} - \vec{n}\otimes\vec{n}\right) - \Delta\,. \tag{C.5}$$

Inserting these results into (4.81)

$$\begin{aligned}
\frac{1-c_{12}}{s_{12}}\omega^{(1)}_{13} &= \frac{1-c_{12}}{s_{12}}\vec{t}\,\mathbb{K}_{(1)}\vec{t}\,ds = \frac{1-c_{12}}{s_{12}}\Big[\frac{\vec{n}^{(1)}\times\vec{n}^{(2)}}{s_{12}}\mathbb{K}_{(1)}\frac{\vec{n}^{(1)}\times\vec{n}^{(2)}}{s_{12}}\Big]ds\\
&= \frac{1-c_{12}}{s_{12}^2}\vec{n}^{(2)}\mathbb{K}^{\dagger}_{(1)}\vec{n}^{(2)}\frac{ds}{s_{12}} = \frac{1}{1+c_{12}}\vec{n}^{(2)}\mathbb{K}^{\dagger}_{(1)}\vec{n}^{(2)}\frac{ds}{s_{12}}\\
&= \frac{1}{1+c_{12}}\vec{n}^{(2)}\big[\bar{\kappa}^{(1)}\big(\mathbb{I}-\vec{n}^{(1)}\otimes\vec{n}^{(1)}\big) - \Delta^{(1)}\big]\vec{n}^{(2)}\frac{ds}{s_{12}}\\
&= \frac{1}{1+c_{12}}\big[\bar{\kappa}^{(1)}(1-c_{12}^2) - \vec{n}^{(2)}\Delta^{(1)}\vec{n}^{(2)}\big]\frac{ds}{s_{12}}\\
&= \Big[(1-\vec{n}^{(1)}\vec{n}^{(2)})\,\bar{\kappa}^{(1)} - \frac{\vec{n}^{(2)}\Delta^{(1)}\vec{n}^{(2)}}{1+\vec{n}^{(1)}\vec{n}^{(2)}}\Big]\frac{ds}{|\vec{n}^{(1)}\times\vec{n}^{(2)}|}
\end{aligned}$$

and using the integral representation by δ-functions

$$\frac{1-c_{12}}{s_{12}}\omega^{(1)}_{13} = \int_{D_1\cap D_2}\Big[(1-\vec{n}^{(1)}\vec{n}^{(2)})\,\bar{\kappa}^{(1)} - \frac{\vec{n}^{(2)}\Delta^{(1)}\vec{n}^{(2)}}{1+\vec{n}^{(1)}\vec{n}^{(2)}}\Big]\delta(\vec{n}^{(1)}\vec{r}_A)\,\delta(\vec{n}^{(2)}\vec{r}_A)\,d^3r_A\,, \tag{C.6}$$

this reproduces the first part of Wertheim's decomposition ([92]), from which derive the 1-particle weight functions by Taylor-expanding *sin* and *cos* in tensor products of their normal vectors.

The integral representation used in (C.6) extends the integration along the line element ds to the entire embedding space. This and similar relations are readily derived from the linear coordinate transformation

$$\eta = \vec{n}\vec{p}\,,\;\; \zeta = \vec{m}\vec{p}\,,\;\; \xi = \vec{e}_1x + \vec{e}_2y + \vec{e}_3z \tag{C.7}$$

at the point $\vec{p} = (x,y,z)$ and its corresponding Jacobi determinant:

$$d\eta\wedge d\zeta\wedge d\xi = |\det(\vec{n},\vec{m},\vec{e})|\;dx\wedge dy\wedge dz = |\vec{n}\times\vec{m}|\;d^3p\,. \tag{C.8}$$

Applied for the integral of an arbitrary test function F and two δ-functions

$$\int F(\vec{p})\,\delta(\vec{n}\vec{p})\,\delta(\vec{m}\vec{p})\,d^3p = \int F(\eta,\zeta,\xi)\;\delta(\eta)\,\delta(\zeta)\,\frac{d\eta\,d\zeta\,d\xi}{|\vec{n}\times\vec{m}|} = \int\widetilde{F}(\xi)\frac{d\xi}{|\vec{n}\times\vec{m}|}\,, \tag{C.9}$$

it reduces to the line integral along ξ, as used in equation (C.6).

With one δ-function included, the corresponding transformation

$$\eta = \vec{n}\vec{p}\,,\quad \zeta = \xi = \vec{e}_1x + \vec{e}_2y + \vec{e}_3z \tag{C.10}$$

and $\vec{e}\wedge\vec{e} = \vec{e}$ yields the result:

$$\int F(\vec{p})\,\delta(\vec{n}\vec{p})\,d^3p = \int F(\eta,\zeta,\xi)\;\delta(\eta)\,\frac{d\eta\,d\zeta\,d\xi}{|\vec{e}\vec{n}|} = \int\widetilde{F}(\zeta,\xi)\frac{dS_n}{|\vec{e}\vec{n}|} = \int\widetilde{F}(\zeta,\xi)\,dS \tag{C.11}$$

with $\det(\vec{n},\vec{e},\vec{e}) = \vec{e}\vec{n}$ and the differential surface element dS_n in the outward pointing $\vec{n}$ direction.

Analogously, the integral of three δ-functions reduces to a sum of intersection points $\{\mathrm{pt}\}$ in the variables

$$\eta = \vec{n}\vec{p}\,, \quad \zeta = \vec{m}\vec{p}\,, \quad \xi = \vec{l}\vec{p}\,, \tag{C.12}$$

solving the algebraic equation $\eta = \zeta = \xi = 0$

$$\int F(\vec{p})\,\delta(\vec{n}\vec{p})\,\delta(\vec{m}\vec{p})\,\delta(\vec{l}\vec{p})\,d^3p = \sum_{\{\mathrm{pt}\}} \frac{\widetilde{F}(\mathrm{pt})}{|(\vec{n}\times\vec{m})\,\vec{l}\,|} \tag{C.13}$$

yields the inverse Jacobi determinant related to three intersecting surfaces.

To derive the 3-particle intersection term proposed by Tarazona in the zero-dimensional limit [85], observe that the 3-particle Euler form (4.82) reduces to the surface of the spherical triangle $\mathrm{area}(\Delta \subseteq S^2)$, whose sides are bounded by S^1 of unit radius. Following our arguments of [55], this allows to rewrite the triangular surface by its corresponding volume section $\mathrm{area}(S^2) = 3\mathrm{vol}(B_3)$ of a ball B_3, which is then approximated by the volume of the tetrahedral simplex $\det(\vec{n}_1,\vec{n}_2,\vec{n}_3)/6$, corresponding to $1/6$ of its Jacobi denterminent J. Including the prefactor $1/6$ from (4.87), the leading correction of the 3-particle intersection probability thus reduces to

$$\frac{1}{6}\frac{1}{4\pi} J\,\mathrm{area}(\Delta \subseteq S^2) = \frac{1}{8\pi} J\,\mathrm{vol}(B_3|_\Delta) = \frac{1}{48\pi}|(\vec{n}_1\times\vec{n}_2)\,\vec{n}_3|^2 + \ldots\,, \tag{C.14}$$

whose first term agrees with the functional introduced by Tarazona [85]. Higher order corrections can be derived by subdiving the spherical cap Δ into a finer grid of tetrahedons. But the simple relationship between its volume and the Jacobi determinant would be lost, resulting in a significantly more complex functional expression.

Bibliography

[1] Abrams, D.S., Prausnitz, J.M.: Statistical thermodynamics of liquid mixtures: A new expression for the excess gibbs energy of partly or completely miscible systems. AIChE Journal **21**, 116–128 (1975)

[2] Allen, P., Tildesley, D.: Computer Simulation of Liquids. Oxford Science Publ. Clarendon Press (1989)

[3] Alvarez-Gaumé, L., Ginsparg, P.: The structure of gauge and gravitational anomalies. Ann. Phys. **161**, 423–490 (1985)

[4] Atkins, P., de Paula, J.: Atkins' Physical Chemistry. Oxford University Press, Oxford (2010)

[5] Baxter, J.: Lattice Theories of the Liquid State. Pergamon Press, Oxford (1963)

[6] Baxter, R.: Ornstein-zernike relation for a disordered fluid. Aust. J. Phys. **21**, 563–569 (1968)

[7] Baxter, R.: Distribution Functions, vol. VIII A, pp. 267–334. Academic Press, New York (1971)

[8] Bernig, A.: Algebraic integral geometry (2010). arXiv:1004.3145

[9] Blaschke, W.: Vorlesungen über Integralgeometrie. Deutscher Verlag der Wissenschaften (1955)

[10] Bott, R., Tu, L.W.: Differential Forms in Algebraic Topology. Springer (1995)

[11] Brader, J.M., Esztermann, A., Schmidt, M.: Colloidal rod-sphere mixtures: Fluid-fluid interfaces and the onsager limit. Phys. Rev. E **66**(3), 031,401 (2002)

[12] Carnahan, N.F., Starling, K.E.: Equation of state for nonattracting rigid spheres. J. Chem. Phys. **51**, 635–636 (1969)

[13] Chapman, W.G., Gubbins, K.E., Jackson, G., Radosz, M.: Saft: Equation of state model for associating fluids. Fluid Phase Equilb **52**, 31 (1989)

[14] Chapman, W.G., Gubbins, K.E., Jackson, G., Radosz, M.: New reference equation of state for associating liquids. Ind. Eng. Chem. Res. **29**, 1709 (1990)

[15] Chern, S.S.: On the kinematic formula in the euclidean space of n dimensions. Am. J. Math. **74**, 227–236 (1952)

[16] Chern, S.S.: Integral formulas for hypersurfaces in euclidean space and their applications to uniqueness theorems. Indiana Univ. Math. J. **8**, 947–955 (1959)

[17] Chern, S.S.: On the kinematic formula in integral geometry. J. Math. Mech. **16**, 101–118 (1966)

[18] Esztermann, A., Reich, H., Schmidt, M.: Density functional theory for colloidal mixtures of hard platelets, rods, and spheres. Phys. Rev. E **73**, 011,409 (2006)

[19] Evans, R.: The nature of the liquid-vapour interface and other topics in the statistical mechanics of non-uniform, classical fluids. Adv. Phys. **28**, 143–200 (1979)

[20] Flory, P.: Thermodynamics of high polymer solutions. J. Chem. Phys. **9**, 660 (1941)

[21] Flory, P.: Thermodynamics of high polymer solutions. J. Chem. Phys. **10**, 51–61 (1942)

[22] Fredenslund, A., Jones, R.L., Prausnitz, J.M.: Group-contribution estimation of activity coefficients in nonideal liquid mixtures. AIChE Journal **21**, 1086–1099 (1975)

[23] Guggenheim, E.: Mixtures. Clarendon Press, Oxford (1952)

[24] Guggenheimer, H.W.: Differential Geometry. Dover Publications, New York (1963)

[25] Hansen-Goos, H., Mecke, K.: Fundamental measure theory for inhomogeneous fluids of nonspherical hard particles. Phys. Rev. Lett. **102**(1), 018,302 (2009)

[26] Hansen-Goos, H., Mecke, K.: Tensorial density functional theory for non-spherical hard-body fluids. J. Phys.: Condens. Matter. **22**, 364,107 (2010)

[27] Hansen-Goos, H., Mecke, K.: Tensorial density functional theory for non-spherical hard-body fluids. J. Phys.: Condens. Matter **22**, 364,107 (2010)

[28] Hansen-Goos, H., Roth, R.: Density functional theory for hard-sphere mixtures: The white-bear version mark ii. J. Phys.: Condens. Matter **18**, 8413–8425 (2006)

[29] Helgason, S.: Differential Geometry, Lie Groups, and Symmetric Spaces. Academic Press (1978)

[30] Hsieh, C.M., Sandler, S.I., Lin, S.T.: Improvements of cosmo-sac for vapor-liquid and liquid-liquid equilibrium predictions. Fluid Phase Equilibria **297**, 90–97 (2010)

[31] Hsiung, C.C.: A First Course in Differential Geometry. International Press, Boston (1981)

[32] Huggins, M.: Solutions of long chain compounds. J. Chem. Phys. **9**, 440 (1941)

[33] Isihara, A.: Determination of molecular shape by osmotic measurement. J. Chem. Phys. **18**(11), 1446–1449 (1950)

[34] Kaouche, A., Leroux, P.: Mayer and Ree-Hoover weights of infinite families of 2-connected graphs. Seminaire Lotharingien de Combinatoire **61 A**, B61Af (2009)

[35] Kierlik, E., Rosinberg, M.: Free-energy density functional for the inhomogeneous hard-sphere fluid: Application to interfacial adsorption. Phys. Rev. A **42**, 3382 (1990)

[36] Kihara, T.: The second virial coefficient of non-spherical molecules. J. Phys. Soc. Japan **6**(5), 289–296 (1951)

[37] Kihara, T.: Virial coefficients and models of molecules in gases. Rev. Mod. Phys. **25**, 831–843 (1953)

[38] Klamt, A.: Conductor-like screening model for real solvents: A new approach to the quantitative calculation of solvation phenomena. J. Phys. Chem. **99**, 2224–2235 (1995)

[39] Klamt, A.: COSMO-RS: From Quantum Chemistry to Fluid Phase Thermodynamics and Drug Design. Elsevier Science, Amsterdam (2005)

[40] Klamt, A., Eckert, F., Arlt, W.: Cosmo-rs: An alternative to simulation for calculating thermodynamic properties of liquid mixtures. Annu. Rev. Chem. Biomol. Eng. **1**, 101–122 (2010)

[41] Klamt, A., Reinisch, J., Eckert, F., Graton, J., Questel, J.Y.L.: Interpretation of experimental hydrogen-bond enthalpies and entropies from cosmo polarisation charge densities. Phys. Chem. Chem. Phys. **15**, 7147–7154 (2013)

[42] Klamt, A., Reinisch, J., Eckert, F., Hellweg, A., Diedenhofen, M.: Polarisation charge densities provide a predictive quantification of hydrogen bond energies. Phys. Chem. Chem. Phys. **14**, 955–963 (2012)

[43] Klamt, A., Schüürmann, G.: Cosmo: A new approach to dielectric screening in solvents with explicit expression for the screening energy and its gradient. J. Chem. Soc., Perkin Trans. **2**, 799–805 (1993)

[44] Korden, S.: Deriving the rosenfeld functional from the virial expansion. Phys. Rev. E **85**(4), 041,150 (2012)

[45] Korden, S.: Density functional theory for hard particles in n dimensions. Commun. Math. Phys. **337**, 1369–1395 (2015). arXiv:1403.2054

[46] Korden, S.: Distribution functionals for hard particles in n dimensions (2015). arXiv:1502.04393

[47] Korden, S.: Lattice-fluid models derived from density functional theory (2015). arXiv:1503.02327

[48] Landau, D., Binder, K.: A Guide to Monte Carlo Simulations in Statistical Physics. Cambridge University Press (2000)

[49] Landau, L.D., Lifschitz, E.M.: Lehrbuch der Theoretischen Physik, vol. 3. Akademie-Verlag Berlin, Berlin (1979)

[50] Landau, L.D., Lifschitz, E.M., Pitajewski, L.P.: Lehrbuch der Theoretischen Physik, vol. 5. Akademie-Verlag Berlin, Berlin (1987)

[51] Larsen, B., Rasmussen, P.: A comparision between the quasichemical model and two-fluid local-composition models. Fluid Phase Equilibria **28**, 1–11 (1986)

[52] Lin, S.T., Sandler, S.I.: A priori phase equilibrium prediction from a segment contribution solvation model. Ind. Eng. Chem. Res. **41**, 899–913 (2002)

[53] Manssori, G.A., Carnahan, N.F., Starling, K.E., Leland, T.W.: Equilibrium thermodynamic properties of the mixture of hard spheres. J. Chem. Phys. **54**, 1523 (1971)

[54] Marechal, M., Goetze, H.H., Härtel, A., Löwen, H.: Inhomogeneous fluids of colloidal hard dumbbells: Fundamental measure theory and monte carlo. J. Chem. Phys **135**, 234,510 (2011)

[55] Marechal, M., Korden, S., Mecke, K.: Deriving fundamental measure theory from the virial series: Consistency with the zero-dimensional limit. Phys. Rev. E **90**, 042,131 (2014)

[56] Maurer, G., Prausnitz, J.: On the derivation and extension of the uniquac equation. Fluid Phase Equilibria **2**, 91–99 (1978)

[57] McDonald, I.R., Hansen, J.P.: Theory of Simple Liquids. Elsevier Science, University of Cambridge (2008)

[58] Minkowski, H.: Volumen und oberfläche. Math. Ann. **57**, 447–495 (1903)

[59] Morita, T., Hiroike, K.: A new approach to the theory of classical fluids, i. Prog. Theor. Phys. **23**, 1003–1027 (1960)

[60] Morita, T., Hiroike, K.: A new approach to the theory of classical fluids, ii. Prog. Theor. Phys. **24**, 317–330 (1960)

[61] Morita, T., Hiroike, K.: A new approach to the theory of classical fluids, iii. Prog. Theor. Phys. **25**, 537–578 (1961)

[62] Phan, S., Kierlik, E., Rosinberg, M., Bildstein, B., Kahl, G.: Equivalence of two free-energy models for the inhomogeneous hard-sphere fluid. Phys. Rev. E **48**, 618 (1993)

[63] Phillips, J., Schmidt, M.: Bulk phase behaviour of binary hard platelet mixtures from density functional theory. Phys. Rev. E **81**, 041,401 (2010)

[64] Pitzer, K.S.: Electrolyte theory - improvements since debye and hückel. Acc. Chem. Res. **10**, 371–377 (1977)

[65] Prausnitz, J., Lichtenthaler, R., de Azevedo, E.G.: Molecular Thermodynamics of Fluid-Phase Equilibria. Prentice-Hall, Englewood Cliff, NJ (1999)

[66] Prigogine, I.: The Molecular Theory of Solutions. North-Holland Pub. Co., Amsterdam (1957)

[67] Ree, F.H., Hoover, W.G.: Fifth and sixth virial coefficients for hard spheres and hard disks. J. Chem. Phys. **40**, 939 (1964)

[68] Ree, F.H., Hoover, W.G.: Reformulation of the virial series of classical fluids. J. Chem. Phys **41**, 1635 (1964)

[69] Ree, F.H., Hoover, W.G.: Seventh virial coefficients for hard spheres and hard disks. J. Chem. Phys **46**, 4181 (1967)

[70] Ree, F.H., Keeler, N., McCarthy, S.L.: Radial distribution function of hard spheres. J. Chem. Phys **44**, 3407–3425 (1966)

[71] Reichl, L.: A Modern Course in Statistical Physics. Wiley (2009)

[72] Reiss, H., Frisch, H.K., Lebowitz, J.L.: Statistical mechanics of rigid spheres. J. Chem. Phys. **31**(2), 369–380 (1959)

[73] Riddell, R.J., Uhlenbeck, G.E.: On the theory of the virial development of the equation of the state of monoatomic gases. J. Chem. Phys. **21**, 2056 (1953)

[74] Rosenfeld, Y.: Scaled field particle theory of the structure and the thermodynamics of isotropic hard particle fluids. J. Chem. Phys. **89**(7), 4272–4287 (1988)

[75] Rosenfeld, Y.: Free-energy model for the inhomogeneous hard-sphere fluid mixture and density-functional theory of freezing. Phys. Rev. Lett. **63**(9), 980–983 (1989)

[76] Rosenfeld, Y.: Density functional theory of molecular fluids: Free-energy model for the inhomogeneous hard-body fluid. Phys. Rev. E **50**(5), R3318–R3321 (1994)

[77] Rosenfeld, Y.: Free energy model for the inhomogeneou hard-body fluid: Application of the gauss-bonnet theorem. Mol. Phys. **86**, 637–647 (1995)

[78] Rosenfeld, Y., Levesque, D., Weis, J.: Free-energy model for the inhomogeneous hard-sphere fluid mixture - triplet and higher-order direct correlation-functions in dense fluids. J. Chem. Phys. **92**(11), 6818–6832 (1990)

[79] Roth, R.: Fundamental measure theory for hard-sphere mixtures: A review. J. Phys.: Condens. Matter **22**, 063,102–063,120 (2010)

[80] Roth, R., Evans, R., Lang, A., Kahl, G.: Fundamental measure theory for hard-sphere mixtures revisited: The white bear version. J. Phys.: Condens. Matter **14**, 12,063–12,078 (2002)

[81] Samios, J., Durov, V.: Novel Approaches to the Structure and Dynamics of Liquids: Experiments, Theories and Simulations. Nato Science Series II. Springer Netherlands (2013)

[82] Santalo, L.A.: Integral Geometry and Geometric Probability. Addison-Wesley (1976)

[83] Schmidt, M.: Fluid structure from density-functional theory. Phys. Rev. E **62**(4), 4976–4981 (2000)

[84] Schneider, R., Weil, W.: Stochastic and Integral Geometry. Springer (2008)

[85] Tarazona, P.: Density functional for hard sphere crystals: A fundamental measure approach. Phys. Rev. Lett. **84**, 694–697 (2000)

[86] Tarazona, P., Rosenfeld, Y.: From zero-dimensional cavities to free-energy functionals for hard disks and hard spheres. Phys. Rev. E **55**, R4873–R4876 (1997)

[87] Taylor, M.P., Lipson, J.: On the born-green-yvon equation and triplet distributions for hard spheres. J. Chem. Phys. **97**, 4301–4308 (1992)

[88] Thiele, E.: Equation of state for hard spheres. J. Chem. Phys. **39**, 474–479 (1963)

[89] Uhlenbeck, G.E., Ford, G.W.: The Theory of Linear Graphs with Applications to the Theory of the Virial Development of the Properties of Gases, *Studies in Statistical Mechanics*, vol. 1. Interscience Publishers (1962)

[90] Wertheim, M.S.: Exact solution of the percus-yevick integral equation for hard spheres. Phys. Rev. Lett. **10**, 321–323 (1963)

[91] Wertheim, M.S.: Analytic solution of the percus-yevick equation. J. Math. Phys. **5**, 643–651 (1964)

[92] Wertheim, M.S.: Fluids of hard convex molecules i. basic theory. Mol. Phys. **83**, 519–537 (1994)

[93] Wertheim, M.S.: Fluids of hard convex molecules ii. two-point measures. Mol. Phys. **89**, 989–1004 (1996)

[94] Wertheim, M.S.: Fluids of hard convex molecules iii. the third virial coefficient. Mol. Phys. **89**, 1005–1017 (1996)

[95] Wertheim, M.S.: Third virial coefficient of hard spheroids. Mol. Phys. **99**, 187–196 (2001)

[96] Weyl, H.: On the volume of tubes. Am. J. Math. **61**, 461–472 (1939)

[97] Wilson, G.: Vapor-liquid equilibrium. xi. a new expression for the excess free energy of mixing. J. Am. Chem. Soc. **86**, 127–130 (1964)

[98] Wittkowski, R., Löwen, H., Brand, H.R.: Derivation of a three-dimensional phase-field-crystal model for liquid crystals from density functional theory. Phys. Re. E **82**(3), 031,708 (2010)

[99] Zinn-Justin, J.: Quantum Field Theory and Critical Phenomena. Oxford Science Publ. (2002)